Declassified and Approved For Release 2013/09/24 : CIA-RDP10-02196R000400060004-1

Russian Original Vol. 39, No. 5, November, 1975

May, 1976

SATEAZ 39(5) 953-1034 (1975)

Return to [redacted] for file (Apr 26 1976)

SOVIET ATOMIC ENERGY

АТОМНАЯ ЭНЕРГИЯ
(ATOMNAYA ENERGIYA)

TRANSLATED FROM RUSSIAN

CONSULTANTS BUREAU, NEW YORK

Declassified and Approved For Release 2013/09/24 : CIA-RDP10-02196R000400060004-1

Declassified and Approved For Release 2013/09/24 : CIA-RDP10-02196R000400060004-1

SOVIET ATOMIC ENERGY

Soviet Atomic Energy is a cover-to-cover translation of *Atomnaya Énergiya*, a publication of the Academy of Sciences of the USSR.

An agreement with the Copyright Agency of the USSR (VAAP) makes available both advance copies of the Russian journal and original glossy photographs and artwork. This serves to decrease the necessary time lag between publication of the original and publication of the translation and helps to improve the quality of the latter. The translation began with the first issue of the Russian journal.

Editorial Board of *Atomnaya Énergiya:*

Editor: M. D. Millionshchikov

Deputy Director
I. V. Kurchatov Institute of Atomic Energy
Academy of Sciences of the USSR
Moscow, USSR

Associate Editor: N. A. Vlasov

A. A. Bochvar
N. A. Dollezhal'
V. S. Fursov
I. N. Golovin
V. F. Kalinin
A. K. Krasin
V. V. Matveev
M. G. Meshcheryakov
P. N. Palei
V. B. Shevchenko
V. I. Smirnov
A. P. Vinogradov
A. P. Zefirov

Copyright © 1976 Plenum Publishing Corporation, 227 West 17th Street, New York, N.Y. 10011. All rights reserved. No article contained herein may be reproduced, stored in a retrieval system, or transmitted, in any form or by any means, electronic, mechanical, photocopying, microfilming, recording or otherwise, without written permission of the publisher.

Consultants Bureau journals appear about six months after the publication of the original Russian issue. For bibliographic accuracy, the English issue published by Consultants Bureau carries the same number and date as the original Russian from which it was translated. For example, a Russian issue published in December will appear in a Consultants Bureau English translation about the following June, but the translation issue will carry the December date. When ordering any volume or particular issue of a Consultants Bureau journal, please specify the date and, where applicable, the volume and issue numbers of the original Russian. The material you will receive will be a translation of that Russian volume or issue.

Subscription
$87.50 per volume (6 issues)

Single Issue: $50
Single Article: $15

Prices somewhat higher outside the United States.

CONSULTANTS BUREAU, NEW YORK AND LONDON

227 West 17th Street
New York, New York 10011

Published monthly. Second-class postage paid at Jamaica, New York 11431.

Soviet Atomic Energy is abstracted or indexed in *Applied Mechanics Reviews, Chemical Abstracts, Engineering Index, INSPEC—Physics Abstracts and Electrical and Electronics Abstracts, Current Contents,* and *Nuclear Science Abstracts.*

Declassified and Approved For Release 2013/09/24 : CIA-RDP10-02196R000400060004-1

Declassified and Approved For Release 2013/09/24 : CIA-RDP10-02196R000400060004-1

SOVIET ATOMIC ENERGY

A translation of *Atomnaya Énergiya*

May, 1976

Volume 39, Number 5 November, 1975

CONTENTS

Declassified and Approved For Release 2013/09/24 : CIA-RDP10-02196R000400060004-1

Declassified and Approved For Release 2013/09/24 : CIA-RDP10-02196R000400060004-1

CONTENTS

(continued)

The Russian press date (podpisano k pechati) of this issue was 10/23/1975. Publication therefore did not occur prior to this date, but must be assumed to have taken place reasonably soon thereafter.

Declassified and Approved For Release 2013/09/24 : CIA-RDP10-02196R000400060004-1

Declassified and Approved For Release 2013/09/24 : CIA-RDP10-02196R000400060004-1

ARTICLES

RESULTS OF TESTS AND OPERATION OF A MODULAR SODIUM–WATER STREAM GENERATOR

O. D. Kazachkovskii, V. F. Bai,
V. A. Borisyuk, V. I. Kondrat'ev,
A. S. Mazanov, N. N. Nechaev,
A. M. Smirnov, V. S. Sroelov (SSSR),
F. Dubshek, K. Lokhman,
V. Tomash, and I. Sobotka (ChSSR)

UDC 621.039.534.63

The modular design of steam generators with a sodium coolant is extremely promising for nuclear power stations. As a result of the structural simplicity, the dimensions of the individual steam-generator units are small. A steam generator of any power can be assembled from standard carefully checked modules. The possibilities of organizing series production of modules, easy transportation, and modular assembly are great advantages.

From the point of view of safety, hazard localization is possible in modular steam generators within the bounds of a single module of low power and also its replacement without disassembly of the entire steam generator. By comparison with frame generators, modular generator have more complexly branching sodium and steam communications; however, their weight characteristics are commensurate.

After a series of test bench trials on modules with a power of 1 MW, a modular steam generator of Czechoslovakian design was installed in the primary loop of the BOR-60 facility and was brought into operation on July 20, 1973 for verification of the thermal-hydraulic characteristics, operating efficiency, and behavior under the conditions of sodium and water interaction.

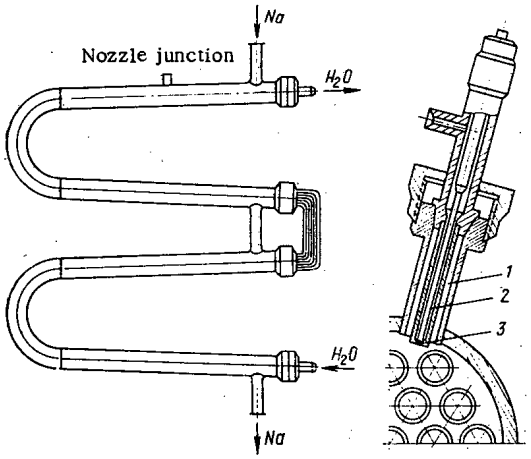

Fig. 1. Diagram of steam feed into the steam-generator intertube space: 1) nozzle junction; 2) shut-off needle valve; 3) nozzle.

Translated from Atomnaya Énergiya, Vol. 39, No. 5, pp. 315-319, November, 1975. Original article submitted November 29, 1974; revision submitted July 2, 1975.

©1976 Plenum Publishing Corporation, 227 West 17th Street, New York, N.Y. 10011. No part of this publication may be reproduced, stored in a retrieval system, or transmitted, in any form or by any means, electronic, mechanical, photocopying, microfilming, recording or otherwise, without written permission of the publisher. A copy of this article is available from the publisher for $15.00.

Declassified and Approved For Release 2013/09/24 : CIA-RDP10-02196R000400060004-1

Declassified and Approved For Release 2013/09/24 : CIA-RDP10-02196R000400060004-1

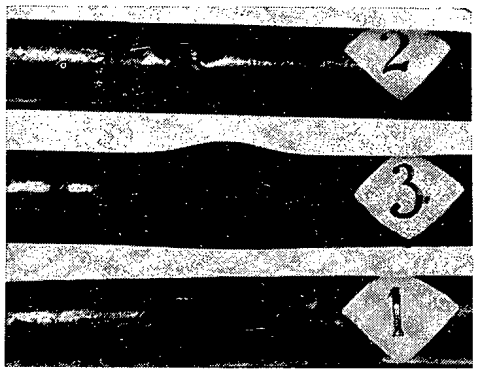

Fig. 2

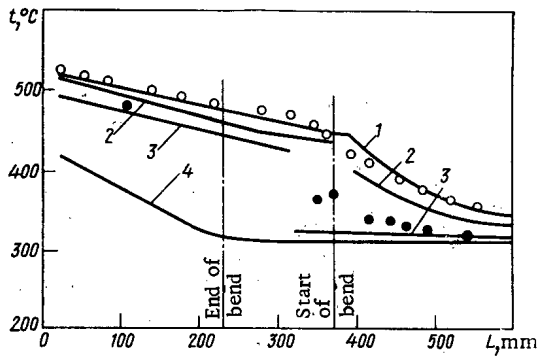

Fig. 3

Fig. 2. External view of failed steam-generature tubes.

Fig. 3. Comparison of the experimental and calculated temperature distribution along the module: 1, 2, 3, 4) Sodium temperature, outside and inside tube surface, and water surface respectively; O and ●) experimental values of sodium and water temperatures.

TABLE 1. Steady-state Operating Cycles of the Czechoslovakian Steam Generator

Parameters	Cycles							
	1	2	3	4	5	6	7	8
Power, MW	1,98	5,25	12,5	20,6	23,6	30	19,3	21,4
Sodium flow rate, m^3/h	410	415	400	410	410	525	410	410
Sodium temperature, °C								
at inlet	260	320	380	440	465	445	450	445
at outlet	245	280	280	280	280	265	300	280
Steam flow rate, tons/h	3,28	9,2	20,4	31	35	42	28,6	30
Temperature, °C								
of feed water	164	194	198	198	198	160	198	160
of superheated steam	260	320	375	435	450	430	450	435
of steam in flow splitter (ahead of separator)	240	291	295	295	295	275	340	295
Superheated steam pressure, kg/cm^2	34	78	82	82	82	82	82	82
Magnitude of blow-off, tons/h	0,75	0,9	0 95	2	2	1,1	—	1,55

Design of the Czechoslovakian Modular Steam Generator

This is a straight-through steam generator (with a power of 30 MW) with an actuating separator installed between the evaporator and the superheater. The surface of the heat exchanger is formed from eight identical parallel filaments each consisting of two evaporator modules, a superheater module, and connecting conduits with diameter 80 mm. The evaporator and superheater modules represent a heat exchanger of U-shaped design and of the "tube-inside-tube" type. The surrounding jacket of the modules is made of tubes with diameter 159 mm and wall thickness 7.1 mm. The inside bundles are formed from nine tubes: in the steam superheater the tube diameter and wall thickness are 18 and 2.5 mm of SANICRO-3 steel; in the evaporator it is 18 × 3 mm of NT8Kh6 steel. Water and steam circulate through the tubes and sodium circulates in the intertube space. The tubes of the modules are mounted in spacer grids and in double tubular panels screened on the sodium size. The double tubular panel prevents seepage of water into the sodium in the case of unsealing of the welded joints. Ths space between the tubular panels is filled with an inert gas and is connected to the leak detection system.

At the inlet to each heat-exchanger tube of the module, a washer with a 4 × 4 mm opening is installed which provides equivalence of the hydrodynamic characteristics of the evaporator tube. Moreover, at the inlet to each module of the evaporator a baffle grid is positioned containing 37 openings with diameter 3 mm for uniform distribution of the feed water through the individual tubes of the modules. The evaporator and steam superheater modules are grouped in individual mounting blocks together with the electric heating elements in a protective housing sealed with heat insulators.

Declassified and Approved For Release 2013/09/24 : CIA-RDP10-02196R000400060004-1

Declassified and Approved For Release 2013/09/24 : CIA-RDP10-02196R000400060004-1

TABLE 2. Coolant Temperature, °C

Coolant	No. of filaments of steam generator							
	1	2	3	4	5	6	7	8
Sodium at inlet to steam generator	440	440	440	440	440	440	440	440
Sodium at outlet from steam superheater:								
in the initial period	406	410	402	404	410	407	396	400
after wash-out	404	406	402	398	404	407	406	400
Sodium at outlet from second stage evaporator:								
in the initial period	310	392	328	316	356	326	321	322
after wash-out	308	316	312	310	315	316	314	315
Sodium at outlet from steam generator								
in the initial period	267	325	275	276	300	272	272	280
after wash-out	278	280	275	270	283	278	274	280
Steam ahead of separator								
in the initial period	310	392	335	316	392	333	338	342
after wash-out								
Superheated steam								
in the initial period	433	431	438	435	433	437	437	434
after wash-out	436	435	436	437	432	430	436	436

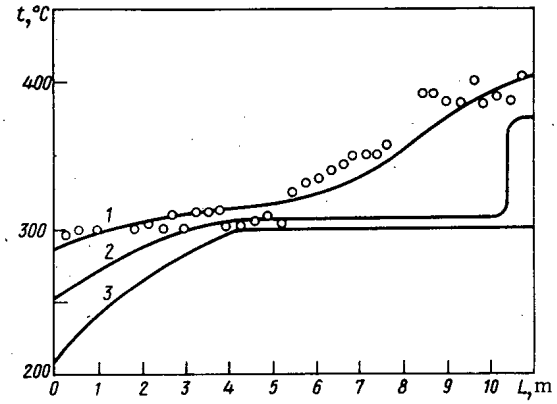

Fig. 4

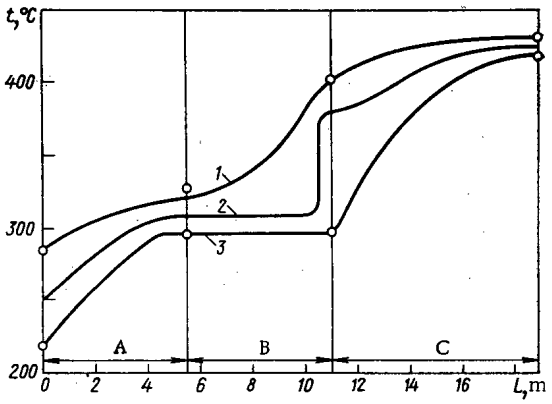

Fig. 5

Fig. 4. Temperature distribution along the length of the evaporator: 1, 2, 3) temperature of sodium, internal surface of tube, and water and steam–water mixture respectively: —) calculation; O) experimental temperatures of sodium along the length of the steam generator.

Fig. 5. Temperature distribution along the length of the steam generator: A and B) evaporators of first and second stages; C) steam superheater; other symbols as in Fig. 4.

Steam Generator Measurement System

In order to measure the parameter of the operating cycles, three systems are installed in the steam generator: emergency condition signalling, functional measurements, and experimental measurements.

NiCr–Ni thermocouples in sheaths with outside diameter of 3.2 mm were used as sensors in the experimental temperature measurement circuit. The ends of the thermocouples are insulated from the walls of the metal sheath.

The temperature was recorded with a 100-point data unit UM20-Metra Blansko. The NiCr–Ni thermocouples, with hot and cold junction temperatures of 500 and 50°C, have an emf equal to 19.52 mV. The error in the data unit for these temperatures amounts to ± 0.25°C. The permissible error of the NiCr–Ni thermocouples with reference to a standard up to 500°C is ± 7.2°C. The cold-junction temperature of the thermocouples was maintained by a ZPA-12 thermostat within the limits of 50 ± 1.5°C.

Investigations on Modular Steam Generators with a Power of 1 MW

Investigation of the Interaction of Sodium with Water. The purpose of the investigations was to study the interacting processes between sodium and water in the modules for the BOR-60, refining the monitoring

Declassified and Approved For Release 2013/09/24 : CIA-RDP10-02196R000400060004-1

Declassified and Approved For Release 2013/09/24 : CIA-RDP10-02196R000400060004-1

methods (especially in the case of small leaks), testing the emergency-system operation for the discharge of reaction products, and isolation of the steam generator with respect to water and sodium.

The experiment consisted of feeding steam taken from the outlet collector of the steam generator through a nozzle junction in the module intertube space (Fig. 1) in order to simulate leakage into one of the steam-generator tubes.

Actuation of the emergency protection and shut-down of the steam feed into the sodium were carried out by the operator after failure of one or several tubes of the bundle. The instant of burn-through of the tubes was fixed by pulsations of the sodium and water flow rates and by the increase of pressure in the degassifier as a result of the release of hydrogen.

As the experiments showed, the modular steam-generator emergency system, the operating principle of which is based on measurements of the flow-rate pulsations of the sodium by differential flow-rate meters, is efficient in operation and sufficiently rapid-acting even in the case of small leakages. In the majority of cases, over 100 sec of a steam-leakage flow rate of $6 \cdot 10^{-3}$ kg/sec into the sodium leads to considerable damage of the steam-generator tubular bundle (Fig. 2). The position of the tubes relative to the steam jet, fed from the nozzle, in this experiment is shown in Fig. 1. Failure of the tubes occurs either as a result of the corrosive action of the reacting jet (tubes 1 and 2), or as a consequence of the loss of strength characteristics of the steel as a result of an increase of temperature in the reaction zone up to ~1000°C (tube 3).

Investigation of Heat Exchange. On the test bench of the Scientific-Research Institute of Nuclear Reactors, a study was undertaken of heat exchange, heat exchange crisis of the second order, and of the temperature pulsations in modular steam generators. The thermal power of the test bench (600 kW) did not permit the nominal mass flow rates of water in the 19-tube module to be produced. Therefore, only six working tubes were left in the modules which were arranged around the periphery of the tube bundle. The remaining tubes were deadened and served as pressurizers, which permitted investigations to be carried out over a range of mass flow rates of 400-850 kg/(m^2 · sec). However, the sodium flow rate in the steam generator was lower than nominal by a factor of ~3.

In Fig. 3, the experimental temperature distribution in the steam generator is compared with that calculated on a computer by the generally accepted procedure. The agreement between the calculated and experimental temperature values was satisfactory when the values of the thermal conductivity λ of NT8Kh6 steel were 22 ± 1.6 kcal/(m · h · °C) and t = 400°C, and with the introduction of a correction for the separation of drops at the bend of the module. The limiting steam contents, obtained experimentally over a range of flow rates of $400 \leq jW \leq 800$ kg/(m^2 · sec), are higher than the values calculated by Doroshchuk's recommendations.* The maximum deviation amounts to ~0.2. The difference between the experimental and theoretical relations probably is explained by the geometry of the stream generator: the magnitude of the limiting steam content, as a result of the separation of drops from the flow at the bend, may depend on the origination point of the second-order crisis.

The experiments on the investigation of the statistical characteristics show that the temperature pulsations of the wall in the crisis zone are determined to a considerable degree by the flow-rate pulsations.

Flow-rate pulsations, which are unimportant from the operating point of view (~1%), might lead to temperature pulsations with double amplitude of up to 30°C.

Start-Up and Steady-State Cycles of a Steam Generator with a Power of 30 MW

In the first stage of the investigations, the BOR-60 facility operated with the Czechoslovakian steam generator connected into the first loop of the second circuit, and with an air heat exchanger subconnected to the second loop. Start-up of the steam generator was carried out in the steam cycle without preliminary filling with water of the steam–water circuit.

First of all, the nominal sodium flat rate of ~400 m^3/h was established. Feed water in the evaporator was supplied simultaneously with rise of power of the reactor at the same rating (300-500 liters/h) that superheated steam came from the evaporator outlet. The steam-generator pressure was adjusted at first by the discharge of steam through the steam conduits' blow-off lines and then (above 10-12 atm) by means

*V. E. Doroshchuk, Heat Exchange Crisis as a result of the Boiling of Water in the Tubes [in Russian], Énergiya, Moscow (1970).

Declassified and Approved For Release 2013/09/24 : CIA-RDP10-02196R000400060004-1

Declassified and Approved For Release 2013/09/24 : CIA-RDP10-02196R000400060004-1

of automatic channels of the reducing-cooling installations. The feed-water supply was increased until the appearance of a stable level in the separator.

With further increase of steam-generator output, the supply of feed-water was regulated according to the level in the separator. The rate of heating-up of the installations was maintained during startup within the limits of 60-70°C/h. In every steady-state cycle, the parameters of which are shown in Table 1, the modular steam generator operated for a long time, which permitted a conclusion to be drawn concerning its stable operation over a wide range of loads.

In the initial period of operation, a deviation of the temperature from nominal (up to ~30%) was observed in two filaments (out of eight) due to the different hydraulic characteristics of the evaporator module on the water side (from analysis of the thermal balances of the steam superheater filaments, it follows that the sodium flow rates through the filaments are almost identical). One of the probable causes of the deviation might be clogging of the evaporator baffle devices. In order to eliminate this, the steam generator was washed out with a reverse flow of feed water and operated for 1 day in a cycle with reduced feed-water pressure (see Table 1, cycle 6).

The results of measurement of the sodium and steam temperatures in the modular steam-generator filaments for cycle 4 (see Table 1) in the initial period of operation and after washing out are shown in Table 2. It follows from Table 2 that as a result of the wash-out the temperature values over all the filaments were levelled. The difference in the temperature values of the sodium at the outlet from the filaments of the steam generator is found to be within the limits of error of the measuring instruments. It should be noted that the readings of the steam temperature sensors before the separator, considerably exceed the saturation temperature. This is a consequence of the imperfection of the measurement system. The fact is that the thermocouples, with the sheath insulated from the walls by a regulus, are in a gaseous medium with a temperature which exceeds the saturation temperature.

Calculations of the temperature distribution over the length of the heat removal surface were carried out for obtaining the parameters at which the steam generator operated for a longer time. The calculated and experimental values of the distribution in the modular steam generator (Fig. 4) refer to the average values of the parameters of all eight modules, and there is a satisfactory agreement between the experimental and calculated values of the sodium temperature. The somewhat lower experimental values of the temperatures in the first module of the evaporator and the larger values in the second module can be explained by the fact that the thermocouples of the first module were located in a gaseous medium with a lower temperature, and the thermocouples of the second module were in a medium with a higher temperature.

Figure 5 shows the calculated curve of the temperature measurement along the length of the steam generator. According to the calculations, the magnitude of the temperature jump at the inside surface of the tube in the zone of transition to worsened heat exchange amounts to 75°C.

This is somewhat dangerous and indicates further work on the steam generator and its subsequent investigation is needed.

Emergency Conditions

During operation of the facility with an air heat exchanger and with the modular steam generator, when the shielding is actuated the sodium circulating pumps of the loops are cut-out. With a delay of 30-60 sec, the feed pump is cut-out, after which the steam generator is disconnected from the loop by means of a slide valve. Some time (~10 min) before total reduction of the pressure in the steam generator, purging from the separator is opened.

The measurements showed that in all the elements of the steam generator, the rate of change of temperature during an emergency shutdown is insignificant, and there are no large temperature changes. This shows that conformity is necessary between power reductions and reduction of the coolant flow rates in the facility. Further cooling of the steam generator is ensured by forced circulation of the sodium through the circuit.

Thus, the first stage of operation showed that the modular steam generator of Czechoslovakian design functions stably in the separator cycle at a power of 5-30 MW. Operation does not cause difficulties in the case of manual and automatic control of the feed-water supply. In the case of decompression of the tube, systematic (chain) failure of the tube bundle takes place as a result of the corrosion–erosion action of

Declassified and Approved For Release 2013/09/24 : CIA-RDP10-02196R000400060004-1

Declassified and Approved For Release 2013/09/24 : CIA-RDP10-02196R000400060004-1

the reacting jet and also loss of the strength characteristics of the tube wall material as a result of increase of temperature in the reaction zone. For modular steam generators, differential-magnetic flowmeters could be used as reliable sensors for recording the flow.

Declassified and Approved For Release 2013/09/24 : CIA-RDP10-02196R000400060004-1

Declassified and Approved For Release 2013/09/24 : CIA-RDP10-02196R000400060004-1

HYDRAULICS OF THE ACTIVE ZONE OF THE VVR-M REACTOR

G. A. Kirsanov, K. A. Konoplev, R. G. Pikulik, and Zh. A. Shishkina

UDC 621.039.53

The active zone of the VVR-M reactor [1, 2] has the cross-sectional shape of a hexagon with an inscribed-circle diameter of 540 mm and a height of 500 mm; it is sited in an aluminum tank under a 3.5-m-thick layer of water (Fig. 1). The pressure drop in the active zone is limited by this level of water. The fuel-element assembly of the VVR-M reactor (Fig. 2) consists of three coaxial tubular fuel elements, the outer tube having a hexagonal form. The tubes are bonded into the fuel-element assembly by mechanical fixing methods. Water runs from top to bottom in the gaps formed by the fuel-element tubes. For convenience of recharging the active zone, the fuel-element assemblies are connected into technological sections of three assemblies each. Each fuel-element assembly has a support by means of which the lower part is fixed into the supporting lattice of the reactor. Above the support lattice is a guide lattice facilitating the placement of the assemblies in the corresponding sockets of the support lattice (Fig. 3). In their upper regions the assemblies come into contact with head bands which specify the gaps between the fuel elements of neighboring assemblies.

The active zone of the reactor is surrounded by a metallic beryllium reflector containing apertures for nine horizontal and 11 vertical channels. The whole reflector is also penetrated by vertical apertures 6 mm in diameter for the passage of the cooling water. The loading of the active zone of the reactor varies over a wide range depending on the number and shape of the experimental devices lying within the zone. Various devices (water cavities, radiation filters, ampoules, channels, beryllium displacers, etc.) are inserted into the active zone in place of extracted fuel-element assemblies. For purposes of fixing in the support lattice, the experimental devices and displacers are furnished with supporting pieces matching the configuration of those in the fuel-element assemblies. The main problem of our present investigation was that of measuring the hydraulic characteristics of individual elements in the active zone of the VVR-M reactor in order to determine possible power reserves and obtain the data needed for thermal and hydraulic calculations.

Measurement of the Water Flow Not Taking Part in Cooling the Fuel Elements and the Hydraulic Resistances of Various Elements of the Active Zone. The flow of water not taking part in cooling the fuel elements is made up of leakages through the apertures in the beryllium reflector, through the gaps between the reactor channels and the reflector, and though the gaps between the reactor vessel and the reflector. In order to measure this flow rate the active zone of the reactor was entirely unloaded and its contents replaced on the reactor lattice by a blank plug, such that the gap along the perimeter of the plug between the walls and the reflector was equal to the gap between the reflector and the fuel elements. We measured the water flow in the first circuit of the reactor as a function of the pressure loss in the reflector (Fig. 4, curve 1). The water flow so measured includes not only that passing through the reflector but also that passing through the gap between the plug and reflector along the plug perimeter. Allowance for the latter was facilitated by the fact that the water velocity in this gap was equal to the water velocity in the channels of the fuel element assemblies, owing to the fact that their hydraulic diameters were equal. In order to measure the dependence of the water velocity in the assembly channels on the pressure loss, the active zone was first charged with the fuel elements and experimental devices. After this we measured the pressure loss in the active zone for various water flow rates in the first reactor circuit (Fig. 4, curve 2). The mean water velocity in the assembly channels was determined from the difference between the flow rates

Translated from Atomnaya Énergiya, Vol. 39, No. 5, pp. 320-323, November, 1975. Original article submitted November 6, 1974; revision submitted June 2, 1975.

©1976 Plenum Publishing Corporation, 227 West 17th Street, New York, N.Y. 10011. No part of this publication may be reproduced, stored in a retrieval system, or transmitted, in any form or by any means, electronic, mechanical, photocopying, microfilming, recording or otherwise, without written permission of the publisher. A copy of this article is available from the publisher for $15.00.

Declassified and Approved For Release 2013/09/24 : CIA-RDP10-02196R000400060004-1

Declassified and Approved For Release 2013/09/24 : CIA-RDP10-02196R000400060004-1

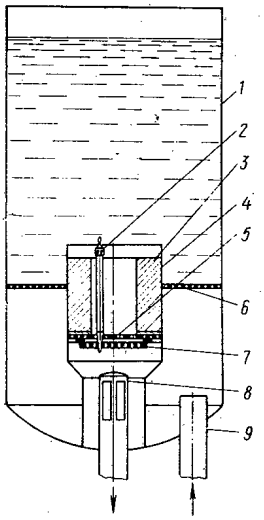

Fig. 1

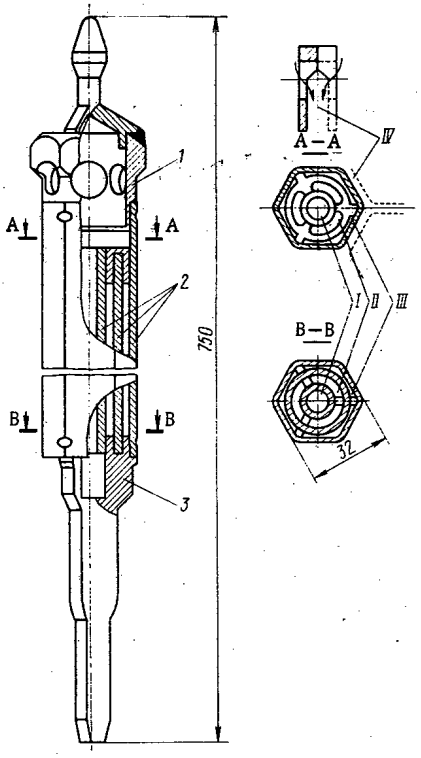

Fig. 2

Fig. 1. Arrangement of the active zone: 1) tank; 2) fuel-element assembly; 3) beryllium reflector; 4) reactor vessel; 5, 6, 7) guide, guard, and support lattices; 8, 9) suction and pressure-head pipes.

Fig. 2. Fuel-element assemblies of the reactor: 1) head; 2) fuel elements; 3) support; I-IV) numbers of assembly channels.

TABLE 1. Distribution of the Hydraulic Resistance of the Active Zone with Respect to Its Elements

Type of active-zone charging	Hydraulic resistance of active zone	Resistance proportion, %		
		of inlet and outlet	of friction in assembly channels	of lattices
Complete	5,5	41	39	20
Working	5,0	44	43	13

when the active zone was charged with fuel elements and when these were replaced by the plug, maintaining the same pressure losses and open cross section of the active zone.

The relationship between the mean water velocity in the assembly channels and the pressure loss in the active zone (Fig. 5) enables us to allow for the flow of water in the gap between the plug and reflector, and to determine how the flow of water through the reflector of the reactor depends on the pressure loss in the active zone (Fig. 4, curve 3). The water flow not taking part in cooling the fuel elements is no greater than $12 \pm 1\%$ of the flow in the first circuit of the reactor over the whole range of possible flow rates.

Hydraulic Resistances of the Active-Zone Elements in the VVR-M Reactor. These were measured in a special test bed constituting a reduced hydraulic model of the reactor with a vessel holding 37 fuel-element assemblies.

Declassified and Approved For Release 2013/09/24 : CIA-RDP10-02196R000400060004-1

Declassified and Approved For Release 2013/09/24 : CIA-RDP10-02196R000400060004-1

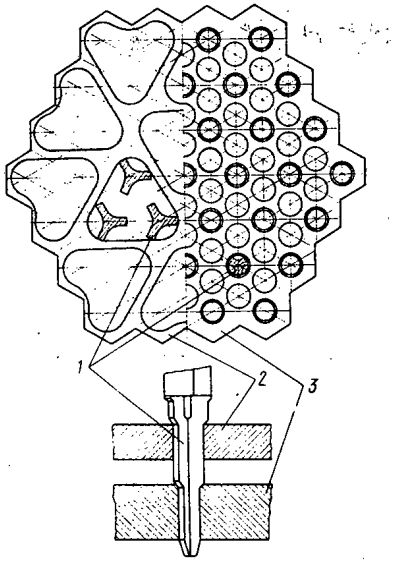

Fig. 3

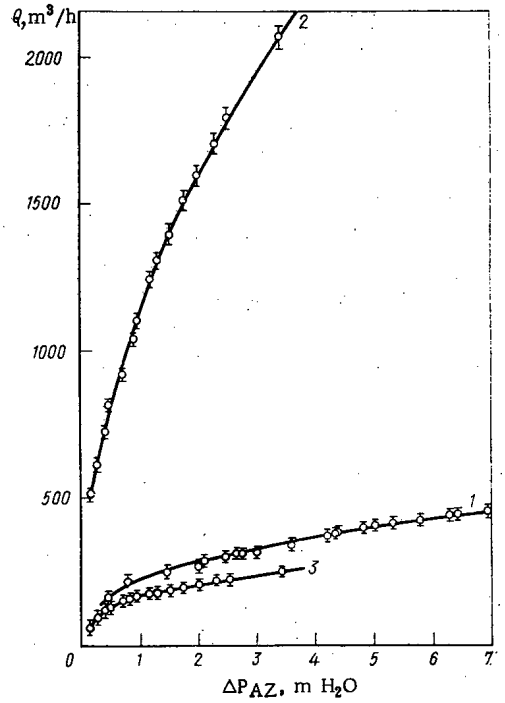

Fig. 4

Fig. 3. Shape of the lattices and arrangement of the supports carrying fuel-element assemblies in the reactor lattices: 1) fuel-element assembly support; 2, 3) guide and support lattices of the reactor.

Fig. 4. Water flow in the first circuit of the reactor and water flow passing through the reflector as functions of the pressure drop in the active zone.

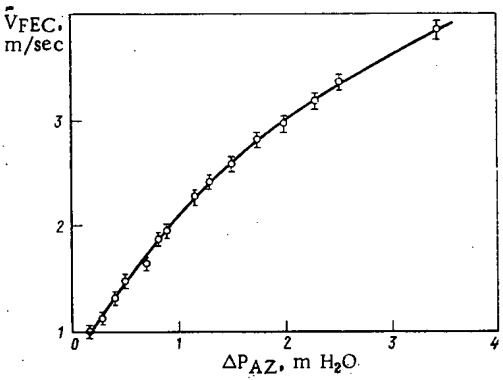

Fig. 5. Mean water velocity in the fuel-element assembly channels as a function of the pressure drop in the active zone.

The hydraulic resistance was calculated from the equation

$$\xi = \frac{2\Delta P}{\rho V^2}, \qquad (1)$$

where ΔP is the pressure loss; V, ρ are the velocity and density of the water.

Measurements of the hydraulic resistances of the guide and support lattices (together with the fuel-element assembly supports) relative to the velocity of the incident flow showed that $\xi_{l\,0} = 3.4 \pm 0.1$. The resistance of the two lattices without the supports of the fuel-element assemblies $\xi_l = 2.4 \pm 0.1$. (Here and subsequently we give the mean-square errors of the results of the measurements).

If the active zone of the reactor is fully charged with fuel elements, its hydraulic resistance (including the fuel-element assembly channels and the support and guide lattices), referred to as the average water velocity in the channels of the fuel-elements assemblies, is $(\xi_{AZ})\bar{V}_{FEC} = 5.5 \pm 0.1$ in the velocity range 1.8-3.0 m/sec; the hydraulic resistance of the lattices referred to the water velocity in the channels of the fuel-element assembly in the same velocity range is $(\xi_{l\,0})V_{FEC} = 1.10 \pm 0.04$.

The hydraulic resistance of the fuel-element assemblies referred to as the average water velocity in the channels equals

$$\bar{\xi}_{FEC} = \bar{\xi}_{in} + \bar{\xi}_{out} + \xi_{fr}\, l/d = 4.35 \pm 014$$

represents the sum of the average local resistances (inlet and outlet) and the product of the frictional resistance and the relative length of the channel.

Declassified and Approved For Release 2013/09/24 : CIA-RDP10-02196R000400060004-1

Declassified and Approved For Release 2013/09/24 : CIA-RDP10-02196R000400060004-1

It should be noted that the assembly channels differ from one another as regards cross-sectional geometry at the inlet and outlet, owing to the presence of the spacers, and so have differing hydraulic resistances. The hydraulic resistances indicated are the average values for an active zone consisting of many fuel-element assemblies, which in the present case is considered as a single construction.

In order to determine the proportion of frictional resistance in the total hydraulic resistance of the active zone, we measured the frictional resistances of various assembly channels over the velocity range 1-5 m/sec. The measurements were carried out in the inner tube of the fuel-element assembly, in the gap between the two circular tubes, and also in the gap between the circular and hexagonal tubes, by reference to the pressure drop in a section of channel 200 mm long lying at over 40 hydraulic diameters from the inlet, for a fixed water velocity in the channel. In all cases there was a systematic discrepancy between the experimental values of the frictional resistance and those calculated from the Nikuradze formula

$$\xi_{fr} = 0.00332 + 0.221\,\mathrm{Re}^{-0.237}. \tag{2}$$

The experimental values are approximately 10% lower than the calculated. The frictional pressure losses in the assembly channels average 49% of the pressure losses in the fuel element assembly. The proportion of the local resistances (inlet and outlet) in the hydraulic resistance of the fuel-element assemblies is very considerable and on average amounts to 51%.

Calculation of the Hydraulic Resistance of the Active Zone in the VVR-M Reactor for the Case of Arbitrary Charging with Fuel Elements and Experimental Devices. The devices inserted into the active zone (together with the fuel elements) usually reduce the open cross section of the active zone and the contribution of the hydraulic resistances of the lattices in the total hydraulic resistance of the active zone; this is due to the fact that some of the experimental devices (for example, the water cavities) have fewer supporting stems than the number of active-zone cells which they occupy.

Thus, the hydraulic resistance of the lattices has different values according to the charging of the active zone. If we assume that the pressure losses in the parts of the lattice with or without assembly supports are equal, we may derive the following equation for the mean hydraulic resistance of the lattices, referred to the water velocity in the assembly channels, for any degree of charging of the active zone with fuel elements and experimental devices

$$(\bar{\xi}_l)_{V_{FEC}} = \frac{1}{\left[\left(1-\frac{m}{n}\right)\frac{1}{\sqrt{\xi_{l0}}}+\frac{m}{n}\frac{1}{\sqrt{\xi_l}}\right]^2}\,(S/nS_c)^2, \tag{3}$$

where n is the number of cells in the active zone of the reactor, S_c is the area of a cell, m is the number of cells occupied by experimental devices without supports, S is the open cross section of the active zone for the specified charging of the latter with fuel elements and experimental devices.

The average hydraulic resistance of the active zone equals

$$\bar{\xi}_{AZ} = \bar{\xi}_{FEC} + (\bar{\xi}_l)_{V_{FEC}}. \tag{4}$$

The average water velocity in the fuel-element assembly channels for known pressure losses in the active zone may be calculated thus:

$$\bar{V}_{FEC} = \sqrt{\frac{2\Delta P_{AZ}}{\bar{\xi}_{AZ}\rho}}. \tag{5}$$

The error in the value of $\bar{V}_{FEC}$ derived from Eq. (5) is determined by the errors in the original quantities ($\bar{\xi}_{FEC}$, $\xi_{l\,0}$ and ξ_l) and is no greater than 3%. The values of $\bar{V}_{FEC}$ calculated for the same charging of the active zone as that at which the pressure-loss dependence of the water velocity in the assembly channels was measured differ from the experimental values by 4.5%. This should be regarded as good agreement, since the mean-square error of the velocity measurement was 2.5%. Thus, the proposed method provides the necessary accuracy for determining the mean water velocity in the channels of the fuel-element assemblies in thermal reactor calculations.

When the active zone is completely filled with fuel elements, or when the zone is occupied to the same extent as that for which the water velocity in the assembly channels was measured, the contributions

Declassified and Approved For Release 2013/09/24 : CIA-RDP10-02196R000400060004-1

Declassified and Approved For Release 2013/09/24 : CIA-RDP10-02196R000400060004-1

of the various elements of the active zone to its hydraulic resistance calculated by means of Eqs. (3) and (4) are as in Table 1.

Hydraulic Characteristics of the Fuel-Element Assembly Channels of the VVR-M Reactor. The set of fuel elements in the VVR-M reactor is made up of four types of channels of the same hydraulic diameter, which differ considerably as regards the reduced value of the open cross section at the channel inlet and outlet due to the presence of spacers (Fig. 2). Thus, each channel has its own value of hydraulic resistance. For parallel operation of the channels in the active zone, each will therefore have its own water velocity, differing from the mean velocity determined from the average hydraulic characteristics of the active zone considered as a single structure. The necessity of studying the hydraulic characteristics of the individual channels is obvious, since the maximum permissible power of the VVR-M reactor is determined by the characteristics of the hydraulically least favorable channel.

The fuel-element assembly model was furnished with shock tubes for measuring the pressure loss in each channel over a section 200 mm long, lying at over 40 hydraulic diameters from the inlet section. The measurements were made in a hydraulic test-bed. From the measured pressure losses and Eq. (2) we calculated the water velocity in each channel and its ratio with respect to the average velocity determined from the known values of the water flow and the open cross section of the group of thirty-seven fuel-element assemblies in the hydraulic test-bed: $K_i = V_i/\overline{V}_{FEC}$. The arithmetic mean values of K_i for channels I-IV were respectively 1.18 ± 0.05; 0.89 ± 0.04; 1.05 ± 0.05; 0.86 ± 0.05.

If we approximate the experimental measurements by a curve passing 10% below that of Eq. (2), the K_i values for this case will exceed those quoted by 5.5%.

As we should expect, the best channel in the set of fuel-element assemblies is the channel of the inner tube I; the inlet and outlet sections of this tube have no spacers. The worst is channel IV, formed by hexagonal tubes.

The measured relationships (ratios) enable us to determine the local resistances for each channel. By equating the pressure losses in each channel to those in the whole set we have

$$(\xi_{in\,i} + \xi_{out\,i} + \xi_{fr}\, l/d)\,\frac{\rho\,(K_i \overline{V}_{FEC})^2}{2} = \overline{\xi}_{FEC}\frac{\rho \overline{V}^2_{FEC}}{2}; \qquad (6)$$

here $\xi_{in\,i}$ and $\xi_{out\,i}$ are the local resistances of the i-th channel. The sum of these for channels I-IV respectively equals 0.81 ± 0.18; 3.19 ± 0.22; 1.61 ± 0.22; 3.49 ± 0.35.

The foregoing results are sufficient for estimating the power reserves of the VVR-M reactor, and also for refining thermal calculations of the active zone.

The authors wish to thank B. S. Razov, V. M. Sokolov, A. N. Gubinskii, and A. N. Syasin, who took part in the construction of the hydraulic test-bed and in the corresponding measurements.

LITERATURE CITED

1. V. V. Goncharov, 2nd Geneva Conference, Paper No. 2185.
2. D. M. Kaminker and K. A. Konoplev, 3rd Geneva Conference (1964), Paper No. 23/R-325.

Declassified and Approved For Release 2013/09/24 : CIA-RDP10-02196R000400060004-1

Declassified and Approved For Release 2013/09/24 : CIA-RDP10-02196R000400060004-1

ANALOG SIMULATION OF THE SPATIAL KINETICS OF A REACTOR

B. N. Seliverstov, N. P. Rudov, F. F. Voskresenskii, P. A. Gavrilov, and A. M. Fomin

UDC 621.039.512

The exact solution of the transient neutron-diffusion differential equations for a simple (but not point-type) reactor model involves serious computing difficulties. Various approximations are accordingly required for the solution of such problems. The most convenient procedure is the so-called cell method of solving spatially dependent kinetic equations by analog computing techniques.

The cell method allows us to divide the reactor into zones or cells and to derive a system of transient equations including the mean neutron fluxes or the strength of each cell. The spatial part of the problem lies in determining the parameters on which the cross flow of neutrons from one cell to another depends. When the cells are small the analysis may be regarded as a finite-difference method.

By comparison with digital computation, the analog method of solving the problem on the foregoing approximation enables the various calculations relating to reactor kinetics to be carried out in a more operative manner for cases of complex geometry and arbitrarily specified boundary conditions; the dynamic characteristics of the energy-evolution fields may furthermore be studied under conditions corresponding to real practical methods of apparatus regulation.

Several papers have recently been published in regard to the construction of space–time reactor models [1-5], but the question of computing methods and the actual manufacture of the models has not been discussed in sufficient detail.

In this paper we shall consider methods of choosing a discrete mathematical model for spatially dependent reactor kinetics and certain special aspects relating to the adjustment of the model.

For simplicity of discussion we shall consider the diffusion equations in the single-group modified approximation, with one group of delayed neutrons, written in variational form:

$$M^2\nabla^2\delta\Phi+(K_{\infty_0}-1-\beta K_{\infty_0})\,\delta\Phi+(1-\beta)\;\times\Delta K_\infty\Phi+(1-\beta)\,\Delta K_\infty\delta\Phi+\lambda\delta C=l\frac{\partial\delta\Phi}{\partial\tau}\,; \tag{1}$$

$$\frac{\beta}{l}(K_{\infty_0}\delta\Phi+\Delta K_\infty\Phi_0+\Delta K_\infty\delta\Phi)-\lambda\delta C=\frac{\partial\delta C}{\partial\tau}\,, \tag{2}$$

where $\delta\Phi$, δC are the relative changes in the neutron flux and the delayed-neutron source concentration respectively (the index "0" refers to the steady-state values, the rest of the notation is as generally accepted).

In view of the very slight influence of the delayed neutrons on the neutron diffusion the term $\beta\Delta K_\infty\delta\Phi$ in Eqs. (1) and (2) may be neglected. If the width of the perturbation spectrum is no greater than β/l we may put $\partial\,\delta\Phi/\partial\tau=0$ in Eq. (1), which also simplifies the system of equations.

Solving Eqs. (1) and (2) after applying a Laplace transformation in $\delta\Phi$ to this system and assuming that $1-[\beta S/(S+\lambda)]\approx 1$, we obtain

$$M^2\nabla^2\delta\Phi+\delta\Phi\left(K_{\infty_0}-1-\frac{\beta K_\infty S}{S+\lambda}\right)+\Delta K_\infty\Phi_0+\Delta K_\infty\delta\Phi=0. \tag{3}$$

Translated from Atomnaya Énergiya, Vol. 39, No. 5, pp. 324-328, November, 1975. Original article submitted December 13, 1974.

©1976 Plenum Publishing Corporation, 227 West 17th Street, New York, N.Y. 10011. No part of this publication may be reproduced, stored in a retrieval system, or transmitted, in any form or by any means, electronic, mechanical, photocopying, microfilming, recording or otherwise, without written permission of the publisher. A copy of this article is available from the publisher for $15.00.

Declassified and Approved For Release 2013/09/24 : CIA-RDP10-02196R000400060004-1

Declassified and Approved For Release 2013/09/24 : CIA-RDP10-02196R000400060004-1

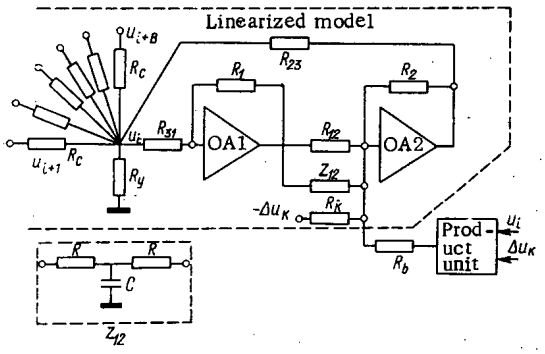

Fig. 1

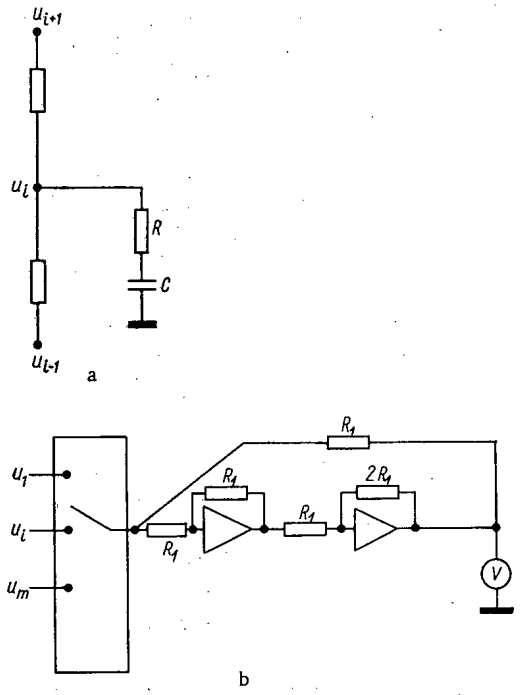

Fig. 2

Fig. 1. Apparatus representing the dynamic equation for a unit cell of the network model.

Fig. 2. Basic electrical circuit of one cell in the model (a), and circuit for measuring the potentials in the cells of the model for the plateau zone (b).

In order to simulate the diffusion of neutrons on the analog principle, we may use the distribution of electric current through a set of ohmic resistances connected into a chain or a two-(or more) dimensional network. If the network is made in an ordered manner, the Kirchhoff Equations describing the processes taking place in this network should coincide with the finite-difference approximations of the diffusion differential equation in the same coordinate system. This approximation is based on the use of a Taylor series.

Neglecting terms on the order of the square of the mesh length in the expansion we obtain the difference form of the Laplacian for an orthogonal lattice

$$\Delta\Phi = \Phi''_{xx} + \Phi''_{yy} \approx \frac{\Phi_1 - 2\Phi_0 + \Phi_3}{h_x^2} + \frac{\Phi_2 - 2\Phi_0 + \Phi_4}{h_y^2}$$

with a uniform step (mesh $h_x = hy$). The division of the region into rectangles is not the only one possible. The region may also be divided up into a system of regular hexagons or triangles. For a network comprising hexagons we may use the Taylor series to express the flux functions at three peripheral points in terms of the values of the function and its derivatives at the central nodal point. Rejecting terms of the order of h, we obtain

$$\Delta\Phi = \frac{4}{3}\,\frac{\Phi_1 + \Phi_2 + \Phi_3 - 3\Phi_0}{h^2}.$$

A greater accuracy is provided by a network formed of regular triangles, which has an error of the order of h^4

$$\Delta\varphi = \frac{2}{3}\,\frac{\Phi_1 + \Phi_2 + \Phi_3 + \Phi_4 + \Phi_5 + \Phi_6 - 6\Phi_0}{h^2}.$$

Thus, for networks with equal steps the foregoing difference functions give an error of the order of h^{n-2}, where n is the number of rays converging at a nodal point.

From the condition of similarity between the physical equation and the equation governing the currents at the i-th node of the model (based on the Kirchhoff law), the analog of Eq. (3) takes the following

Declassified and Approved For Release 2013/09/24 : CIA-RDP10-02196R000400060004-1

Declassified and Approved For Release 2013/09/24 : CIA-RDP10-02196R000400060004-1

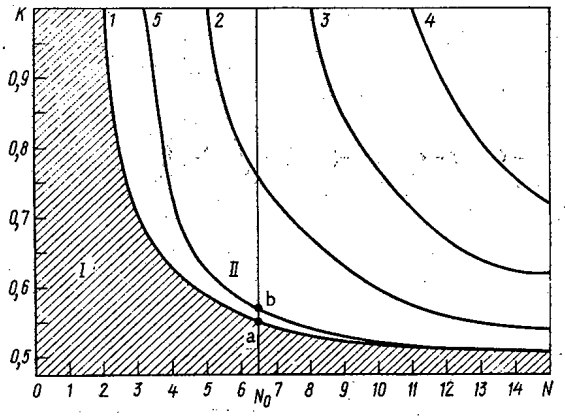

Fig. 3. Dependence of the roots of the characteristic equation on the number of subdivisions N: 1) λ_1 (N); 2) λ_2 (N); 3) λ_3 (N); 4) λ_4 (N); 5) dependence of K^*_1 on the number of subdivisions N; I) and II) subcritical and supercritical regions.

form (the apparatus representing the dynamic equation for a unit cell of the network model is illustrated in Fig. 1):

$$\frac{R^*}{R_c}\nabla^2\bar{u}_i-\frac{\bar{u}_iR^*}{R_y}+\frac{\bar{u}_iR_2R^*}{R_{12}R_{23}}+\frac{\bar{u}_iR_2R^*}{R_{23}Z_{12}}-\frac{\bar{u}_iR^*}{R_{23}}-\frac{\bar{u}_iR^*}{R_{31}}+\frac{R_2R^*}{R_kR_{23}}\Delta\bar{u}_k+\frac{\bar{u}_iR_2R^*}{R_bR_{23}}\cdot\frac{\Delta\bar{u}_k}{100}=0;$$

where $\nabla^2\bar{u}_i=\left(\sum_{k=1}^{n}\bar{u}_{i+k}+n\bar{u}_i\right)\alpha$; $\bar{u}_i=\frac{u_i}{u^*}$; $\Delta\bar{u}_k=\mu_k\Delta K_\infty$; μ_k is a scale factor. The parameters of the circuit elements in the model are determined from the following equations:

$$R_k=\alpha\frac{R^*R_2}{\Delta K_{\infty\max}R_{23}}\cdot\frac{M^{2*}}{h^2};\quad R_c=\frac{R^*M^{2*}}{M^2};$$

$$R_y=\alpha\frac{M^{2*}R^*R_{31}}{h^2R_{31}-2M^{2*}R^*};\quad R_{23}=\alpha\frac{R^*(R_2-R_{12})M^{2*}}{h^2(1-\beta)K_{\infty_{0i}}R_{12}};$$

$$R=\frac{R_2R_{12}}{\beta(R_2-R_{12})2};\quad C=\frac{4\beta(R_2-R_{12})}{\lambda R_2R_{12}};$$

$$R_b=\alpha\frac{R_2R^*M^{2*}}{R_{23}\Delta K_{\infty\max}h^2};\quad Z_{12}=\frac{(S+\lambda)R_2R_{12}}{\lambda\beta(R_2-R_{12})}.$$

The values of the parameter α selected in relation to the geometry of the unit cell are determined as follows: one-dimensional model – 1; two-dimensional model – 1, 4/3, and 2/3 for rectangular, triangular, and hexagonal networks respectively. The physical value of the neutron flux is expressed in terms of voltage by the equation

$$\Phi_i=u_i\frac{\Phi^*}{u^*},$$

where $u^*=100(R_{12}/R_2)$; Φ^* is the maximum value of the flux expected in the calculation, * symbolizes the normalized factor.

The quantities R^*, M^{2*}, R_{31}, R_2 and R_{12} in the equations may to a certain extent be selected arbitrarily and subject to the following considerations. Firstly, the resistance R_2 should be greater than R_{12}, i.e., the transmission factor of the second dc amplifier should be greater than unity. This requirement arises from the equation for R_{23}, since R_2-R_{12} should be greater than zero. It is desirable that the coefficient of the second amplifier should be no greater than 2-3, since any increase in the sensitivity of the network greatly complicates its adjustment. Secondly, the sum of the resistances $R_{23}+R_y$ should be no less than the permissible load for the amplifiers used in the network. Thirdly, the resistance R_{31} should preferably be made an order of magnitude larger than the network resistances R_c (c = cell), so as to eliminate its influence on the current cross-flows.

Declassified and Approved For Release 2013/09/24 : CIA-RDP10-02196R000400060004-1

Declassified and Approved For Release 2013/09/24 : CIA-RDP10-02196R000400060004-1

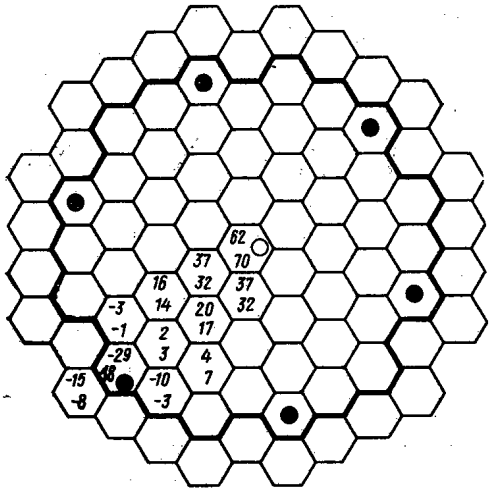

Fig. 4. Perturbed energy-evolution distributions obtained from a physical calculation and from an analog spatial model of the reactor (upper and lower figures respectively) in % of the specific initial value: ○) perturbation introduced; ●) compensation of the perturbation; ——,) line separating the plateau and peripheral zones.

It should be noted that in general multiplication devices are required in those cells of the model in which, for some reason or other, K_∞ changes. For small deviations of the neutron flux (10-20%) multiplying devices are not needed for those points at which changes occur in K_∞.

Simulation of the spatially dependent kinetic characteristics in the plateau region (zone of equalized neutron flux) enables us to economize with respect to a certain number of operational amplifiers. The original equations for simulating the cells in the plateau region in the absence of perturbation are obtained from Eq. (3) on the assumption that $\Delta K_\infty = 0$, $K_{\infty_0} = 1$. This greatly simplifies the realization of the structural cell. Figure 2a shows the basic electrical circuit for such a cell, the parameters being found from the equations

$$\frac{1}{CR} = \lambda; \quad \frac{h^2}{M^2}\frac{1}{R_c} = \frac{1}{R\beta}.$$

The potentials in the cells of the plateau zone may be measured by means of the circuit illustrated in Fig. 2b. The electrical circuits of the unit cells in the peripheral zone and those of the plateau cells in which a perturbation ΔK_∞ is introduced are analogous to the circuit of Fig. 1.

In order to obtain valid quantitative results in the cell model, it is extremely important to adjust the reactor model to the "critical" state. Let us consider this question in more detail.

It is well known [1] that the transmission function for passing from point to point in the cellular model under consideration has the following form for a cell of arbitrary geometry

$$W(S) = \frac{\left(\frac{1}{\lambda}S + 1\right)K_1}{T\frac{1}{\lambda}S^2 + \left(T + \frac{1}{\lambda^*}\right)S + 1},$$

where $T = \frac{lK_1}{N^2}\xi$; $\frac{1}{\lambda^*} = \frac{1}{\lambda}\left(1 + \frac{K_{\infty_0}\beta K_1}{N^2}\xi\right)$; $\xi = \left(\frac{Z}{M}\right)^2$. Here Z is the equivalent diameter of the active zone of the reactor, in which K_1 is defined as

$$K_1 = \frac{1}{n - h^2\frac{K_\infty - 1}{M^2}\frac{1}{\alpha}}. \qquad (4)$$

Declassified and Approved For Release 2013/09/24 : CIA-RDP10-02196R000400060004-1

Declassified and Approved For Release 2013/09/24 : CIA-RDP10-02196R000400060004-1

The number n is determined by the form of the network of step h; it depends on the geometry chosen for the unit cell, and equals the number of rays of the network converging to the nodal point.

The expression for K_1 is formally valid for a homogeneous reactor with an infinitely large number of subdivisions, i.e., $h \to 0$.

For a finite number of subdivisions the reactor model represented by a set of transmission functions W(S), in which K_1 is calculated from Eq. (4), does not correspond to the critical state. Figure 3 shows the way in which K_1 depends on the number of subdivisions of the active zone in a one-dimensional critical reactor. For such a reactor without any reflector we have the equation

$$\frac{K_{\infty_0}}{M^2} = \frac{\pi^2}{Z^2}.$$

Substituting this expression into Eq. (4) we obtain $K^*(N) = 1/[2-(\pi^2/N^2)]$ where N is the number of subdivisions of the active zone. The curve $K_1(N)$ corresponds to the minimum roots $\lambda_1(N)$ of the characteristic equation for $S = 0$, expressed in relation to the number of subdivisions.

We see from Fig. 3 that the curves $K_1^*(N)$ and $K_1(N)$ intersect asymptotically as $N \to \infty$, i.e., the physical properties of the discrete critical will only correspond strictly to those specified when $N \to \infty$. In other words, if the critical reactor is represented by a discrete model with a finite number of subdivisions N_0 and specified values of $K_{\infty 0}$ and M^2, according to the arrangement envisaged the "model" reactor will be in a "supercritical" state.

If we ensure a "critical" state of the discrete model by moving from point b to point a (Fig. 3), the physical parameters of the discrete system will deviate from the specified values by a certain finite amount (or error), and this error will be the smaller, the greater the value of N_0. This illustration of the one-dimensional version reflects the principal characteristic of the analog method of solution involving a coarse-step representation of the active zone of the reactor; it requires special accuracy in calculating the transmission factors of the elementary (unit) cells of the network.

Thus, for any finite subdivision of the active zone of the reactor the discrete model will be in a "supercritical" state if the model is adjusted on the basis of the values of K_∞ obtained from the physical calculation of the critical reactor. If the values of K_1 are not defined as the roots of an N-th-order characteristic equation, where N is the number of unit cells in the active zone, which is an extremely complicated matter for two-dimensional geometry, the adjustment of such a cellular model will present appreciable difficulties. For the network simulating the homogeneous active zone, we must repeatedly vary the values of the resistance R_{23} in all cells of the active zone so as to make them approach exactly the same value. The criterion representing the "critical" state of the network model is the existence of a linear law of power variation, (after the jump associated with the prompt neutrons) when the reactivity undergoes an abrupt perturbation (linear model); the runaway or amplitude–phase–frequency characteristics of the average powers should coincide with the similar characteristics of the point linear-reactor model, at least up to a frequency of $\omega = \beta/l$.

The problem of adjusting the model is greatly simplified if we are studying the kinetics of a reactor with a clearly expressed plateau zone.

In this case the number of resistances R_{23} requiring variation diminishes to $N - P$, where P is the number of unit cells in the plateau region and N is the total number. If, moreover, the periphery of the active zone is a ring with a width of one unit cell (independently of the number of cells in the plateau zone), the transmission coefficient for the transmission function (4) of the peripheral zone will be determined from the equation $K_1 = 2\ 1/n$, where n characterizes the unit-cell geometry. In this case we use Eq. (4) to determine the value of K_∞ for the peripheral zone, whereas for the plateau region the value of K_∞ is unity. The values of K_∞ for the plateau and peripheral zones enable us to calculate the corresponding values of R_{23}.

Sometimes when simulating spatially dependent reactor kinetics (in cases in which for a variety of reasons it is impossible to simulate the structural cell of the reactor under consideration by one unit cell of the network) complexities arise in determining the correspondence between the perturbation actually introduced into the reactor and its mathematical analog.

We see from Eq. (3) that the external perturbation amounts to the change in the local value of K_∞. However, the initial "weighting" data for the perturbations caused by the extraction of a fuel element or

Declassified and Approved For Release 2013/09/24 : CIA-RDP10-02196R000400060004-1

Declassified and Approved For Release 2013/09/24 : CIA-RDP10-02196R000400060004-1

control rod (or by temperature and density effects) are usually expressed in terms of K_{eff}. Owing to limited technical capabilities, the practical representation of all the structural cells in power reactors (usually over a thousand) on the network is quite impossible. If the unit cell of the spatial model is geometrically similar to the structural cell, the problem is greatly simplified.

We may envisage two ways of calibrating the perturbations for a linear model, i.e., for the case in which the deviations of the neutron flux may be regarded as small (not more than 20% of the nominal value): by analyzing the starting-up period corresponding to the mean reactor power T_S, and by using perturbation theory.

The first method is analogous to the rod-weighting method used in assembly experiments. It is well known that, for point kinetics, in the linear approximation we have the equation

$$\delta K_{eff} = \frac{\beta}{T_s \lambda}, \tag{5}$$

relating the change in the effective neutron breeding factor to the reactor start-up period. Thus, if the period of the neutron flux averaged over all cells in the network is measured, we may use Eq. (5) to calibrate the perturbation in units of reactivity. It should be noted that as the perturbation diminishes, i.e., the period increases, the accuracy of the calibrations is reduced. There is a certain "threshold" perturbation, depending on the scale selected, for which the reactor period cannot be recorded with the required accuracy because of the drift intrinsic to the electronic model.

The second method uses the following equation of perturbation theory

$$\rho = \frac{\int \Delta K_\infty \Phi_0^2 \, dV}{\int K_\infty \Phi_0^2 \, dV}, \tag{6}$$

where dV is the volume of the cell over which the perturbation is uniformly distributed, while integration is carried out over the whole active zone. For a discrete space–time model of the reactor Eq. (6) may be converted to the following form:

$$\Delta K_\infty = \rho \frac{\sum_1^N K_\infty (\Phi_{i0})^2}{(\Phi_{i0})^2},$$

where ρ is the change in reactivity due to the particular perturbation, while the summation extends over all the cells of the network model. Thus for known physical characteristics of the active zone and a known reactivity ρ introduced into the reactor we may determine the perturbations in units of ΔK_∞ for the unit cell of the network model.

After the network model of the spatially dependent reactor kinetics has been adjusted to the critical state and the characteristic perturbations and the means of compensating external perturbations have been calibrated, if any substantial temperature or density effects (influencing the reactivity) also exist, a system of inertial feedback links is established among the unit cells, the sign and depth of the feedback being respectively determined by the sign and magnitude of the temperature and density coefficients of reactivity, while the inertia is determined by the specific heat and thermal resistance of the fuel and moderator.

Since the mechanism underlying the inertial action of the feedback links is determined by a complex heat-transfer process, and (strictly speaking) is described by a system of differential equations of high order, in problems of network simulation it is more convenient to use approximations of the first or second orders, according to the ratio of the fuel and moderator time constants.

The accuracy of the solution obtained in network models is characterized by Fig. 4, which compares the perturbed steady-state distribution of energy evolution obtained in a coarse-step network model with the results of the electronic-computer calculation of a similar field in a reactor incorporating a reflector. The unit cell of the network model includes seven unit cells of the digital model. We see from Fig. 4 that the results agree satisfactorily in the plateau zone, but in the peripheral region they differ substantially. This is mainly because the simulation was carried out on the one-group approximation, as a result of which the influence of the reflector on the neutron flux distribution in the peripheral zone was not taken into account.

Declassified and Approved For Release 2013/09/24 : CIA-RDP10-02196R000400060004-1

Declassified and Approved For Release 2013/09/24 : CIA-RDP10-02196R000400060004-1

LITERATURE CITED

1. B. N. Seliverstov, V. V. Belousov, and A. I. Efanov, in: Control of Nuclear Power Installations [in Russian], Vol. 4, Atomizdat, Moscow (1970), p. 13.
2. P. T. Potapenko and Yu. I. Naidin, ibid., p. 22.
3. P. T. Potapenko, in: Analog and Analog-Digital Computing Technique [in Russian], No. 6, Sovet-skoe Radio, Moscow (1973).
4. W. Proctor et al., Nuclear Power, No. 82, 49 (1963).
5. R. Murray, C. Binghaim, and C. Matvin, Nucl. Sci. Engng., 18, 481 (1964).

Declassified and Approved For Release 2013/09/24 : CIA-RDP10-02196R000400060004-1

Declassified and Approved For Release 2013/09/24 : CIA-RDP10-02196R000400060004-1

METHODS OF REGULATING THE FIELDS OF ENERGY EVOLUTION IN LARGE POWER REACTORS

B. N. Seliverstov, N. P. Rudov, and F. F. Voskresenskii

UDC 621.039.562

In making practical use of a large power reactor, it is essential to maintain the prespecified shape of the field of energy evolution constant, since undue deformations of the latter may lead to serious accidents. The sensitivity of the energy field to deformation and local changes in the physical characteristics of the active zone increases with the size of the reactors and with the smoothing of the neutron flux. Classical systems for the automatic control of integrated power are incapable of compensating for local surges of energy evolution.* Hence in order to preserve the specified profile of energy evolution and eliminate local surges it is essential to include a special automatic system.

At the present time provision is made for the operator to maintain the spatial distribution of energy evolution by means of manual control rods. However, in view of the increasing requirements imposed upon the accuracy of energy-profile maintenance and the complexity of all the problems incumbent upon the operator, the question of automating control of the energy distribution is now one of first-order importance.

In developing a system for controlling the spatial energy distribution it is essential to allow for the technological specifications governing the use of the reactor, and also for the structure of the internal feedback mechanism, which determines the predisposition of the reactor in question to spatial instabilities of energy evolution.

By "technological specifications" in the use of the reactor we mean primarily the purpose for which it is to be employed and the modes of charging and recharging the fuel elements.

In the operation of large power reactors of the channel type there is a tendency toward "on-line" recharging, i.e., the expanded fuel is replaced by fresh material without reducing the power or stopping the reactor. This has a positive influence on the economy of nuclear power stations. Designers of control systems for the spatial distribution of energy evolution are thus faced with a completely specific problem, since the site, magnitude, and velocity of the perturbation are specified in advance.

Other problems are associated with stabilizing the spatial oscillations of the energy-evolution fields associated with the interaction of neutron-physical and thermotechnical processes. In this case the specific characteristics of the control system are determined by the characteristic frequency of the spatial oscillations of the energy-evolution fields. Usually one distinguishes between low-frequency xenon oscillations (fluctuations), the period of which varies from tenths of an hour to several hours, and high-frequency oscillations characteristic of large boiling reactors, having positive feedback with respect to vapor content. Here the period of the spatial oscillations may be a matter of seconds.

It should be noted that the reasons for the misalignment of the reactor energy fields maynot liesolely in the tendency of the particular reactor toward various kinds of instability, but also in possible anomalies of a technological character, for example, the redistribution of the rate of flow of the coolant and of the inlet temperatures with respect to the various fuel channels, and so forth. The most complicated case is naturally that in which the reactor possesses all the foregoing dynamic characteristics and also requires continuous "on-line" recharging of the fuel.

*By "classical" control system we mean a many-control-rod, synchronously-coupled control system operating by reference to the average current signal of peripheral ionization chambers.

Translated from Atomnaya Énergiya, Vol. 39, No. 5, pp. 329-333, November, 1975. Original article submitted December 13, 1974.

©1976 Plenum Publishing Corporation, 227 West 17th Street, New York, N.Y. 10011. No part of this publication may be reproduced, stored in a retrieval system, or transmitted, in any form or by any means, electronic, mechanical, photocopying, microfilming, recording or otherwise, without written permission of the publisher. A copy of this article is available from the publisher for $15.00.

Declassified and Approved For Release 2013/09/24 : CIA-RDP10-02196R000400060004-1

Declassified and Approved For Release 2013/09/24 : CIA-RDP10-02196R000400060004-1

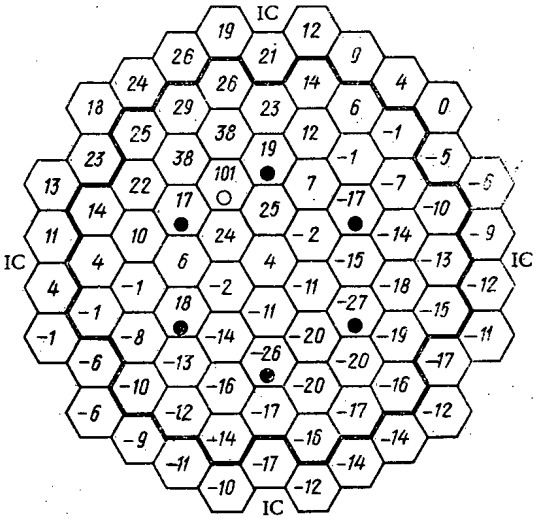

Fig. 1

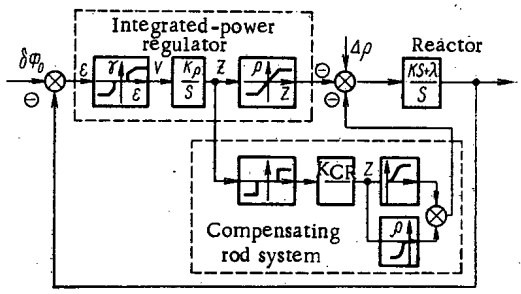

Fig. 2

Fig. 1. Deviations from the nominal distribution of energy evolution on suppressing the perturbation by means of an integrated-power regulator: ○) regulator rods; ●) perturbation introduced; IC) ionization chamber; —) boundary between the plateau and peripheral zones.

Fig. 2. Block diagram of the integrated-power regulator and structural arrangement of the regulation system incorporating the compensating rods.

Let us consider some of the arrangements for regulating the energy fields employed in present-day power reactors. The efficiency of these systems may be demonstrated by considering the two-dimensional network model of a hypothetic reactor without any feedback links, having a hexagonal lattice of cells for which the ratio of the square of the diameter to the migration area equals $2.5 \cdot 10^3$.

Local perturbations of the neutron breeding coefficient ΔK_∞, simulating the replacement of expended fuel by a fresh supply, were introduced into the plateau zone.* In simulating the ionization chambers outside the active zone we assumed that the contribution to the readings of the chamber due to the neutron flux arising from cells lying at a distance r was given by the law $\varphi = \frac{1}{r^2} \exp\left(-\frac{\xi}{r}\right)$ where the value of ξ characterized the attenuation of the signal.† Thus a signal proportional to $\sum_{i=1}^{N} \varphi_i$ (where N is the number of cells in the active zone of the reactor) falls on each ionization chamber.

For large values of ξ such as correspond to the real case of large, but not "rigidly connected" active zones, the neutron flux of the central cells takes hardly any part in determining the signal to the integrated-power regulator. Clearly, in maintaining the integrated reactor power constant the "classical" regulator will not eliminate local surges of energy evolution, especially when the zone of perturbation lies a long way from the regulator (control) rods. Figure 1 illustrates the distribution of the energy-evolution deviations obtained on using the most traditional, so-called "classical" scheme for regulating the integrated power of the reactor. The structural arrangement of the integrated-power regulator is shown in Fig. 2.

Let us now consider some improved systems for regulating the integrated power using the peripheral ionization chambers.

Integrated Reactor Power Control System Incorporating Compensating Rods [1]. The selected number of compensating rods (Fig. 2) are brought into play on a signal from the intermediate terminals of the regulator. After the rods of the automatic regulator have passed into the zone of action of the end switches,

*In order to obtain easily understood results, we assumed that the local perturbation ΔK_∞ equalled 10β where β is the effective proportion of delayed neutrons.

†The expression for φ constitutes an approximation to the experimental relationships.

Declassified and Approved For Release 2013/09/24 : CIA-RDP10-02196R000400060004-1

Declassified and Approved For Release 2013/09/24 : CIA-RDP10-02196R000400060004-1

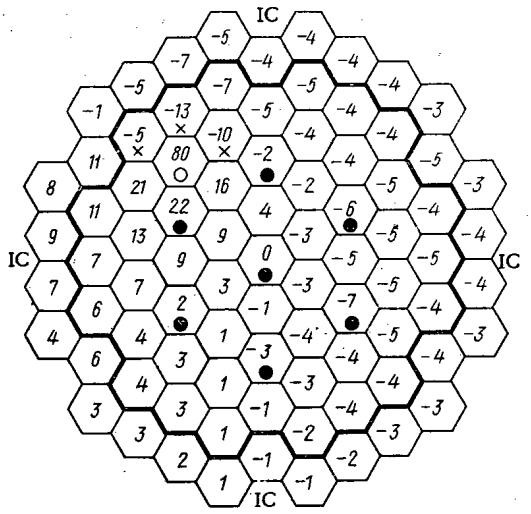

Fig. 3

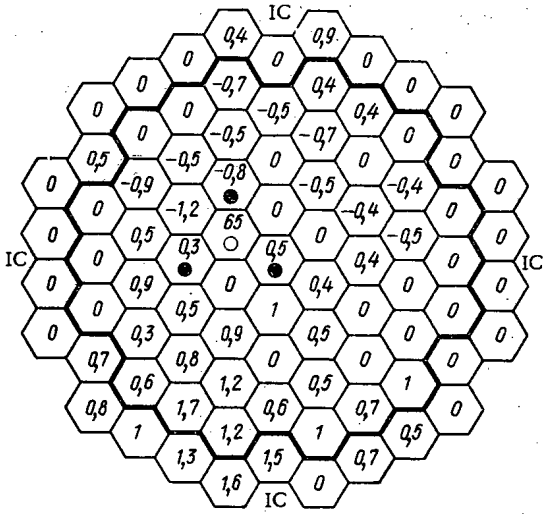

Fig. 4

Fig. 3. Distribution of the deviations from a certain nominal energy distribution on suppressing the perturbation with an integrated-power regulator, aided by three simultaneously introduced compensating rods: x) compensating rods (remaining notation as in Fig. 1).

Fig. 4. Distribution of the deviations from a certain nominal energy distribution on suppressing the perturbation with an integrated-power regulator, aided by an altered structural distribution of the regulating rods (notation as in Fig. 1).

the selected compensation rods are moved at a constant velocity until the automatic-regulator rods again pass out of the zone of action of the end switches.

The main parameters of this system are the number of compensating rods brought into action and the insensitivity zone ΔL of these rods. In choosing the insensitivity zone of the compensating rods one is forced into a compromise, since a reduction in the zone ΔL leads to a certain improvement in the energy-evolution distribution but worsens the stability condition, which in the linear approximation amounts to the satisfaction of the inequality

$$\frac{1}{\lambda}+\frac{1}{K_{CR}q}>\frac{1}{K_{reg}},$$

where λ is the average decay constant of the delayed neutrons, q is the harmonic linearization coefficient falling with increasing insensitivity zone ΔL; K_{CR}, K_{reg} are the amplification factors of the compensating system and the regulator respectively.

The choice of the number of compensating rods is primarily determined by their compensating capacity and also by their disposition relative to the fuel element being recharged. The best version is that in which the perturbation is localized by near-lying compensation rods. It is also essential to satisfy the conditions of nuclear safety, since the variation of a large number of absorbers may, in the case of failures, lead to emergency situations. Figure 3 shows the distribution of the deviations in energy evolution on suppressing the perturbation with an integrated-power regulator aided by three connected compensation rods.

It is not difficult to see that there will be no increase in the maximum of the local surge in energy evolution if several similar rechargings are carried out at the same time, subject to a suitable organization of the compensation system. The distance between the points of perturbation should be greater than five migration lengths.

Integrated Power Control System with an Altered Disposition of the Regulating Rods. On compensating the perturbations in the manner just discussed, the rigidly fixed disposition of the automatic-control rods, in conjunction with asymmetrical perturbations relative to the center of the active zone, leads to an increased nonuniformity in energy distribution a long way from the point of perturbation. The energy distribution over the active-zone region may be improved if the compensating rods in the region of the fuel

Declassified and Approved For Release 2013/09/24 : CIA-RDP10-02196R000400060004-1

Declassified and Approved For Release 2013/09/24 : CIA-RDP10-02196R000400060004-1

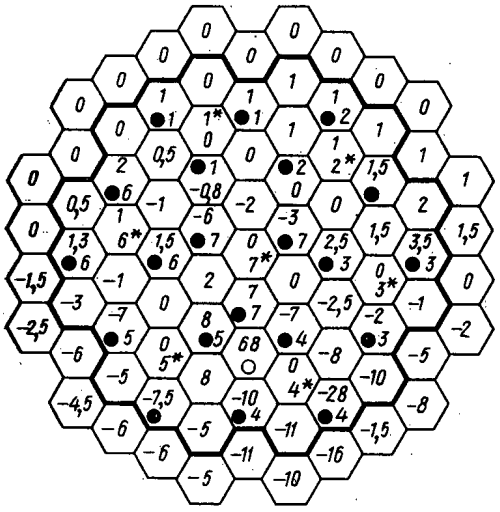

Fig. 5

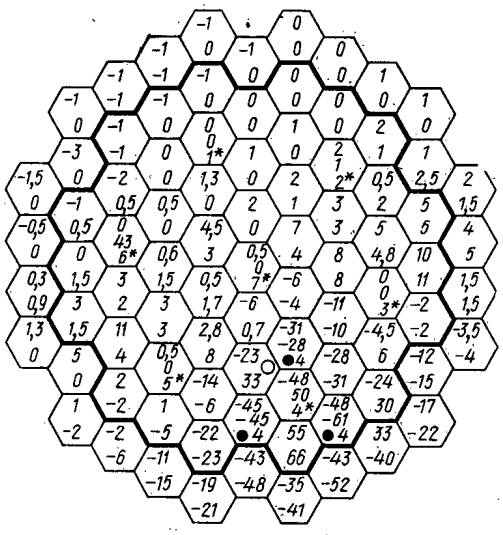

Fig. 6

Fig. 5. Distribution of the energy deviations from a certain nominal distribution, subject to multichannel suppression of the perturbation: ●i) rods of the local regulator served by the i-th chamber inside the reactor; i*) monitoring chamber inside the reactor for three neighboring rods (remaining notation as in Fig. 1).

Fig. 6. Distribution of energy evolution relative to a certain nominal distribution during the multichannel suppression of perturbation, after a preliminary power reduction in the zone of the perturbation (The top figures correspond to the energy deviations relative to the nominal values after reducing the power in the zone of action of the fourth regulator, the lower figures after introducing the perturbation; the remaining notation is as in Fig. 5).

undergoing replacement operate in the guise of an automatic regulator. Figure 4 illustrates the distribution of energy deviation for this mode of regulation. We see from Fig. 4 that over the whole region of the active zone, except of course the perturbed region, the energy deviations lie within the range of error of the simulation system.

Apart from the flexibility of control, the automatic-regulator type of operation has better dynamic characteristics, so that the transient processes take place more smoothly than in the relay case. A shortcoming of this arrangement is the demand for increased reliability of all the executive devices and the necessity of using different compensating rods for different recharging operations.

Multichannel System for Controlling Fields of Energy Evolution Using Monitoring Sensors Inside the Reactor. This arrangement is generally regarded as an advance on those already considered [2]; it maintains the energy profile constant in the reactor, not only while recharging the fuel elements, but also during any unforseen service anomalies. In addition to this, a multichannel regulation system with a well-developed array of sensors inside the reactor is capable (subject to a correct choice of parameters) of stabilizing the spatial instability of the fields of energy evolution over a wide frequency range.

The multichannel regulator comprises a group of local regulators with autonomous sensors connected to each other through the active zone. The number of local regulators or regulation zones is chosen after considering the diffusion and thermophysical characteristics of the active zone and providing for the specified monitoring efficiency. By monitoring efficiency we mean the smallest possible ratio of the maximum neutron flux recorded by the sensors to the true value of the maximum flux [3].

Figure 5 illustrates the distribution of the energy deviations from the steady-state case, subject to multichannel regulation. We see from Fig. 5 that this multichannel form of regulation is in no way inferior as regards the maintenance of spatial energy evolution to the arrangements already considered, and it is superior to these in its ability to maintain the required distribution in the event of any unintentional random perturbations or any kind of instability.

Another important advantage of the multichannel arrangement is the fact that in the case of large intentional local perturbations of reactivity requiring a preliminary reduction in the reactor power, the

Declassified and Approved For Release 2013/09/24 : CIA-RDP10-02196R000400060004-1

Declassified and Approved For Release 2013/09/24 : CIA-RDP10-02196R000400060004-1

multichannel control system avoids a universal reduction in reactor power, since the power only has to be reduced locally in the region of the envisaged perturbation. Figure 6 shows the energy deviations from a certain nominal value for this method of compensating perturbations.

In addition to the foregoing multichannel control system, we may also encounter another version in which the ordinary integrated-power regulator works in conjunction with a system of local regulators. The great advantage of the first arrangement is the monotypic nature of its structure; a disadvantage is the necessity of rapid action (it must be no worse than that of the ordinary automatic-control system), independently of the characteristic times of the field surges; this demands very reliable and practically inertia-free local sensors. In addition to this, in order to realize the transient power conditions it is essential to synchronize the settings of each local regulator.

An advantage of structural schemes of the second type is that the required rapidity of action of the subsidiary local automatic control system is determined by the actual characteristic times of the misalignments. This enables a broader set of internal reactor monitoring sensors to be employed. Furthermore, since the automatic control system is capable of operating independently of the system of local automatic regulator, it may simply be brought into action as and when needed [4].

LITERATURE CITED

1. A. P. Bovin et al., 3rd Geneva Conference (1964), Paper 28 (R) 321.
2. P. T. Potapenko and Yu. I. Naidin, in: Control of Nuclear Power Installations [in Russian], No. 4, Atomizdat, Moscow (1970), p. 32.
3. P. T. Potapenko, At. Énerg., 24, No. 4, 340 (1968).
4. I. Ya. Emel'yanov, Izv. Akad. Nauk SSSR, Énergetika i Transport, No. 3 (1974), p. 97.

Declassified and Approved For Release 2013/09/24 : CIA-RDP10-02196R000400060004-1

Declassified and Approved For Release 2013/09/24 : CIA-RDP10-02196R000400060004-1

ANALYSIS OF THE STABILITY OF THE NEUTRON-FIELD CONTROL SYSTEMS IN A POWER REACTOR

B. N. Seliverstov, N. P. Rudov, and F. F. Voskresenskii

UDC 621.039.512:621.039.562

Modern high-power reactors are characterized by large active zones and a high specific power of each unit volume in the active zone. When the reactor is in operation, the neutron field is distorted, as a result of various physical processes, and this may lead to accidents.

The creation of automatic-control systems increases the degree of maintenance of the neutron field, alleviates the work of the operator, improves safety, and increases the economic efficiency of the reactor as a whole [1].

One of the most important criteria of the efficiency on a neutron-field control system is its stability. This problem becomes even more important when using inertial monitoring sensors situated inside the reactor.

There are a number of ways of constructing neutron-field regulators. The simplest of these is a group of local automatic regulators in which each regulator has its own internal sensor, servo drive, and control rod (or group of rods). As a result of the coupling which exists between different neutron fluxes of the active zone, the neutron-field control system belongs to the class of multiply connected automatic-control systems.

An analysis of the operation of such multiply connected systems involves a great deal of calculation owing to the high order of the differential equations describing the dynamics of the system.

The equations may be greatly simplified by writing them in matrix form and using matrix-type structural arrangements (Fig. 1). In Fig. 1 W_{ob} is the transmission matrix of the object being regulated (the reactor) with dimensions $n \times n$ (here n is the number of local automatic regulators); W_{reg} is the transmission matrix of the neutron-field regulator (by virtue of the identical nature of the local regulators); $\delta\Phi$, ΔK, $\delta\Phi_0$ are the vectors of the output variables perturbing the system and specifying the action upon it:

$$W_{reg} = W_{reg}E, \tag{1}$$

where E is the unit matrix and W_{reg} is the transmission function of the local automatic regulator.

Each element in the transmission matrix of the object characterizes the transmission of particular actions in a linear dynamic system and reflects the dependence of each output of the system on each of its inputs. Since the influence of a perturbation in the j-th regulation channel on the i-th channel is equivalent to the influence of the i-th perturbation in the j-th channel, the matrix W_{ob} will be symmetrical.

Let us consider the form of the elements in the transmission matrix of a reactor without any power feedback.

At the initial instant after the introduction of an abrupt perturbation into the neutron breeding coefficient, there is a corresponding redistribution of the neutron flux with respect to the active zone of the reactor by virtue of the higher harmonics of the interaction [2]. This process ends in fractions of a second, after which a certain asymptotic period of change in the neutron flux is established, this being the same for all channels within the plateau zone (zone of uniform flux).

Translated from Atomnaya Énergiya, Vol. 39, No. 5, pp. 333-336, November, 1975. Original article submitted December 13, 1974.

©1976 Plenum Publishing Corporation, 227 West 17th Street, New York, N.Y. 10011. No part of this publication may be reproduced, stored in a retrieval system, or transmitted, in any form or by any means, electronic, mechanical, photocopying, microfilming, recording or otherwise, without written permission of the publisher. A copy of this article is available from the publisher for $15.00.

Declassified and Approved For Release 2013/09/24 : CIA-RDP10-02196R000400060004-1

Declassified and Approved For Release 2013/09/24 : CIA-RDP10-02196R000400060004-1

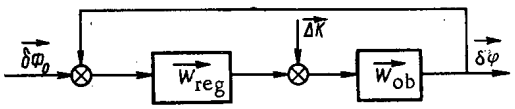

Fig. 1. Matrix structural scheme of a multiply connected automatic neutron-field control system.

Neglecting the time required for the redistribution of the neutron flux on account of the higher harmonics, we may express the matrix $\mathbf{W}_{ob}$ in the form

$$\mathbf{W}_{ob}=\left\|\begin{matrix}\frac{K_1S+\lambda}{S} & \frac{K_{12}S+\lambda}{S} & \dots \\ \frac{K_{12}S+\lambda}{S} & \frac{K_1S+\lambda}{S} & \dots \\ \frac{K_{1n}S+\lambda}{S} & \dots & \frac{K_1S+\lambda}{S}\end{matrix}\right\|, \tag{2}$$

where $K_1 > K_{1i}$, $i \neq 1$. In matrix form the equation characterizing the operation of the multiply connected automatic control system is

$$(\mathbf{E}+\mathbf{W}_{ob}\mathbf{W}_{reg})\,\delta\Phi=\mathbf{W}_{ob}\Delta\mathbf{K}+\mathbf{W}_{ob}\mathbf{W}_{reg}\delta\Phi_0. \tag{3}$$

If the local automatic regulators are disposed at a fair distance from each other (several migration lengths), the form of $\mathbf{W}_{ob}$ becomes simpler. It is well known that for a fairly slight perturbation Δk_∞ the change in the shape of the neutron field associated with the prompt neutrons extends over a finite part of the active zone lying close to the region of perturbation. Hence in the case of fairly well-separated local automatic regulators

$$\mathbf{W}_{ob}=\left\|\begin{matrix}\frac{K_1S+\lambda}{S} & \frac{K_2S+\lambda}{S} & \dots & \frac{K_2S+\lambda}{S} \\ \dots & \dots & \dots & \dots \\ \frac{K_2S+\lambda}{S} & \dots & \frac{K_2S+\lambda}{S} & \frac{K_1S+\lambda}{S}\end{matrix}\right\|=\frac{K_1S+\lambda}{S}\mathbf{E}+\frac{K_1S+\lambda}{S}\mathbf{B}, \tag{4}$$

where $\mathbf{E}$ is the unit matrix

$$\mathbf{B}=\left\|\begin{matrix}0 & 1 & 1 & \dots & 1 \\ 1 & 0 & 1 & \dots & 1 \\ \dots & \dots & \dots & \dots & \dots \\ 1 & \dots & \dots & \dots & 10\end{matrix}\right\|, \quad K_2 \ll K_1. \tag{5}$$

Let us determine the conditions for the stable operation of a multiply connected automatic-control system for the particular case in which the local automatic regulators lie at a distance of several migration lengths from one another.

Allowing for the form of the matrix $\mathbf{W}_{reg}$ (1) and that of the object transmission matrix (4), we apply the decomposition method to the original multiply connected automatic-control system [3]. We introduce new coordinates, connected to the old coordinates by a nondegenerate coordinate transformation matrix C:

$$\Theta=\mathbf{C}^{-1}\delta\Phi;\ \mathbf{Q}=\mathbf{C}^{-1}\Delta\mathbf{K};\ \Psi=\mathbf{C}^{-1}\delta\Phi_0,$$

where Θ, $\mathbf{Q}$ are the vectors of the quantity to be regulated and the perturbation in the new coordinate system respectively; Ψ is the vector of the actions specifying the envisaged changes. The equation of the multiply connected automatic-control system in the new coordinate system may be written thus:

$$\left[\mathbf{E}+\left(\frac{K_1S+\lambda}{S}\mathbf{E}+\frac{K_2S+\lambda}{S}\mathbf{C}^{-1}\mathbf{B}\mathbf{C}\right)\mathbf{W}_{reg}\right]\Theta=$$
$$=\left(\frac{K_1S+\lambda}{S}\mathbf{E}+\frac{K_2S+\lambda}{S}\mathbf{C}^{-1}\mathbf{B}\mathbf{C}\right)(\mathbf{Q}+\mathbf{W}_{reg}\Psi).$$

The matrix $\mathbf{B}^*=\mathbf{C}^{-1}\mathbf{B}\mathbf{C}$ is similar to the matrix $\mathbf{B}$, so that their characteristic numbers coincide. If we take the matrix of the canonical basis as $\mathbf{C}$, we obtain the simplest canonical form of the matrix $\mathbf{B}$ [4]. In the present case the matrix $\mathbf{B}$ is symmetrical. The canonical forms of symmetrical matrices are always diagonal, while their characteristic numbers are always real, i.e.,

Declassified and Approved For Release 2013/09/24 : CIA-RDP10-02196R000400060004-1

Declassified and Approved For Release 2013/09/24 : CIA-RDP10-02196R000400060004-1

$$\mathbf{B}^* = \mathbf{C}^{-1}\mathbf{B}\mathbf{C} = \begin{Vmatrix} \lambda_1 & 0 & \dots & 0 \\ 0 & \lambda_2 & \dots & 0 \\ \dots & \dots & \dots & \dots \\ 0 & \dots & \dots & 0\lambda_n \end{Vmatrix}.$$

Remembering the form of the matrix B, it is not hard to determine its characteristic numbers (eigenvalues):

$$\lambda_1 = \lambda_2 = \dots = \lambda_{n-1} = -1, \ \lambda_n = n-1,$$

where n is the number of local automatic regulators.

Thus, by using the nondegenerate transformation matrix C we may pass to an equivalent system consisting of singly connected systems, the structure of n − 1 systems being identical. The characteristic equation of the closed system ($\lambda = -1$) is:

$$1 + W_{\text{reg}}(K_1 - K_2) = 0. \tag{6}$$

In an analogous way, for $\lambda = n - 1$ the characteristic equation will be:

$$1 + W_{\text{reg}}\left[K_1 + K_2(n-1) + \frac{n\lambda}{S}\right] = 0. \tag{7}$$

By way of example, let us consider a typical form of the transmission function of the regulator:

$$W_{\text{reg}} = \frac{K_{\text{reg}}}{S(T_1 S + 1)(T_2 S + 1)}. \tag{8}$$

Applying the Gurwitz criterion to Eqs. (6) and (7), we obtain the stability condition

$$K_{\text{reg}} < \frac{T_1 + T_2}{T_1 T [K_1 + K_2(n-1)]} - \frac{(T_1 + T_2)^2 n\lambda}{T_1 T_2 [K_1 + K_2(n-1)]^2}. \tag{9}$$

We see from Eq. (9) that with increasing n the coefficients K_{reg} have to be reduced in order to ensure the stability of the multiply connected automatic-control systems. In other words, with increasing number of local automatic regulators the stability of the multiply connected neutron-field automatic-control system becomes less favorable. In addition to this, it follows from Eq. (9) that with increasing distance between the local automatic regulators (for n = const) the stability of the multiply connected automatic-control systems worsens, although, strictly, on the basis of the assumptions here made, such an assertion is only valid for n = 2.*

Analogous results may be obtained in a more general form on the following assumption. At a certain instant of time let a perturbation $\Delta k_{\infty}^{\text{int}}$ uniformly distributed over the active zone be created, in which $\Delta k_{\infty i}^{\text{int}} = \Delta k_{\infty j}^{\text{int}}$. By virtue of the identical nature of the local regulators we may consider that the laws governing the changes in $\delta\Phi_i(t)$ and $\Delta k^{\text{reg}}(t)$ are identical within all of the plateau zone. Then as a result of the mutually consistent correspondence between the Laplace transformation and the time characteristics of the system the following equations will be satisfied:

$$\begin{aligned} \delta\Phi_i(S) &= \delta\Phi_j(S) = \delta\Phi; \\ \Delta k_i^{\text{reg}}(S) &= \Delta k_j^{\text{reg}}(S) = \Delta k. \end{aligned} \tag{10}$$

Allowing for the form of the object matrix (2) and Eq. (10), the equation of the multiply connected automatic-control system (3) may easily be transformed into the equation of the following singly connected system:

$$\left(1 + W_{\text{reg}} \sum_{j=1}^{n} W_{ij}\right) \delta\Phi = \sum_{j=1}^{n} W_{ij}\Delta k + W_{\text{reg}} \sum_{j=1}^{n} W_{ij}\delta\Phi_{0j}, \tag{11}$$

*The foregoing method of analyzing the stability of multiply connected automatic-control systems is most effective for large power reactors with $L^2/M^2 \geq 1000$, for example, those of the Beloyarsk and Leningrad Nuclear Power Stations (L is the characteristic dimension of the reactor, M is the migration length).

Declassified and Approved For Release 2013/09/24 : CIA-RDP10-02196R000400060004-1

Declassified and Approved For Release 2013/09/24 : CIA-RDP10-02196R000400060004-1

where $\sum_{j=1}^{n} W_{ij}$ is the sum of the elements of the i-th line in the matrix W_{ob}. In order to ensure a reserve of computing capability, it is convenient to take $\max_{1 \leqslant i \leqslant n} \sum_{j=1}^{n} W_{ij}$. Remembering that $W_{ij} = \frac{K_{ij}S+\lambda}{S}$, we obtain the following stability condition for $W_{reg} = \frac{K_{reg}}{S(T_1S+1)(T_2S+1)}$:

$$K_{reg} < \frac{T_1+T_2}{T_1T_2K} - \frac{(T_1+T_2)^2}{T_1T_2} \frac{n\lambda}{K^2}, \tag{12}$$

where

$$K = K_1 + \left(\sum_{\substack{j=1 \\ i \neq j}}^{n} K_{ij}\right)_{max}.$$

It is not difficult to see that condition (12) coincides with (9) if as coefficient K_2 in the latter we take $K_2^* = K_2^* = \max_{1 \leqslant i \leqslant n} \frac{\sum_{j=1}^{n} K_{ij}}{n-1}$.

In analyzing the stability of the multiply connected automatic-control system regulating the neutron flux in a reactor with negative feedback, the transmission matrix W_{ob} may be greatly simplified if we use the laws of the adiabatic method and express it in the form

$$W_{ob} = HW_r, \tag{13}$$

where W_r is the transmission function of the point model of the reactor with negative feedback, H is the static matrix of transfer coefficients of order n × n describing the deviations of the neutron flux.

Applying the decomposition method with respect to the matrix equation (3) of the closed, multiply connected automatic-control system with due allowance for Eq. (13), and also remembering the identical nature of the local regulators, we may obtain an equivalent system of n singly connected mutually independent systems (by virtue of the symmetry of the matrix H). The characteristic numbers of the matrix are not as simple in form as those considered earlier, and have to be calculated with an electronic computer [5].

For the multiply connected system to be stable, the stability of all n singly connected systems of the equivalent system must be ensured. It is thus sufficient to apply any criterion of stability n times.

The neutron-field regulator comprising a group of local automatic regulators just considered executes two functions: It regulates both the neutron field and the average power. However, whereas the neutron-flux-distribution regulator does not have to be very fast acting, the average-power regulator must be very rapid in order to ensure normal safe operation of the reactor.

Thus, it is of practical interest to consider automatic-control systems consisting of two subsystems: one to regulate the neutron field (local automator regulator group) and one to regulate the average power (automatic regulator), the rapidity of action of the second system being an order of magnitude greater than that of the first.

The influence of the perturbations of Δk_{∞}^{i} on the average power of the reactor, in accordance with the statistical weights of the constituents, is exactly the same for any cell of the plateau zone, and is described by the transmission function of the point reactor, W_r. For the particular system under consideration we may write

$$\delta\Phi_i = \sum_{j=1}^{n} W_{ij}\varepsilon_j - W_{i_{AR}}\Delta k_{AR}, \tag{14}$$

where $\varepsilon_j = \Delta k_j - \Delta k^j_{reg}$; Δk^j_{reg}, Δk_{AR} are respectively the changes in the k_∞ of the j-th local automatic regular and the average power regulator; W_{iAR} is the transmission function allowing for the influence of the automatic regulator rods on the deviations of the neutron flux in the i-th cell. Allowing for the operating principles of the average-power regulator, we may write

$$\Delta k_{AR} = \frac{W_{AR}W_r}{1+W_{AR}W_r} \sum_{j=1}^{n} \varepsilon_j = W \sum_{j=1}^{n} \varepsilon_j, \tag{15}$$

Declassified and Approved For Release 2013/09/24 : CIA-RDP10-02196R000400060004-1

Declassified and Approved For Release 2013/09/24 : CIA-RDP10-02196R000400060004-1

where W_{AR} is the transmission function of the automatic regulator. In Eq. (15) W is the transmission function of the closed average-power regulation system. Since the rapidity of action of the latter system is much greater than that of the local automatic regulators, the average-power regulating system is decoupled in time from the local-automatic-regulator system.

Putting

$$W_{AR}=\frac{K_{AR}}{S(TS+1)}, \quad W_r=\frac{K_r(S+\lambda)}{S},$$

we obtain

$$W=\frac{\Delta K_{AR}}{\sum_{j=1}^{n}\varepsilon_j}\Bigg|_{S\to 0}=1. \tag{16}$$

Allowing for Eqs. (15) and (16), we may rewrite Eq. (14) thus

$$\delta\Phi_i=\sum_{j=1}^{n}(W_{ij}-W_{iAR})\varepsilon_j. \tag{17}$$

Let us consider the interaction of the neutron-field regulator and the average-power regulator for a reactor free from temperature-dependent reactivity effects. In this case

$$W_{ij}=\frac{K_{ij}S+\lambda}{S}, \quad W_{iAR}=\frac{K_{iAR}S+\lambda}{S}. \tag{18}$$

Allowing for (17) and (18), the matrix equation of the closed multiply connected automatic control system (3) may be written as follows:

$$(\mathbf{E}+\mathbf{K}\mathbf{W}_{reg})\,\delta\Phi=\mathbf{K}\Delta\mathbf{K}+\mathbf{K}\mathbf{W}_{reg}\delta\Phi_0, \tag{19}$$

where

$$\mathbf{K}=\begin{Vmatrix} K_{11}-K_{1AR}K_{12}-K_{1AR}\ldots K_{1n}-K_{1AR} \\ \ldots\ldots\ldots\ldots\ldots\ldots\ldots \\ K_{n1}-K_{rAR}\ldots\ldots K_{11}-K_{nAR}\end{Vmatrix}. \tag{20}$$

Allowing for the identical nature of the local regulators (1) and applying the decomposition method to Eq. (19), we obtain an equivalent system consisting of n singly connected systems, which are described by equations of the following form:

$$(1+\lambda_i W_{reg})\,\Theta_i=\lambda_i W_{reg}\Psi_i+\lambda_i Q_i,$$

where λ_i is an eigenvalue of the matrix (20).

It is convenient to analyze stability in a singly connected system with $\lambda=\lambda_{max}$, which may be determined from the equation

$$\lambda_{max}\leqslant K_{11}+\max_{1\leqslant i\leqslant n}\sum_{\substack{j=1\\ i\neq j}}^{n}|K_{ij}-K_{iAR}|.$$

Using the Gurwitz criterion, we obtain the condition for the stability of a multiply connected automatic-control system with regulators characterized by the following transmission function of form (8):

$$K_{reg}<\frac{T_1+T_2}{T_1T_2}\frac{1}{\lambda_{max}}, \tag{21}$$

where T_1 and T_2 are the time constants of the local automatic regulators – see Eq. (20).

Comparing Eqs. (21) and (12), we see that the system of local automatic regulators is more stable when operating in combination with the average-power regulator than without it. This is explained by the change in the form of the transmission function of the object (the object is described by a static chain), which increases the reserve of stability of the system and reduces the maximum eigenvalue of the object matrix, i.e., the amplification factor of the transmission function of the open system of the singly connected

Declassified and Approved For Release 2013/09/24 : CIA-RDP10-02196R000400060004-1

Declassified and Approved For Release 2013/09/24 : CIA-RDP10-02196R000400060004-1

scheme diminishes. In an analogous way we may obtain a similar result for a reactor with negative feedback due, for example, to temperature-dependent reactivity effects.

LITERATURE CITED

1. B. N. Seliverstov, N. P. Rudov, and F. F. Voskresenskii, At. Énerg. 39, No. 5, 334 (1975).
2. P. T. Potapenko, in: Control of Nuclear Power Installations [in Russian], No. 4, Atomizdat, Moscow (1970), p. 5.
3. V. T. Morozovskii, Multiply Connected Automatic Control Systems [in Russian], Énergiya, Moscow (1970).
4. R. F. Gantmakher, Theory of Matrices [in Russian], Nauka, Moscow (1967).
5. E. V. Filipchuk, P. T. Potapenko, and A. N. Kosilov, At. Énerg., 35, No. 5, 317 (1973).

Declassified and Approved For Release 2013/09/24 : CIA-RDP10-02196R000400060004-1

Declassified and Approved For Release 2013/09/24 : CIA-RDP10-02196R000400060004-1

SOLUBILITY OF FLUORIDES OF CERTAIN ELEMENTS IN LIQUID URANIUM HEXAFLUORIDE

N. S. Nikolaev and A. T. Sadikova

UDC 541.123.23:546.791.6:546.16

In connection with the development of modern methods of isotopic separation of uranium, the requirements for quality of uranium hexafluorides have increased, which has required an elucidation of the behavior of individual impurity elements in liquid uranium hexafluoride. The source of contaminants is the technological processes and operations on the processing of uranium raw materials and irradiated materials (fragment elements). The general background contamination consists of both volatile and nonvolatile fluorides. The problem is complicated by the fact that most of the chemical elements are impurities in uranium hexafluoride.

It can be assumed that in industrial UF_6, impurities will not be present in a saturation state. Consequently, the solubility serves as an index of the contamination limit of UF_6 by a given element. And yet, the information on the solubility of impurities in UF_6 is extremely limited [1-4].

This work discusses the solubilities of impurity elements in the form of fluorides in liquid UF_6 at temperatures above the triplet point.

The soluble components used were fluorides of the alkali elements (Na, K, Rb, Cs), the alkaline-earth elements (Ca, Sr, Ba) and Mg, the rare-earth elements (La, Pr, Nd, Sm, Eu, Gd, Ho), Sc and Y, three d-transition elements (Cu, Ni, Fe), Cd and Al, Ti, and Th, Nb and Ta, xenon difluoride,* and, finally

*Provided by the I. V. Kurchatov Atomic Energy Institute.

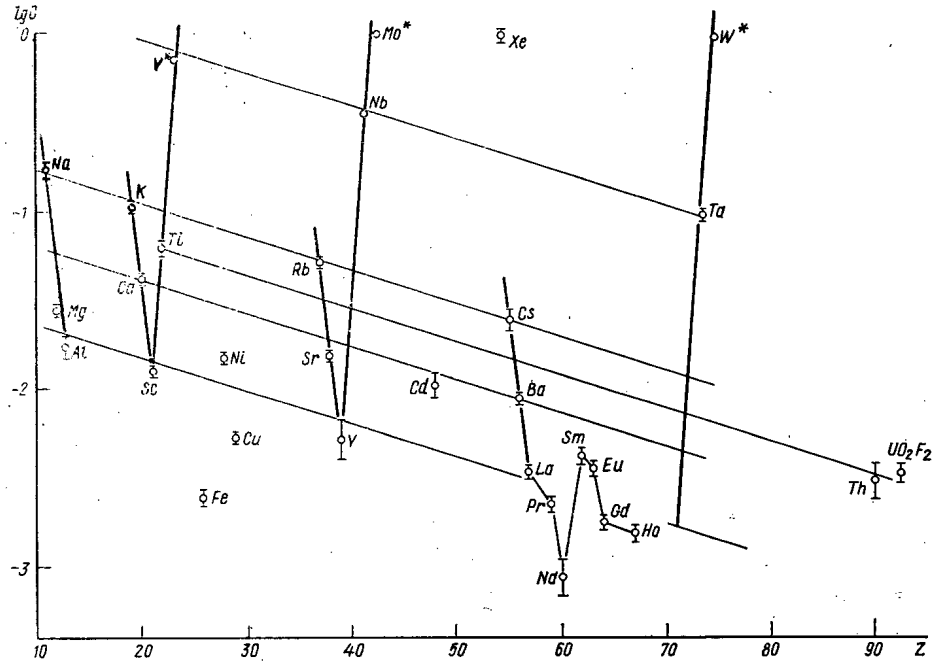

Fig. 1. Solubility diagram of metal fluorides in liquid UF_6.

Translated from Atomnaya Énergiya, Vol. 39, No. 5, pp. 338-343, November, 1975. Original article submitted December 18, 1974.

©1976 Plenum Publishing Corporation, 227 West 17th Street, New York, N.Y. 10011. No part of this publication may be reproduced, stored in a retrieval system, or transmitted, in any form or by any means, electronic, mechanical, photocopying, microfilming, recording or otherwise, without written permission of the publisher. A copy of this article is available from the publisher for $15.00.

Declassified and Approved For Release 2013/09/24 : CIA-RDP10-02196R000400060004-1

Declassified and Approved For Release 2013/09/24 : CIA-RDP10-02196R000400060004-1

TABLE 1. Solubility of Fluorides of Various Elements in Liquid Uranium Hexafluoride

Periodic system group	Fluoride	C, %	C, moles/1000 g	Mean-square error	T, °C
I	NaF	0,71	$1,7 \cdot 10^{-1}$	0,05	220
	KF	0,61	$1,0 \cdot 10^{-1}$	0,03	220
	RbF	0,59	$5,6 \cdot 10^{-1}$	0,03	220
	CsF	0,38	$2,5 \cdot 10^{-2}$	0,05	220
II	MgF_2	0,17	$2,7 \cdot 10^{-2}$	0,01	220
	CaF_2	0,32	$4,1 \cdot 10^{-2}$	0,02	220
	SrF_2	0,20	$1,6 \cdot 10^{-2}$	0,01	220
	BaF_2	0,17	$9,6 \cdot 10^{-3}$	0,01	220
III	AlF_3	0,15	$1,8 \cdot 10^{-2}$	0,03	220
	ScF_3	0,13	$1,3 \cdot 10^{-2}$	0,01	220
	YF_3	0,077	$5,3 \cdot 10^{-3}$	0,02	220
	LaF_3	0,068	$3,4 \cdot 10^{-3}$	0,001	220
	PrF_3	0,046	$2,3 \cdot 10^{-3}$	0,005	220
	NdF_3	0,018	$8,5 \cdot 10^{-4}$	0,003	220
	SmF_3	0,091	$4,4 \cdot 10^{-3}$	0,011	220
	EuF_3	0,077	$3,7 \cdot 10^{-3}$	0,016	220
	GdF_3	0,037	$1,8 \cdot 10^{-3}$	0,004	220
	HoF_3	0,036	$1,6 \cdot 10^{-3}$	0,006	220
IV	TiF_4	0,78	$6,3 \cdot 10^{-2}$	0,05	220
	ThF_4	0,10	$3,2 \cdot 10^{-3}$	0,01	220
V	NbF_5*	6,86	$3,7 \cdot 10^{-1}$		100
	TaF_5	2,86	$1,0 \cdot 10^{-1}$		100
VI	UO_2F_2*	0,107	$3,4 \cdot 10^{-3}$	0,01	220
0	XeF_2*	16,7	1,0	0,3	100
	FeF_3	0,029	$2,5 \cdot 10^{-3}$	0,003	220
	NiF_2	0,154	$1,6 \cdot 10^{-2}$	0,006	220
	CuF_2	0,057	$5,5 \cdot 10^{-3}$	0,002	220
	CdF_2	0,17	$1,1 \cdot 10^{-2}$	0,02	220

*The results obtained correspond to the data of [1, 2, 3].

uranyl fluoride, which is practically always present in UF_6, i.e. 27 fluorides of different elements, representing all the groups of the periodic system, as well as uranyl fluoride, were investigated. All the fluorides were prepared in the laboratory and conformed to the basic requirement – they were absolutely anhydrous.

The solubility was determined in a 30-ml copper autoclave at 50-60 atm. The assembly of the autoclave (with setup of the lid) was performed by means of steel flanges with bolts using a Teflon gasket. A 20-30-g portion of UF_6 was introduced into the autoclave (the volume of the liquid phase did not exceed 6 cm^3), with the fluoride to be dissolved in amounts sufficient for the formation of a solid phase, and it was placed in a crucible furnace with regulated heating. The solubility was determined at 220 ± 5 and 100 ± 5°C for nonvolatile and volatile fluorides, respectively.

The sample was exposed at the set temperature for 30-40 h (with mixing), then the solution was allowed to stand at the same temperature for another 40 h which was 3-4 times greater than the time necessary for reaching equilibrium. After standing, the autoclave was rapidly immersed in liquid nitrogen, which corresponded to fixation of the solution (method of quenching).

To determine the solubility of nonvolatile fluorides, UF_6 was removed from the collected sample by evacuation at 80-90°C, and the impurity element was analyzed in the solid residue. To determine the solubility of volatile fluorides (TaF_5, NbF_5, XeF_2), the entire sample collected was subjected to hydrolysis by introducing the sample into ice, and only then was the analysis performed.

All the operations on loading and collection of samples were performed in a dry box, dried with anhydrone and liquid nitrogen (the temperature in the box was lowered to −20°). The results obtained are presented in Table 1.

A systematic study of the solubility of fluorides in UF_6 permitted the establishment of patterns in the solubility of various fluorides. A diagram was compiled (Fig. 1) on which the atomic number of the impurity element was plotted along the x axis, and the logarithm of the solubility along the y axis (the solubility C was expressed in moles per 1000 g of the solution). The values of the solubilities for MoF_6, WF_6, and WF_5, marked by asterisks, were taken from [1] and pertain to a temperature of 70°C. The diagram cited shows a definite periodic correlation of the solubility of various groups of elements in liquid UF_6 with the atomic number of the element.

Within the periods, as the atomic number of the element increases, the solubility decreases from monofluorides to trifluorides, and then increases significantly in the transition to penta- and hexafluorides. In 3-6 periods, the minimum solubility falls on the trifluorides of Al, Sc, Y, and Ln, respectively; moreover, the fluorides of the lanthanides, represented by three "light" (La, Pr, Nb) and four "heavy" elements (Sm, Eu, Gd, Ho), in accord with the structural difference (fluorides of the light lanthanides possess a tysonite structure, while fluorides of the heavy lanthanides possess an yttrium trifluoride structure) were separated according to solubility into two subgroups: in the first the solubility of the lanthanide fluoride decreases with increasing atomic number of the element from La to Nd, while in the second the solubility varies in the following order: $SmF_3 \geq EuF_3 > GdF_3 \geq HoF_3$.

Declassified and Approved For Release 2013/09/24 : CIA-RDP10-02196R000400060004-1

Declassified and Approved For Release 2013/09/24 : CIA-RDP10-02196R000400060004-1

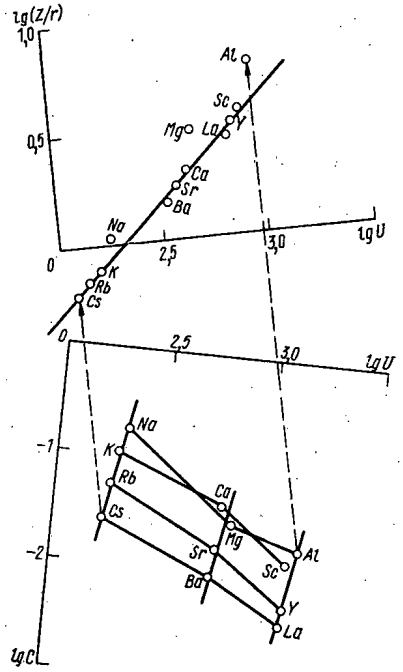

Fig. 2

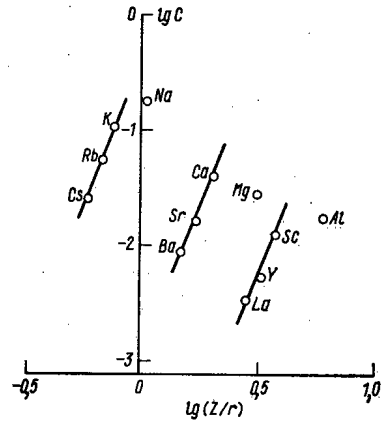

Fig. 3

Fig. 2. Dependence of the variation of the solubility of fluorides of elements of periods 3-6 of the periodic system in UF_6 on the crystal lattice energy. Above the projection, along the visually selected mid-plane, constructed using the methods of description geometry along two projections: lower part of the figure and Fig. 3.

Fig. 3. Dependence of the solubility of fluorides of metals of groups I-III in UF_6 on the polarizing strength of the cation Z/r.

TABLE 2. Comparison of the Solubility of Fluorides of Elements in Uranium Hexafluoride with the Values of Their Crystal Lattice Energies

Periodic system period	Fluoride	C, moles/1000 g	U, kcal/mole [7]
3	NaF	$1{,}7\cdot10^{-7}$	217
	MgF_2	$2{,}7\cdot10^{-2}$	695
	AlF_3	$1{,}8\cdot10^{-2}$	1440
4	KF	$1{,}0\cdot10^{-1}$	194
	CaF_2	$4{,}1\cdot10^{-2}$	624
	ScF_3	$1{,}3\cdot10^{-2}$	1281
5	RbF	$5{,}6\cdot10^{-2}$	184
	SrF_2	$1{,}6\cdot10^{-2}$	588
	YF_2	$5{,}3\cdot10^{-3}$	1275*
6	CsF	$2{,}5\cdot10^{-2}$	172
	BaF_2	$9{,}6\cdot10^{-3}$	566
	LaF_3	$3{,}4\cdot10^{-3}$	1245*

*The energies were calculated according to the Kapustinskii formula.

The lowest solubility among the lanthanide fluorides is possessed by NdF_3, which agrees with the first region of crystal chemical instability established by Dzhurinskii [5], in which, in particular, an extreme value of the solubility is observed.

Declassified and Approved For Release 2013/09/24 : CIA-RDP10-02196R000400060004-1

Declassified and Approved For Release 2013/09/24 : CIA-RDP10-02196R000400060004-1

TABLE 3. Comparison of the Melting Points of Certain Fluorides and Their Solubility in Liquid Uranium Hexafluoride

Fluoride	T_m, °C	C, moles/1000 g	Fluoride	T_m, °C	C, moles/1000 g
AlF_3	1040	$1,8 \cdot 10^{-2}$	ThF_4	600—700	$3,2 \cdot 10^{-3}$
ScF_3	1515	$1,3 \cdot 10^{-2}$	NbF_5	78,9	$3,6 \cdot 10^{-1}$
YF_3	1425	$5,3 \cdot 10^{-3}$	TaF_5	96,8	$1,0 \cdot 10^{-1}$
LaF_3	1726	$3,4 \cdot 10^{-3}$	MoF_6*	17,5	1,0
TiF_4	248	$6,3 \cdot 10^{-2}$	WF_6*	2,3	1,0

*The values of the solubility were taken from [1].

TABLE 4. Comparison of the Experimental Values of the Solubility and Those Calculated According to Eq. (1)

Fluoride	C, moles/1000 g		Discrepancy ΔC
	expt.	calc.	
KF	$1,0 \cdot 10^{-1}$	$0,93 \cdot 10^{-1}$	—0,07
RbF	$5,6 \cdot 10^{-2}$	$5,9 \cdot 10^{-2}$	+0,30
CsF	$2,5 \cdot 10^{-2}$	$3,3 \cdot 10^{-2}$	+0,80
CaF_2	$4,1 \cdot 10^{-2}$	$3,6 \cdot 10^{-2}$	—0,50
SrF_2	$1,6 \cdot 10^{-2}$	$1,54 \cdot 10^{-2}$	—0,06
BaF_2	$9,6 \cdot 10^{-3}$	$6,3 \cdot 10^{-2}$	—3,30
ScF_3	$1,3 \cdot 10^{-2}$	$1,8 \cdot 10^{-2}$	+0,50
YF_3	$5,3 \cdot 10^{-3}$	$6,3 \cdot 10^{-3}$	+1,00
LaF_3	$3,4 \cdot 10^{-3}$	$2,9 \cdot 10^{-3}$	—0,50

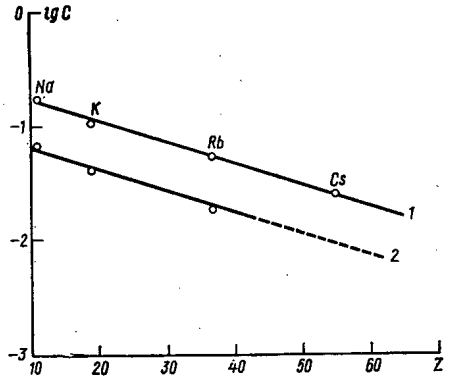

Fig. 4. Solubility of fluorides of the alkali metals in liquid UF_6 at the temperatures 220 (1) and 150 (2) °C.

The decrease in the solubility of the transition from fluorides of the alkali metals through the alkaline-earth fluorides to fluorides of sp(Al) and d(Sc, Y, La) elements, corresponds to an increase in the charge (valence) of the element. The crystal lattice energy of the compound to be dissolved varies radically in the same order. The correlation between the solubility of the fluoride and its crystal lattice energy U is cited in Table 2. For fluorides of the s, sp, and 4f elements, the values of the crystal lattice energies deviate from the assumption of an ionic character of the bonds according to the Born model or the simplified calculations of Kapustinskii [6].

From the data of Table 2 it follows that within the periods the solubility of the fluorides decreases with increasing crystal lattice energy of the fluoride to be dissolved (Fig. 2). The further increase in the solubility of the fluorides in the transition to tetra-, penta-, and hexafluorides is due to the nature of these compounds.

The difference is determined by the fact that fluorides of groups I and II are classed as ionic-type compounds, whereas fluorides of elements with a greater valence are classed as fluorides with a mixed bond type, and the compounds MeF_4 and MeF_5 are closer to molecular, while the hexafluorides are typical molecular compounds with an intramolecular covalent bond. The observed change in the solubility of the fluorides can also be compared with the qualitative characteristic of covalence of the bond in the compound – with the melting point (Table 3).

From Table 3 it is evident that the least soluble trifluorides possess the highest melting points. This agrees with the theoretical calculations, which show that the energy of a mixed ionic–covalent bond of trifluorides is greater than the energy of purely ionic or purely covalent bonds [8].

For tetra- and pentafluorides, a substantial decrease in the melting point is observed, which corresponds to an increase in the covalence of the bond (an exception is ThF_4, the solubility of which is close to the solubility of fluorides of the lanthanides). The hexafluorides, as typical covalent compounds, possess an extremely low level of the melting point; since the bonds between molecules of the hexafluorides are provided for only by van der Waals forces, the passage of the molecules of a soluble hexafluoride into solution occurs with a negligible energy expenditure, which also provides for the increased solubility of the compounds.

The change in the solubility of fluorides of the elements according to groups indicates a decrease in the solubility with increasing atomic number of the element. Such a variation of the solubility is evidently associated with the decrease in the polarizing action of the soluble cation and the increase in its radius. It is known that the polarizing strength of a cation has a negligible influence on the crystal lattice energy. In nonpolar solvents (for example, in uranium hexafluoride), the polarizing action of the cation promotes the

Declassified and Approved For Release 2013/09/24 : CIA-RDP10-02196R000400060004-1

Declassified and Approved For Release 2013/09/24 : CIA-RDP10-02196R000400060004-1

TABLE 5. Values of the Solubilities for Fluorides of the Rare-Earth Elements

Fluoride	C, moles/1000 g		U,* kcal/mole	r_i, Å [8]
	expt.	calc.		
LaF_3	$3,4 \cdot 10^{-3}$	$3,1 \cdot 10^{-3}$	1245	1,04
PrF_3	$2,3 \cdot 10^{-3}$	$3,5 \cdot 10^{-3}$	1260	1,01
NdF_3	$8,5 \cdot 10^{-4}$	$4,4 \cdot 10^{-3}$	1265	0,99
SmF_3	$4,4 \cdot 10^{-3}$	$5,0 \cdot 10^{-3}$	1275	0,97
EuF_3	$3,7 \cdot 10^{-3}$	$5,0 \cdot 10^{-3}$	1275	0,95
GdF_3	$1,8 \cdot 10^{-3}$	$5,3 \cdot 10^{-3}$	1290	0,94
HoF_3	$1,6 \cdot 10^{-3}$	$4,3 \cdot 10^{-3}$	1325	0,894

*The energy was calculated according to the Kapustinskii formula.

formation of a supplementary bond between ions of the substance to be dissolved, as a result of which the stability of this system is increased. Such "extractability" of the dissolved phase in comparison with crystals increases the solubility of the substances as the radius of the cation decreases [9], which is inversely related to the influence of the crystal lattice energy on the solubility. It has been established that when various fluorides dissolve in liquid UF_6, the greatest solubility in the groups is exhibited by fluorides in which the cation possesses a lower radius: in group I the greatest solubility is possessed by NaF, in II by CaF_2, in III by AlF_3, in IV by TiF_4, and finally in V by VF_5. An exception is MgF_2, an important peculiarity of which is the very high crystal lattice energy in comparison with the lattice energy of the fluorides in this group: MgF_2 695 kcal, CaF_2 624 kcal, i.e., the difference is ~70 (!) kcal.

It is known that a quantitative criterion of the polarizing strength of a cation is the ratio of the charge of the cation Z to its radius r. The relationship between the solubility C and the polarizing strength of the cation Z/r in a logarithmic scale for the fluorides of groups I, II, and III is shown in Fig. 3. From the diagrams considered earlier (see Figs. 1-3) it is evident that the solubility of fluorides of the elements is related to the crystal lattice energy of the fluoride to be dissolved and the polarizing strength of the cation. In this case it was found that in space with coordinates log C, log Z/r, and log U, the experimental points found, expressing the solubility of the ionic fluorides in UF_6, lie in one plane (see Fig. 2). This permitted us to find an analytical expression describing the solubility of the fluorides of groups I-III in liquid uranium hexafluoride:

$$\lg C = 7.70 \lg Z/r - 7.36 \lg U + 16.75, \quad (1)$$

where C is the solubility of the metal fluoride; Z/r is the polarizing strength of the soluble cation; U is the crystal lattice energy of the soluble fluoride.

The coefficients in this equation were found by the method of least squares [10]. The equation contains components showing that the solubility of the fluorides is determined by opposite tendencies: by the polarizing strength of the cation and by the crystal lattice energy; the first value of the solubility increases, while the second decreases (Table 4).

The values of the solubility for NaF, MgF_2, and AlF_3 deviate from the established dependence and can be explained by the minimum values of their ionic radii, which differ sharply from the ionic radii of the corresponding element homologs.

We also calculated the solubility according to the equation derived for other ionic compounds. This pertains primarily to fluorides of the rare-earth elements, for which the crystal lattice energy can also be calculated according to the Kapustinskii formula, since the basic valence electrons organize structures of an ionic character (Table 5).

It is evident that for four fluorides out of seven, the experimental and calculated solubilities are in satisfactory agreement. It should be kept in mind that the solubilities of trifluorides of the rare-earth elements occupy the lowest position on the solubility diagram (see Fig. 1), and this determines the highest experimental and analytical tolerance for them. Satisfactory agreement between the calculated and experimental values of the solubility was also obtained for CdF_2, which possesses a fluorite structure, for which calculation of the crystal lattice energy according to Kapustinskii is applicable: $C_{exp} = 1.1 \cdot 10^{-2}$, $C_{calc} = 1.8 \cdot 10^{-2}$.

Considering the arbitrary, semiempirical nature of the value of the crystal chemical radius and taking into account the approximate, and in certain cases (for elements of group III) tentative, nature of the values used for the ionic radii in the calculations of the values of the crystal lattice energies, the agreement of the calculated and experimental values of the solubilities obtained can be considered satisfactory.

Declassified and Approved For Release 2013/09/24 : CIA-RDP10-02196R000400060004-1

Declassified and Approved For Release 2013/09/24 : CIA-RDP10-02196R000400060004-1

We also considered the influence of temperature on the solubility. For fluorides of the alkali metals, an increase in the solubility with the temperature was established (Fig. 4) [11], from which it is evident that the solubility isotherm at 150°C for the alkali fluorides does not violate the general correlation.

In conclusion, let us note that the established pattern evidently is more general and can be extended to the investigated fluorides of groups IV-VI. The place of fluorides of higher valence of groups IV-VI, possessing a more pronounced covalent character,* will be determined by the rule following from the graphical accomodation of such fluorides (see Fig. 1). This is illustrated by the experimental values of the solubilities for pentafluorides of niobium and tantalum, for which the values of the solubility were obtained after the detection of the indicated pattern and fitted well on the diagram. For ionic fluorides, an estimate of the solubility can be performed on the basis of the values of the crystal lattice energies and the polarizing strength of cations of soluble fluorides, in accord with the established principle.

LITERATURE CITED

1. W. Mears, Industr. and Engng. Chem., 50, No. 12, 1771 (1958).
2. V. N. Prusakov and V. K. Ezhov, in: Transactions of the Symposium of the Council of Economic Mutual Aid: Investigations in the Field of Processing of Irradiated Fuel [in Russian], Karlovy Vary, Feb. 26-March 2, 1968, Report KV-68/30.
3. V. K. Ezhov, V. N. Prusakov, and B. B. Chaivanov, At. Énerg., 28, No. 6, 497 (1970); V. K. Ezhov, At. Énerg., 30, No. 4, 383 (1971).
4. U. D. Veryatin et al., At. Énerg., 31, No. 4, 375 (1971).
5. G. A. Bandurkin and B. F. Dzhurinskii, Dokl. Akad. Nauk SSSR, 168, No. 6, 1315 (1966).
6. G. B. Bokii, Crystal Chemistry [in Russian], MGU, Moscow (1960), p. 190.
7. T. Gibb, J. Progress in Inorg. Chem., 3, 400 (1962).
8. M. C. Day and J. Selbin, Theoretical Inorganic Chemistry, Van Nostrand Reinhold (1969).
9. F. A. Cotton and G. Wilkinson, Advanced Inorganic Chemistry, Wiley (1972).
10. L. Z. Rumshinskii, The Mathematical Treatment of Experimental Results [in Russian], Nauka, Moscow (1971), p. 79.
11. N. S. Nikolaev and A. T. Sadikova, At. Énerg., 25, No. 5, 422 (1968).

*Even approximate values of the crystal lattice energy are not available for them.

Declassified and Approved For Release 2013/09/24 : CIA-RDP10-02196R000400060004-1

Declassified and Approved For Release 2013/09/24 : CIA-RDP10-02196R000400060004-1

RADIOLYSIS OF ACID SOLUTIONS OF POTASSIUM IODATE IN CONTACT WITH A SOLUTION OF TRI-n-BUTYL PHOSPHATE IN HEXANE

E. V. Barelko, G. S. Babakina, and I. P. Solyanina

UDC 541.15

One of the important problems arising in the development of extraction schemes of regeneration of spent fuel cells of fast reactors is the investigation of the principles of the behavior of the radioiodine for a reduction of its radiation chemical influence on the extraction reagent and the prevention of contamination of the surrounding environment [1].

The radiolysis of organic substances containing iodine has thus far been studied primarily under conditions of a homogeneous system: in pure hydrocarbons [2-5] and in hydrocarbon solutions of tributyl phosphate (TBP) [6-7].

The yield of radiation chemical capture of molecular iodine according to Schuler [2] in hexane at very low doses was 3.8 molecules/100 eV. The value of $G(-I_2)$ is a function of the dose and temperature, and at large doses it drops to 2.2 molecules/100 eV at 25°C [5]. In the presence of TBP in the same dose range, the yield of radiation chemical capture of I_2 reaches 4.6 molecules/100 eV [6]. Experiments on the radiolysis of molecular iodine in a solution of TBP +hexane, into which HNO_3 was also introduced, gave a value of $G(-I_2)$ equal to 5.5 molecules/100 eV. However, in the radiolysis of a two-phase system [8] containing an aqueous nitric acid solution of fission products and a solution of TBP in a kerosene diluent, the yield of the capture of iodine by the organic phase was only 0.1 molecule/100 eV. In this case the integral dose received by the system reached $2.28 \cdot 10^{20}$ eV/ml, i.e., was comparable with the range of doses of irradiation used in [5, 7]. The low yield of the radiation capture of iodine of the organic phase was explained in [8] by competition of oxygen and oxides of nitrogen with iodine for the accepting of radicals arising in the organic phase under the action of radiation. The chemical forms of iodine were not investigated in this case.

One of the possible forms of radioiodine present in aqueous nitric acid solutions of nuclear fuel sent for extraction processing is iodate [9, 10].

The γ radiolysis of KIO_3 in alkaline solution was investigated in the greatest detail by Haissinsky et al. [11], who established a correlation between the yield of the decomposition of iodate, the sum of the yields of its reduction products and the radiolysis products of water. Practically the only published work devoted to the radiolysis of KIO_3 in an aqueous solution of sulfuric acid gives no idea of the ratios between the reacted initial form and all the forms of iodine produced during radiation reduction, in particular, I_2 [12]. The absence of such data may be associated with the fact that under these conditions iodine readily enters into reverse reactions under the action of radiation.

In this work we discuss the influence of radiation on the process of passage of iodine into a solution of the extraction reagent (TBP +hexane) from acid aqueous solutions of potassium iodate, containing sulfuric and nitric acids (systems deaerated). The procedure of experiments in H_2SO_4 solution under such model conditions substantially simplifies the interpretation of the results, since it eliminates questions of competition of nitric acid and oxygen with forms of iodine for the active intermediate radiolysis products of the aqueous and organic phases. The use of n-hexane as the diluent (instead of the industrial diluent synthine) in turns simplifies the analysis of the radiolysis products, without significantly changing the chemical mechanism of the processes, which is practically the same for saturated hydrocarbons with different chain

Translated from Atomnaya Énergiya, Vol. 39, No. 5, pp. 344-349, November, 1975. Original article submitted October 30, 1974. Revised May 12, 1975.

©1976 Plenum Publishing Corporation, 227 West 17th Street, New York, N.Y. 10011. No part of this publication may be reproduced, stored in a retrieval system, or transmitted, in any form or by any means, electronic, mechanical, photocopying, microfilming, recording or otherwise, without written permission of the publisher. A copy of this article is available from the publisher for $15.00.

Declassified and Approved For Release 2013/09/24 : CIA-RDP10-02196R000400060004-1

Declassified and Approved For Release 2013/09/24 : CIA-RDP10-02196R000400060004-1

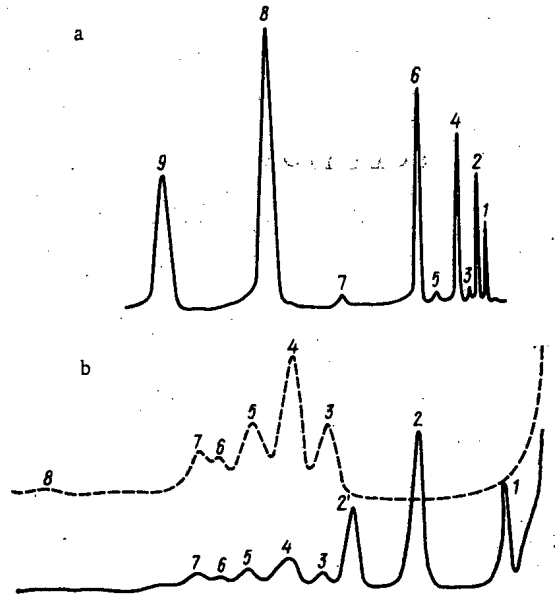

Fig. 1. Chromatogram of the organic phase irradiated in contact with a sulfuric acid solution of iodate (a). Peaks: 1) CH_3I; 2) C_2H_5I; 3) $2\text{-}C_3H_7I$; 4) $1\text{-}C_3H_7I$; 5) $2\text{-}C_4H_9I$; 6) $1\text{-}C_4H_9I$; 7) $1\text{-}C_5H_{11}I$; 8) $2\text{-}C_6H_{13}I$; 9) $1\text{-}C_6H_{13}I$. Chromatogram of the organic phase (b), irradiated in contact with a solution of 0.2 M H_2SO_4 (– – – – – –) and $1.12 \cdot 10^{-2}$ M IO_3^- + 0.2 M H_2SO_4 (———). Peaks: 1) $1\text{-}C_4H_9I$; 2) $2\text{-}C_6H_{13}I$; 2') $1\text{-}C_6H_{13}I$; 3-7) isomers of dodecane; 8) n-dodecane.

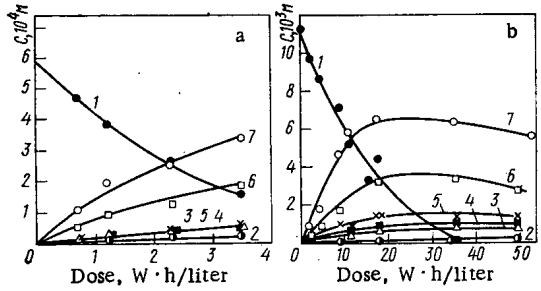

Fig. 2. Kinetic curves of the decomposition of IO_3^- at an initial concentration of $5.6 \cdot 10^{-4}$ M (a) and $1.2 \cdot 10^{-2}$ (b) in a solution of 0.2 M H_2SO_4 and formation of alkyl iodides in the organic phase: ●) decomposition of IO_3^-; ○) ΣRI; □) $\Sigma C_6H_{13}I$; ×) ΣC_4H_9I; Δ) C_2H_5I; ■) ΣC_3H_7I; ◑) CH_3I.

lengths [13]. It is convenient to compare the results obtained with the published data on homogeneous systems, devoted chiefly to the radiolysis of solutions of iodine in n-hexane; such a comparison brings us closer to an understanding of the mechanism of iodination of the organic phase in a more complex, two-phase system.

The irradiation of two-phase systems was performed on a ^{60}Co setup, containing 200,000 gram radium equivalents. The dose rate was 18 W/liter, dose range 0.3-50 W · h/liter. The experiments were conducted in glass ampoules with intensive mixing.

TBP and hexane were subjected to standard purification; cp grade KIO_3, H_2SO_4, and HNO_3 were used. The solutions were prepared in distilled water. The basic method of analysis of the radiolysis products in the organic phase was chromatography.* The instruments were a Khromass-2 (MKh-1312) with mass spectrometric detector and a Tsvet-106 with electron capture detector, a so-called detector of constant rate of recombination of ions (DCR). The standard substances for a comparison of the retention times were alkyl iodides: CH_3I; C_2H_5I; $1\text{-}C_3H_7I$ and $2\text{-}C_3H_7I$; $1\text{-}C_4H_9I$ and $2\text{-}C_4H_9I$; $1\text{-}C_5H_{11}I$; $1\text{-}C_6H_{13}I$ and $2\text{-}C_6H_{13}I$, grade "pure," which were supplementarily purified by boiling over copper shavings, followed by redistillation under vacuum.

Chromatographic Columns and Systems of Analysis. The Tsvet-106: Column length 2.7 m, inner diameter 4 mm, carrier gas "special purity" nitrogen. Gas flow rate: 40 ml/min through the column, 140

*The passage of water into the organic phase was also determined by the method of labeled atoms, using solutions of iodate labeled with ^{131}I, synthesized according to [14], as well as by a spectrophotometric method (on an SF-8 instrument).

Declassified and Approved For Release 2013/09/24 : CIA-RDP10-02196R000400060004-1

Declassified and Approved For Release 2013/09/24 : CIA-RDP10-02196R000400060004-1

TABLE 1. Radiation Chemical Yields of Alkyl Iodides

Substance	Concn. of IO_3^-, M			
	$5,6 \cdot 10^{-4}$	$1,12 \cdot 10^{-3}$	$5,6 \cdot 10^{-3}$	$1,12 \cdot 10^{-2}$
Methyl iodide	0,02	0,02	0,01	0,02
Ethyl iodide	0,06	0,04	0,04	0,13
2-Propyl iodide	0,02	0,06	0,08	0,10
1-Propyl iodide	0,02	0,01	0,04	0,09
2-Butyl iodide	0,01	0,01	0,10	0,06
1-Butyl iodide	0,05	0,13	0,16	0,20
1-Amyl iodide	0,01	0,02	0,08	0,03
3, 2 Hexyl iodide	0,15	0,27	0,50	0,39
1-Hexyl iodide	0,04	0,06	0,19	0,14
$G(\Sigma RI)$	0,38	0,62	1,16	1,16
$G(-IO_3^-)$	0,42	0,64	0,93	1,20

TABLE 2. Radiation Chemical Yields of Alkyl Iodides

Substance	Concn. of IO_3^-, M	
	$1,1 \cdot 10^{-3}$	$1,12 \cdot 10^{-2}$
Methyl iodide	0,02	0,04
Ethyl iodide	0,03	0,06
Σ 1,2-Propyl iodides	0,02	0,06
Σ 1,2-Butyl iodides	0,02	0,06
1-Amyl iodide	0,01	0,02
Σ 2-3-Hexyl iodides	0,31	0,58
1-Hexyl iodide	0,07	0,16
$G(\Sigma RI)$	0,48	0,97
$G(-IO_3^-)$	0,54	1,11

TABLE 3. Content of Alkyl Iodides in the Mixture, %

Compounds	Two-phase systems with IO_3^-		Homogeneous systems with I_2	
	25% TBP + hexane	hexane	20% TBP + hexane [6]	hexane [6]
Σ 1,2,3-Hexyl iodides	50	80	35	75
Σ 1,2-Butyl iodides	20	5	35	8
Σ (C_1-C_3) iodides	30	15	30*	17

*Calculated from the data of [6] according to the difference between $G(-I_2)$ and $G\Sigma(BuI + HeI)$.

ml/min through the detector, column temperature 70°C, input 180°C. Stationary phase Chromaton-SE-30 (Czechoslovakia). Khromass-2. Length of the capillary column 25 m, diameter 0.2 mm, carrier gas helium, rate of flow 60 ml/min, column temperature 80°C, input 200°C. Stationary phase apiezon L.

The concentration of iodate in the aqueous phase was measured by a polarographic method. The initial and irradiated solutions were neutralized with 1 M NaOH and then diluted with water to a background concentration of 0.1 M.

The results of radiolysis of a sulfuric acid solution of iodate ($1.12 \cdot 10^{-3}$ M), conducted in the range of doses 1-30 W·h/liter, showed that the radiation yield of the decomposition of iodate does not exceed 0.02-0.03 molecule/100 eV, which is evidence of its radiation stability under these conditions.

The radiolysis of sulfuric acid solutions of potassium iodate in contact with the organic phase (25% solution of TBP in n-hexane or n-hexane) was investigated in the interval of iodate ion concentrations $5.6 \cdot 10^{-4}$-$1.12 \cdot 10^{-2}$ M. It was found that under the action of radiation there is a passage of iodine into the organic phase; the amount of the iodine transferred depends on the radiation dose and the IO_3^- concentration in solution, and the yield of the decomposition of IO_3^- is far higher than under conditions of radiolysis of the aqueous phase alone. Spectrophotometric analysis of the irradiated organic phase in the ultraviolet and visible regions of the spectrum showed that the basic iodine-containing products detected in the investigated dose range are alkyl iodides, and to a small degree the complex TBP·I_2, the formation of which was ascertained in [15].

Figure 1a presents the general view of the chromatogram of the irradiated organic phase, taken a Tsvet-106 chromatograph with a DCR detector. The peaks detected coincide with the peaks of a standard mixture of C_1-C_6 alkyl iodides in n-hexane solution. The form and resolution of the peaks permitted calculations of the yields of these compounds with an accuracy of ~25% for low-boiling alkyl iodides (C_1-C_3) and with an accuracy within 5-10% for high-boiling alkyl iodides (C_4-C_6).

Figure 1b presents samples of chromatograms (Khromass-2 instrument) where together with the peaks of butyl and hexyl iodides, isomers of dodecane were identified according to [16]: 4,5-diethyloctane, 4-ethyl-5-methylnonane, 5,6-dimethyldecane, 5-methylundecane + 4-ethyldecane, and n-dodecane. For comparison a chromatogram of the same system, irradiated in the absence of iodate, is given; it is evident that when iodine passes into the organic phase, the yield of "dimers" – basic radiolysis products of hexane in the liquid phase – drops sharply.

Declassified and Approved For Release 2013/09/24 : CIA-RDP10-02196R000400060004-1

Declassified and Approved For Release 2013/09/24 : CIA-RDP10-02196R000400060004-1

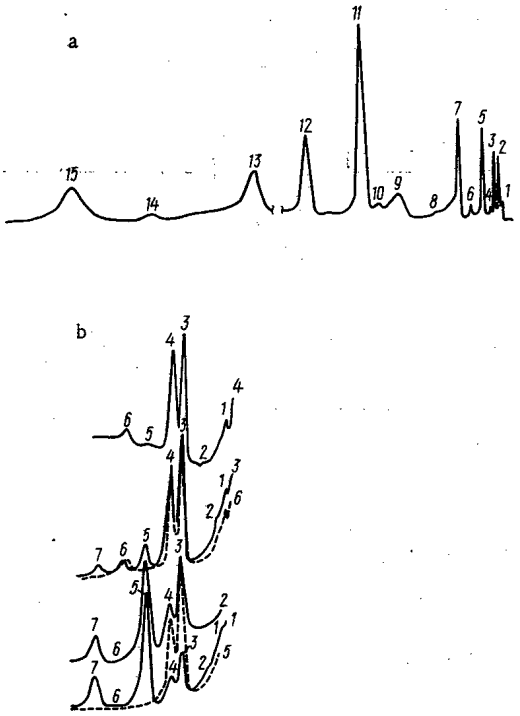

Fig. 3. Samples of chromatograms of the organic phase, irradiated in contact with nitric acid solutions of IO_3^-: a) Tsvet-106 chromatograph; b) Khromass-2. HNO_3 concentration: 1) 0.1 M; 2) 0.2 M; 3) 1 M; 4) 2 M; 5, 6) 0.1 and 1 M (without iodate), respectively. Peaks: 1, 2, 3, 4, 6) products of nitration; 5) 2-hexyl iodide; 7) 1-hexyl iodide.

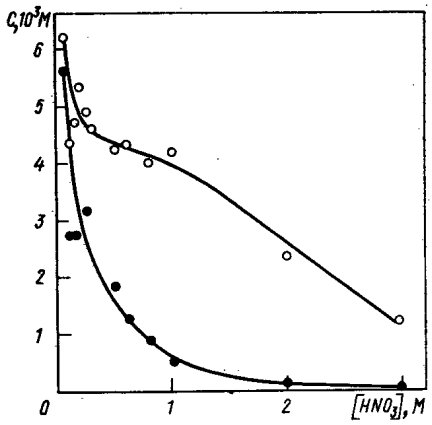

Fig. 4

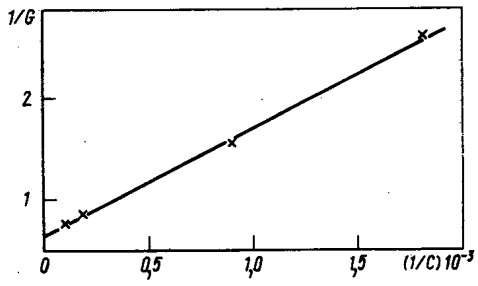

Fig. 5

Fig. 4. Dependence of the concentration of reacted iodate (○) and the sum of the alkyl iodides (●) on the HNO_3 concentration.

Fig. 5. Dependence of 1/G on the iodate concentration in a solution of 0.2 M H_2SO_4.

Figure 2 shows the kinetic curves of the radiolytic decomposition of iodate at initial concentrations of it in the aqueous phase at $5.6 \cdot 10^{-4}$ M and $1.12 \cdot 10^{-2}$ M (1) and, correspondingly, the accumulation of alkyl iodides (2-6) and their sum (7) in the organic phase. From this figure it follows that up to the radiation doses at which approximately half the iodate breaks down, constancy of its decomposition yield, with which

Declassified and Approved For Release 2013/09/24 : CIA-RDP10-02196R000400060004-1

Declassified and Approved For Release 2013/09/24 : CIA-RDP10-02196R000400060004-1

the yields of alkyl iodides are correlated, is noted. This correlation is well observed according to their sum, according to their basis components, especially according to hexyl iodides, and evidently also exists for light iodo derivatives, the accuracy of the determination of which, however, is insufficient for a final conclusion of this kind.

The constancy of $G(-IO_3^-)$ in the case of large initial concentrations of iodate (followed polarographically) was maintained up to high degrees of decomposition; however, the formation of alkyl iodides practically ceased in this case. Individual experiments conducted using iodate (^{131}I) showed that the cessation of the accumulation of alkyl iodides corresponds to a sharp slowdown of the capture of iodine by the organic phase. In experiments with low concentrations of IO_3^-, analogous phenomena were observed qualitatively.

From Table 1 it follows that with increasing iodate concentration, the summary yield of alkyl iodides increases. Within the limits of the error of the analysis, the composition of a mixture of alkyl iodides evidently can be considered unchanged.

Data on the radiolysis of pure hexane in contact with solutions of potassium iodate ($1.12 \cdot 10^{-3}$M; $1.12 \cdot 10^{-2}$ M) in 0.2 M H_2SO_4 are cited in Table 2.

Comparing these results with the data of Table 1, we can see that the yields of the decomposition of iodate and the summary yields of the alkyl iodides formed in this case, determined for two-phased systems containing and not containing TBP, practically coincide within the limits of error of the measurements. However, a substantial difference is the fact that in systems containing TBP, the relative content of butyl iodide in a mixture of alkyl iodides increases approximately 3-4-fold, while the fraction of hexyl iodides drops correspondingly. The data cited are evidence of a direct participation of the extraction reagent in the process of iodination. An analogous effect was also observed in an investigation of process of nitration of hydrocarbon solutions of TBP [17].

Experiments with nitric acid solutions of iodate were conducted at an initial iodate concentration of $1.2 \cdot 10^{-2}$ M and a dose of 12.3 W·h/liter; the HNO_3 concentration was varied from 0.1 to 3 M. An attempt was also made in this case to identify the basic iodine-containing radiolysis products.

Figure 3a presents a typical chromatogram of the organic phase possessing 15 peaks.

By varying the components of the irradiated phases: hexane, TBP +hexane in the organic phase and HNO_3, IO_3^- +HNO_3 in the aqueous phase, and also by comparing the data obtained with data on the radiolysis of IO_3^- in H_2SO_4 solution, it is possible to identify the peaks characterizing the iodine compounds in the investigated system.

1. The peaks 2-7, 11, 12 belong to normal and isomeric alkyl iodides (C_1-C_6).

2. Peaks 13-15 were assigned to the high-boiling radiolysis products of hexane, containing not only iodine, but also fragments of HNO_3 (the NO, NO_2, NO_3 groups).

3. Peak 9 can be assigned to iodine-containing nitric acid compounds, formed from TBP. In the radiolysis of sulfuric acid solutions of iodate, as well as nitric acid solutions that do not contain IO_3^-, peaks 9, 13-15 were not detected.

4. In the case of contact with concentrated solutions of HNO_3, in addition to peaks 1 and 10, the peaks of other alkyl nitrates appeared, the time of emergence of which under the conditions of the chromatographic column used was close to the time of emergence of the alkyl iodides.

The use of chromato-mass spectrometry permitted a distinct identification of 1- and 2-hexyl iodides against a background of the basic nitration solutions, in particular, 1-$C_6H_{11}NO_2$ and 2-$C_6H_{11}NO_2$ (see Figs. 3-6).

From a comparison of the results of analysis obtained by the indicated chromatographic methods, we determined the yields of alkyl iodides (C_1-C_6). From Fig. 4 it can be seen that with increasing HNO_3 concentration from 0.1 to 3 M, the yields of alkyl iodides dropped practically to zero, but a decomposition of iodate is noted, although the radiation yield of this decomposition is substantially lower than in dilute solutions of nitric acid. In this case it approaches the value reached in H_2SO_4 solution. Since the difference between the yield of the decomposition of iodate and the sum of the alkyl iodides formed exceeds the error of their determination, it can be concluded that the decomposing I_3^- is converted to compounds characterized by the chromatographic peaks 9, 13-15 (with increasing HNO_3 concentration, the areas of these peaks actually increase).

Declassified and Approved For Release 2013/09/24 : CIA-RDP10-02196R000400060004-1

Declassified and Approved For Release 2013/09/24 : CIA-RDP10-02196R000400060004-1

The aggregate of the data obtained permit the establishment of some features of the mechanism of the radiation chemical capture of iodine by the organic phase in the radiolysis of two-phased systems containing IO_3^- in the aqueous phase. Thus, comparing the results obtained for sulfuric acid solutions with data on the radiolysis of homogeneous organic systems in the presence of molecular iodine [5, 6], it can be concluded that within the limits of accuracy of the published data and our own data, the composition of alkyl iodides, their relative content in the mixture (Table 3), as well as the nature of the influence of iodine on the yields of isomeric dodecanes (see Fig. 2) in homogeneous and two-phase systems coincide. The data obtained permit us to assume that IO_3^- is reduced in the aqueous phase through lower oxides to I_2.

In view of the low concentration of iodate, it can be considered (according to [11]) that its conversion is related to the indirect action of radiation, absorbed chiefly by water, the reductive components of the radiolysis of which (H atoms) are the basic reagents.

The negligible yield of the reduction of IO_3^- in an aqueous acid solution at concentrations $\sim 5 \cdot 10^{-4}$–$5 \cdot 10^{-3}$ M in the presence of an organic phase increases to the values obtained in [11] for alkaline solutions, and considering reducing equivalents, leads to an approximate agreement with the yield of the reductive component of the radiolysis of water (G_H), calculated from the function $G_H = 5G(-IO_3^-)$ and equal to ~ 4 [18]. At high concentrations of IO_3^-, G_H even exceeds this value. To explain the low yield of the reduction of IO_3^- in aqueous solution, it should be assumed that the reduction of IO_3^- and the iodine-containing compounds in a lower valence state arising in this case is competed with by the oxidation of these compounds by the oxidative component of the radiolysis of water (OH radicals) with regeneration of IO_3^-.

In this case it should be considered that in acid solutions the solvated electron $\bar{e}_{aq}$, existing chiefly in alkaline solutions, is replaced by H atoms, which are weaker toward the reducing agent than $\bar{e}_{aq}$, [18].

Thus, the stimulating role of the organic phase in the radiation reduction of iodate can be explained by rapid extraction of molecular water, protecting it from the oxidizing influence of OH radicals; by interception of the OH radicals themselves by organic molecules at the interface (it is known that the OH radical reacts with saturated hydrocarbons according to the reaction: $RH + OH \rightarrow R + H_2O$ with very low activation energies [19]); by diffusion of H atoms formed in the organic phase, with their participation in the reduction of IO_3^-. The latter assumption would explain the yields of the decomposition of the iodate ion greater than would correspond to the known value of G_H in water. According to [2, 5], molecular iodine extracted from the aqueous phase is attacked by radicals and charged particles of the organic phase, giving alkyl iodides.

Although it is evident that all the enumerated processes in which H and OH participate can play a definite role in the reduction of iodate, the selection of the process controlling the rate of formation of alkyl iodides on the basis of the data obtained is still difficult. A mathematical treatment of this complex system is still premature, and we limited ourselves to a comparison of the data on the dependences of $G(-IO_3^-)$ on the IO_3^- concentration and the dose with simplified models. It was found that this dependence can be described by the expression

$$\frac{1}{G(-IO_3^-)} = \frac{1}{G_0(-IO_3^-)}\left(1 + \frac{K}{[IO_3^-]}\right),$$

obtained on the assumption of the existence of one particle that reduces IO_3^-, which is destroyed according to a first-order law. Figure 5 shows the linear dependence of $1/G(-IO_3^-)$ on $1/[IO_3^-]$. Extrapolation of $1/G(-IO_3^-)$ to zero $1/[-IO_3^-]$ gives a value of $G_0(-IO_3^-)$ corresponding to a value of G_H which is approximately 50% higher than the value of the yield of the reductive component of the radiolysis of water now known [20]. Possible causes of this were indicated above.

Experiments conducted with a nitric acid solution of iodate are evidence of a more complex combination of radiation chemical processes in comparison with sulfuric acid solutions. Thus, the decrease in the yield of the decomposition of iodate in moderately concentrated solutions of HNO_3 in comparison with solutions of H_2SO_4 indicates an inhibiting role of HNO_3. This role may be reduced to an interception of the reductive component of the radiolysis of water, as well as to chemical oxidation of the forms of iodine of lower valence, formed from IO_3^-. Possibly in the presence of nitric acid in the aqueous phase, the extractable forms of iodine also change: together with I_2, products of the type of INO, INO_2, etc. are obtained. The experiments also indicate the possibility of the formation in the investigated system not only of alkyl iodides, but also of bifunctional compounds, containing nitric acid groups and iodine, where the latter predominate in concentrated solutions of HNO_3. It is known that organic radicals formed in the photolysis of mixtures containing hydrocarbons, halogens, and nitrous oxide are capable of giving bifunctional com-

Declassified and Approved For Release 2013/09/24 : CIA-RDP10-02196R000400060004-1

Declassified and Approved For Release 2013/09/24 : CIA-RDP10-02196R000400060004-1

pounds of the type of 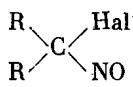 [21]; however, the properties of such compounds have not been studied.

On the basis of our data on chromatography, it can be asserted that the boiling point of such compounds, obtained in radiolysis, is significantly higher than the boiling point of the corresponding alkyl iodides.

LITERATURE CITED

1. Proc. IAEA Symposium "Reprocessing of Highly Irradiated Fuels," Vienna (1970).
2. E. Weber, P. Forsyth, and R. Schuler, Radiation Res., 3, 68 (1955).
3. P. Fessenden and R. Schuler, J. Amer. Chem. Soc., 79, 273 (1957).
4. D. Perner and R. Schuler, J. Phys. Chem., 70, 317 (1966).
5. H. Widmar and F. Gäumen, Helv. Chim. Acta, 46, No. 2, 766 (1963).
6. P. A. Zagorets et al., At. Énerg., 32, No. 5, 422 (1972).
7. P. A. Zagorets et al., At. Énerg., 34, No. 3, 205 (1973).
8. T. Rigg, Nature, No. 10, 933 (1960).
9. I. E. Nakhutin, et al., 4th Geneva Conference, 1971, Reports of the USSR [in Russian], No. 703.
10. E. Tachikawa et al., J. Appl. Rad. and Isotopes, 22, No. 12, 793 (1971).
11. M. Haissinsky, J. Jowe, and W. Szumansky, J. Chem. Phys., 1-2, 572 (1964).
12. N. Todd and S. Witcher, J. Chem. Phys., 20, 1172 (1952).
13. A. Swallow, The Radiation Chemistry of Organic Compounds [Russian translation], IL, Moscow (1963).
14. A. P. Musakin and L. V. Puchkov, Zh. Neorgan. Khim., 4, No. 2, 483 (1959).
15. H. Tsubomura and J. Klugman, J. Amer. Chem. Soc., 82, No. 56, 314 (1960).
16. Radioliz Uglevodorov, Akad. Nauk SSSR, Moscow (1971).
17. E. V. Barelko and I. P. Solyanina, At. Énerg., 38, No. 1, 23 (1975).
18. C. Jonak, E. Hart, and M. Matheson, J. Phys. Chem., 77, 1838 (1973).
19. E. T. Denisov, Rate Constants of Homolytic Reactions [in Russian], Nauka, Moscow (1974).
20. V. N. Kondrat'ev and E. E. Nikitin, Kinetics and Mechanism of Gas Phase Reactions [in Russian], Nauka, Moscow (1974).
21. A. Schoenberg, Preparative Organic Photochemistry, Springer-Verlag (1968).

Declassified and Approved For Release 2013/09/24 : CIA-RDP10-02196R000400060004-1

Declassified and Approved For Release 2013/09/24 : CIA-RDP10-02196R000400060004-1

SUPPRESSION OF VOLUME MODES OF THE FLUTE INSTABILITY IN AN OPEN MIRROR PLASMA BY MEANS OF AN ELECTRODE FEEDBACK SYSTEM

V. V. Arsenin and V. A. Chuyanov

UDC 533.951.8

In a number of recent experiments [1-3] it has been shown that it is possible to suppress surface modes of the flute instability in open mirror plasmas by means of a feedback system which controls an electromagnetic perturbation field outside the plasma. This system consists of electric potential (field) probes at the side surface of the plasma and external side electrodes whose potential is kept proportional to the signals from the corresponding probes by a special electronic circuit. Volume modes are not suppressed in such a system since, first of all, a side probe does not detect oscillations whose field goes to zero near the probe, and second, the field due to the side electrodes decreases toward the axis of the plasma and does not follow the structure of the radially oscillating field produced by the charged plasma particles. Proposed methods of stabilizing the volume modes include controlled sources [4-7] (for example, by means of weak beams acting directly in the plasma volume [6]) or a system with probes and electrodes located at the ends of the plasma [8].

In the present paper it is shown that the largest scale volume modes may also be suppressed (have their growth rate significantly reduced) by means of a surface system (side electrodes) if these modes are made observable by "measuring" the oscillations within the plasma. In this case it is not necessary to measure the disturbance throughout the plasma volume. It is sufficient to know it on a single radius. Since now the field of the surface (external) charges cannot everywhere compensate the space charge, the instability remains but its growth rate can be made arbitrarily small.

Model. Dispersion relations. To simplify the notation we shall use a "plane" model. Let a plasma, located in a uniform external magnetic field $B_0 \| z$, fill the plane layer $0 < x < a$, and have the density distribution

$$N = N_0\left(1 - \frac{x}{a}\right) \tag{1}$$

in this layer. A "gravitational" force with acceleration g acts in the x direction imitating the effect of the inhomogeneity in the external magnetic field in the actual mirror. We assume that the plasma is bounded by a metal surface at $x = 0$, and by a vacuum at $x = a - c$. We shall examine the stability of this distribution with respect to "flute" perturbations in the electrical potential,

$$\Phi = \varphi(x)\cos(ky - \omega t + \zeta)\, e^{\gamma t} + \psi(x)\sin\times(ky - \omega t + \zeta)\, e^{\gamma t}, \tag{2}$$

where the quantities φ, ψ, k, ω, γ, and ζ are real.

For simplicity we shall limit ourselves to the case of a rarefied plasma with $\omega_{0i} \ll \omega_{Bi}$, where $\omega_{0i} = (4\pi e^2 N_0/m_i)^{1/2}$ is the ion Langmuir frequency and $\omega_{Bi} = eB_0/m_i c$ is the ion cyclotron frequency. Then, in the expression for the induced plasma charge density wave, ρ, only the convective term is significant and, after separation of the "cosine" and "sine" parts, the Poisson equation, $\Delta\Phi = -4\pi\rho$, reduces to a system of two equations

$$\varphi'' - k^2\varphi - \lambda\varphi + \mu\psi = 0; \tag{3}$$

$$\psi'' - k^2\psi - \lambda - \mu\varphi = 0, \tag{4}$$

Translated from Atomnaya Énergiya, Vol. 39, No. 5, pp. 350-352, November, 1975. Original article submitted December 13, 1974.

©1976 Plenum Publishing Corporation, 227 West 17th Street, New York, N.Y. 10011. No part of this publication may be reproduced, stored in a retrieval system, or transmitted, in any form or by any means, electronic, mechanical, photocopying, microfilming, recording or otherwise, without written permission of the publisher. A copy of this article is available from the publisher for $15.00.

Declassified and Approved For Release 2013/09/24 : CIA-RDP10-02196R000400060004-1

Declassified and Approved For Release 2013/09/24 : CIA-RDP10-02196R000400060004-1

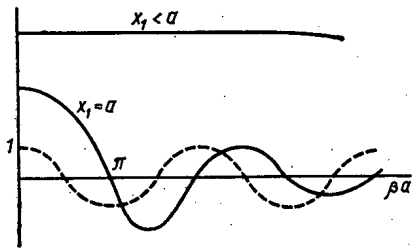

Fig. 1

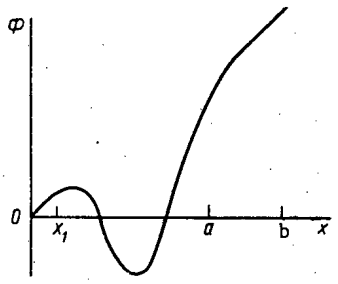

Fig. 2

Fig. 1. For the solution of Eq. (17): ——) the function $\delta \frac{a}{b-a} \frac{\sin \beta x_1}{\beta a}$;

– – –) $\cos \beta a$.

Fig. 2. Radial structure of the oscillations for $\alpha \neq 0$, $\beta \neq 0$.

where, for a two fluid model

$$\lambda(\omega, \gamma) = \frac{k\omega_{0i}^2}{a\omega_{Bi}} \left[\frac{\omega}{\omega^2+\gamma^2} - \frac{\omega+kV}{(\omega+kV)^2+\gamma^2} \right]; \tag{5}$$

$$\mu(\omega, \gamma) = \frac{k\omega_{0i}^2}{a\omega_{Bi}} \left[\frac{\gamma}{\omega^2+\gamma^2} - \frac{\gamma}{(\omega+kV)^2+\gamma^2} \right]. \tag{6}$$

Here $V = g/\omega_{Bi}$ is the drift velocity of the ions in the gravitational field.

The solution which satisfies the boundary conditions on the metal wall, $\varphi(0) = \psi(0) = 0$, is

$$\varphi = A \operatorname{sh} \alpha x \cos \beta x; \tag{7}$$

$$\psi = A \operatorname{ch} \alpha x \sin \beta x, \tag{8}$$

where A is a real constant, and the real quantities, α and β are related to λ and μ by the dispersion relations

$$\alpha^2 - \beta^2 = k^2 + \lambda; \tag{9}$$

$$2\alpha\beta = \mu. \tag{10}$$

The wave numbers α and β, as well as the frequency spectrum, are determined by the boundary conditions at the free surface ($x = a$) of the plasma.

If a metal wall is located at $x = b$, a distance from the plasma boundary much less than the characteristic wavelength k^{-1}, then [to within $k(b-a)$] $\varphi(a) = \psi(a) = 0$. Here, $\alpha = 0$; and $\beta = n\pi/a$. The oscillations in the n-th mode are unstable with density and have $\omega_{0i}^2 = \omega_{Bi} \frac{V}{a} (k^2a^2 + n^2\pi^2)$.

Let us assume that at the boundary of the plasma there are boundary conditions which differ from those on a simple conducting wall. Let the potential difference $\Phi(b, y, t) - \Phi(a, y, t)$ across the gap $a < x < b$ be kept (by a system of probes and electrodes with an electronic circuit) proportional to the potential of some interior surface $x = x_1$ with $x_1 < a$:

$$\varphi(b) - \varphi(a) = \delta\varphi(x_1) - \varepsilon\psi(x_1), \tag{11}$$

$$\psi(b) - \psi(a) = \delta\psi(x_1) + \varepsilon\varphi(x_1), \tag{12}$$

where δ and ε are real (For $\varepsilon \neq 0$ there is a phase shift.).* Then, from the continuity of the potential and of the normal component of the induction at the plasma boundary with the vacuum, we obtain (for $k(b-a) \ll 1$) the following system of (dispersion) equations for finding α and β:

$$\alpha a \operatorname{ch} \alpha a \cos \beta a - \beta a \operatorname{sh} \alpha a \sin \beta a - \delta \frac{a}{b-a} \operatorname{sh} \alpha x_1 \cos \beta x_1 + \varepsilon \frac{a}{b-a} \operatorname{ch} \alpha x_1 \sin \beta x_1 = 0; \tag{13}$$

$$\alpha a \operatorname{sh} \alpha a \sin \beta\alpha + \beta a \operatorname{ch} \alpha a \cos \beta a - \delta \frac{a}{b-a} \operatorname{ch} \alpha x_1 \sin \beta x_1 - \varepsilon \frac{a}{b-a} \operatorname{sh} \alpha x_1 \cos \beta x_1 = 0. \tag{14}$$

*We note that to maintain these conditions, measurements at two points ($x = x_1$ and $x = a$) are required.

Declassified and Approved For Release 2013/09/24 : CIA-RDP10-02196R000400060004-1

Declassified and Approved For Release 2013/09/24 : CIA-RDP10-02196R000400060004-1

Oscillations with Different Spatial Structure. We shall examine the system of Eqs. (13)-(14) in the special case of $\varepsilon = 0$, where it takes the form

$$\alpha a \operatorname{ch} \alpha a \cos \beta a - \beta a \operatorname{sh} \alpha a \sin \beta a = \delta \frac{a}{b-a} \operatorname{sh} \alpha x_1 \cos \beta x_1; \tag{15}$$

$$\alpha a \operatorname{sh} \alpha a \sin \beta a + \beta a \operatorname{ch} \alpha a \cos \beta a = \delta \frac{a}{b-a} \operatorname{ch} \alpha x_1 \sin \beta x_1. \tag{16}$$

There exist three types of solutions.

1. $\alpha = 0$, $\beta \neq 0$.* For $\alpha = 0$ Eq. (15) is evidently satisfied and Eq. (16) reduces to the form

$$\beta a \cos \beta a = \delta \frac{a}{b-a} \sin \beta x_1. \tag{17}$$

If $x_1 = a$ an infinite set of β's is obtained, of which the smallest value of β is on the order of a^{-1}. For $x_1 < a$, as can be seen from Fig. 1, the smallest value of βa may become $\gg 1$ (i.e., the oscillations may have shorter wavelengths). For $x_1 \ll a$ a sufficient condition for the absence of roots $\beta x_1 \lesssim 1$ is

$$|\delta| \frac{x_1}{b-a} \gg 1. \tag{18}$$

When Eq. (18) is satisfied, the smallest root βa is of order $\beta_{\min} a \sim |\delta| \frac{a}{b-a}$. From Eq. (9) it follows that as $\beta_{\min} a$ becomes larger for increased δ the threshold for instability with respect to density will increase as $\beta^2_{\min} a^2$ while the growth rate decreases.

2. $\beta = 0$, $\alpha \neq 0$ (Surface Waves). For $\beta = 0$ Eq. (16) is satisfied identically and Eq. (15) takes the form

$$\alpha a \operatorname{ch} \alpha a = \delta \frac{a}{b-a} \operatorname{sh} \alpha x_1. \tag{19}$$

This equation has a nonzero solution if $\delta\, x_1/(b-a) > 1$. This unique solution increases logarithmically with δ. From Eq. (9) it follows that the oscillations are stable provided

$$\alpha > k. \tag{20}$$

This type of wave is possible only for positive δ.

3. The system of Eqs. (15)-(16) may have solutions for which $\alpha \neq 0$ and $\beta \neq 0$ simultaneously. Assuming $x_1 \ll a$ we find roots $\alpha, \beta \ll x^{-1}$. In this region Eqs. (15)-(16) take the form

$$\operatorname{ch} \alpha a \cos \beta a - \frac{\beta}{\alpha} \operatorname{sh} \alpha a \sin \beta a = \delta \frac{x_1}{b-a}; \tag{21}$$

$$\frac{\alpha}{\beta} \operatorname{sh} \alpha a \sin \beta a + \operatorname{ch} \alpha a \cos \beta a = \delta \frac{x_1}{b-a}, \tag{22}$$

$$\operatorname{sh} \alpha a \sin \beta a = 0; \tag{23}$$

from which

$$\operatorname{ch} \alpha a \cos \beta a = \delta \frac{x_1}{b-a}. \tag{24}$$

Since it was assumed that $\alpha \neq 0$, it follows from Eq. (23) that $\beta a = n\pi$, $n = 1, 2, \ldots$. For $\delta > 0$ only even n are allowed as can be seen from Eq. (24); and for $\delta < 0$, odd n. Eq. (24) is soluble for α if $\delta\,(-1)^n \frac{x_1}{b-a} > 1$.

Then $\alpha = \frac{1}{a} \operatorname{Arch} \left[\delta (-1)^n \frac{x_1}{b-a} \right]$.

An instantaneous picture of the potential in the oscillations with $\alpha \neq 0$ and $\beta \neq 0$ is shown in Fig. 2. As opposed to cases 1 and 2, in oscillations of this type there is an additional wave propagating in the x direction. For example, for $\alpha a \gg 1$ the potential in the region $x \gg \alpha^{-1}$ has the form

$$\Phi = Ce^{\alpha x + \nu t} \cos (\beta x - ky + \omega t + \zeta). \tag{25}$$

*The root $\alpha = 0$, $\beta = 0$ corresponds to the trivial solution $\varphi = \psi = 0$.

Declassified and Approved For Release 2013/09/24 : CIA-RDP10-02196R000400060004-1

Declassified and Approved For Release 2013/09/24 : CIA-RDP10-02196R000400060004-1

If the number β (the "radial" mode number) is fixed, then the growth in α as δ increases is a stabilizing influence on the oscillations. We shall demonstrate this in the case of a plasma whose density is much greater than threshold when the growth rate $\gamma \gg kV$ so that the single fluid model is valid. In this case Eqs. (9)-(10) may be rewritten in the form

$$(\alpha - i\beta)^2 - k^2 = \frac{k^2 V \omega_{0i}^2}{a\omega_{Bi}(\omega + i\gamma)^2}. \tag{26}$$

For $\alpha = 0$ this equation gives an instability with $\omega = 0$ and $\gamma = \left[\frac{k^2 V \omega_{0i}^2}{a\omega_{Bi}(\beta + n^2\pi^2)}\right]^{1/2}$. As α increases the growth rate decreases. For $\alpha^2 \gg k^2 + \beta^2$ the growth rate is

$$\gamma \approx \left(\frac{k^2 V \omega_{0i}^2}{a\omega_{Bi}}\right)^{1/2} \frac{\beta}{\alpha^2} *. \tag{27}$$

Thus, a feedback system with external controlling electrodes and probes within the plasma can have a stabilizing effect, not only on the surface modes, but also on the lowest radial modes of volume flute oscillations.

LITERATURE CITED

1. V. Arsenin, V. Zhiltsov, and V. Chuyanov, in: Proc. IAEA Symposium Plasma Physics and Contr. Nucl. Fusion Research, Vol. 11, Vienna (1969), p. 515.
2. V. Chuyanov et al., in: Feedback and Dynamic Control of Plasma, AIP Conference Proceedings, No. 1, New York (1970), p. 180.
3. V. A. Chuyanov and E. G. Merfi, Pis'ma v Zh. Éksperim. i Teor. Fiz., 13, 533 (1971).
4. T. Simonen, T. Chu, and H. Hendel, Phys. Rev. Lett., 23, 568 (1969).
5. H. Furth and P. Rutherford, Phys. Fluids, 12, 2638 (1969).
6. V. A. Chuyanov, Pis'ma v Zh. Éksperim. i Teor. Fiz., 11, 598 (1970).
7. V. V. Arsenin, ibid., p. 267.
8. V. Arsenin, in: Proc. 6th European Conference on Contr. Fusion Plasma Physics, Moscow, July 30-August 4, 1973, p. 625.

*Since stabilized flute oscillations with $\alpha \neq 0$ and $\beta \neq 0$ have negative energy, weak pumping of waves with $\alpha \gg \beta \neq 0$ is accompanied by flow of energy from the plasma.

Declassified and Approved For Release 2013/09/24 : CIA-RDP10-02196R000400060004-1

Declassified and Approved For Release 2013/09/24 : CIA-RDP10-02196R000400060004-1

FOCUSSING INTENSE ELECTRON BEAMS BY A LONGITUDINAL FIELD

V. K. Plotnikov

UDC 537.533.2

In recent years there has been great interest in linear inductive electron accelerators with high-intensity beams and in injectors for various machines used to study collective particle accelerating techniques. In this case there are strict requirements on the beam parameters at the output of a linear inductive electron accelerator. One of these parameters is the phase volume of the transverse motion, which should be minimal. For random choice of the initial values of the parameters of the transverse motion and of the strength of the longitudinal focussing magnetic field, numerical calculations [1] have shown that the effective phase volume of the beam due to nonlinearities in the intrinsic fields increases significantly during the acceleration process. This effect will not occur if there is a stationary distribution function of the particles in phase space. Clearly, it is necessary to seek sufficiently easily realizable stationary distribution functions and external field configurations. A possible type of self-consistent solution of this problem for the case in which the density of particles increases monotonically (a nontubular beam) toward the beam axis is the subject of this paper.*

Derivation of the Self-Consistent Equations. Since the beam is axially symmetric it is convenient to use cylindrical coordinates, r, φ, z (The longitudinal z axis coincides with the beam axis.). We shall assume that the external longitudinal magnetic field H is uniform over the radius. Then the equations of motion in a Gaussian system (in the absence of relativistic conditions in the transverse direction) have the form

$$\frac{1}{\gamma}\frac{d}{dt}(\gamma\dot{r}) = r\dot{\varphi}^2 + 2\Omega r\dot{\varphi} + \frac{e}{m\gamma^3}\frac{\partial U}{\partial r}; \qquad \frac{d}{dt}[\gamma r^2(\dot{\varphi}+\Omega)] = 0. \tag{1}$$

Here $\Omega = eH/2mc\gamma$; e and m are the charge and rest mass of the electron; c is the speed of light; γ is the relativistic correction; U is the potential of the intrinsic electric field of the beam (The term with U also takes into account the effect of the φ-th component of the intrinsic magnetic field of the beam.).

From the second of Eqs. (1), we find an integral of the motion,

$$M = \gamma r^2(\dot{\varphi}+\Omega), \tag{2}$$

which signifies the angular momentum of the particles with respect to the beam axis. Finding $\dot{\varphi}$ from Eq. (2), substituting $\dot{\varphi}$ in the first of Eqs. (1), integrating, and again returning to $\dot{\varphi}$ by substituting from M from Eq. (2), we obtain the second integral of the motion,

$$J = \dot{r}^2 + \Omega^2 r^2 + (r\dot{\varphi} + r\Omega)^2 - \frac{2e}{m\gamma^3}U(r), \tag{3}$$

which is proportional to the energy of transverse motion of the particles.

In view of the axial symmetry of the beam the coordinate φ does not enter in the integrals of the motion. This makes it possible to consider the motion in a three-dimensional phase space, r, $\dot{r}$, $r\dot{\varphi}$ [3]. It is

*The problem of matching a beam with a focussing channel to a longitudinal field was first examined in [2]; however, there only the microscopic phase space distributions of the particles was considered.

Translated from Atomnaya Énergiya, Vol. 39, No. 5, pp. 353-356, November, 1975. Original article submitted October 30, 1974.

©1976 Plenum Publishing Corporation, 227 West 17th Street, New York, N.Y. 10011. No part of this publication may be reproduced, stored in a retrieval system, or transmitted, in any form or by any means, electronic, mechanical, photocopying, microfilming, recording or otherwise, without written permission of the publisher. A copy of this article is available from the publisher for $15.00.

Declassified and Approved For Release 2013/09/24 : CIA-RDP10-02196R000400060004-1

Declassified and Approved For Release 2013/09/24 : CIA-RDP10-02196R000400060004-1

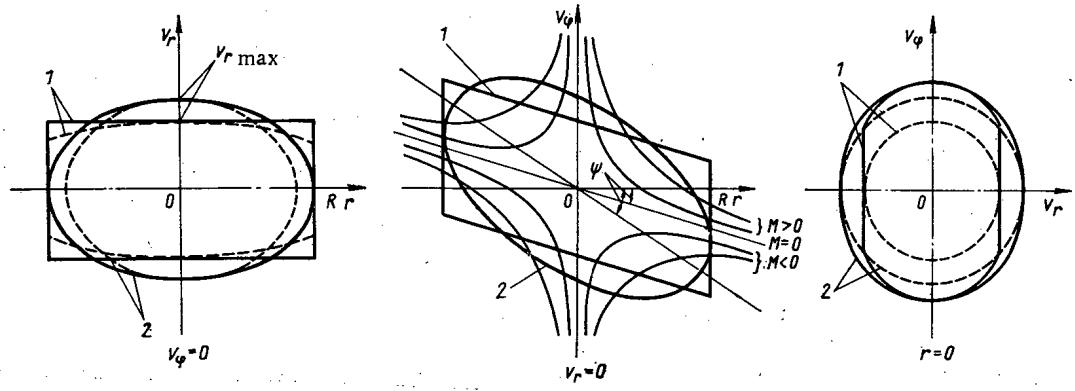

Fig. 1. Projections (——) and cross section (– – – –) of the phase volume of the beam on the phase planes $V_\varphi = 0$, $V_r = 0$, and $r = 0$ for the cases of large (1) and small (2) beam currents.

convenient to do the calculation in the coordinates $x = \frac{r}{R}$; $v_r = \frac{\dot{r}}{\Omega R}$; $v_\varphi = \frac{r\dot{\varphi}}{\Omega R} + \frac{r}{R}$, where R is the radius of the beam. Using the notation $i = \frac{J}{R^2\Omega^2}$ and $\alpha(x) = \frac{eU(x)}{m\gamma^3\Omega^2R^2}$, we obtain an expression for the second integral of the motion (assuming R and Ω to be constant):

$$i = x^2 + v_r^2 + v_\varphi^2 - 2\alpha(x). \tag{4}$$

The phase space distribution function of the particles is stationary if it depends only on the integrals of the motion. We shall consider the case in which the charge density in phase space is given by the function

$$n = (i_0 - i)^q n_0 = [i_0 - x^2 - v_r^2 - v_\varphi^2 + 2\alpha(x)]^q n_0 \quad \text{for} \quad i \leqslant i_0; \tag{5}$$

$$n = 0 \quad \text{for} \quad i > i_0, \tag{6}$$

where i_0 is the integral of the motion corresponding to the boundary of the phase volume; $i_0^q n_0$ is the charge density in the center of the phase volume; and, q is an integer ($q \geq 0$). For $x = 1$, we have $v_r = v_\varphi = 0$. Thus, the value of the integral i_0 (for particles with oscillation amplitude R) is

$$i_0 = 1 - 2\alpha(1) = 1 - 2\alpha_0. \tag{7}$$

Different values of q give different values of the drop in density toward the edge of the beam ranging from an equilibrium density ($q = 0$) to a δ function in the center ($q = \infty$). For intermediate values of q, a bell-shaped density distribution is obtained, which makes it possible (by selecting q) to approximate the actually occuring distribution with some accuracy. From the Poisson equation we find the relation of U to the particle density in real space ρ, and ρ in turn is expressed in terms of n by the relation

$$\rho = \int n\, dv_r\, dv_\varphi, \tag{8}$$

where the integration is over limits determined by Eq. (4) for $i = i_0$. The integration yields

$$\rho = \frac{\pi n_0 R^{2+2q}}{1+q}[1 - 2\alpha_0 - x^2 + 2\alpha(x)]^{1+q}. \tag{9}$$

Substituting the expression for ρ (x) into the formula for U, and U into Eq. (5), we obtain an integral equation for the unknown function α (x):

$$\alpha(x) = \frac{AR^{2q}}{1+q}\int_0^{x^2}\frac{1}{\zeta}\int_0^{\zeta}[1 - 2\alpha_0 - \xi + 2\alpha(\xi)]^{1+q}\, d\xi\, d\zeta. \tag{10}$$

In Eq. (10)

$$A = \frac{\pi mc^2 n_0 R^2}{e\gamma H^2}. \tag{11}$$

Declassified and Approved For Release 2013/09/24 : CIA-RDP10-02196R000400060004-1

Declassified and Approved For Release 2013/09/24 : CIA-RDP10-02196R000400060004-1

The constant A may be expressed in terms of the beam current I by means of the expression

$$\frac{I}{\beta c} = 2\pi \int_0^R \rho(r)\, r\, dr = \frac{2\pi e \gamma H^2 R^{2+2q}}{(1+q)\, mc^2} f_1(A), \tag{12}$$

where the density n_0 is related to A and the beam parameters through Eq. (11). One of the basic beam parameters is the magnitude of the phase volume. Since it is easiest to obtain a measurement of the projection of the phase volume V_r on the r plane, $m\gamma\dot{r}$, we now give the relation between V_r, the beam parameters, the constant A, and the field strength H:

$$V_r = \frac{2eHR}{\pi mc^2} \int_0^1 \sqrt{1 - 2\alpha_0 - x^2 + 2\alpha(x)}\, dx = \frac{2eHR}{\pi mc^2} f^{-1}(A). \tag{13}$$

Equation (10), together with Eqs. (11)-(13), allows us to find self-consistent expressions for the boundary of the stationary phase space volume of the beam and for the radial charge density distribution, and to establish the relations between the beam current, the radius, the phase volume, the energy, and strength of the focussing magnetic field.

The solution to Eq. (10) will now be sought in the form

$$\alpha = \sum_{k=1}^{\infty} C_k x^k. \tag{14}$$

Since a power function of x lies under the integral sign in Eq. (10), writing α as a series also results, after integration, in a series. This series has only even powers of x because of the axial symmetry of the beam. Substituting Eq. (14) in Eq. (10) and equating coefficients of equal powers of x on the right and left sides, we find expressions for C_k in terms of A and α_0, the relationship between which is determined by $\alpha_0 = \alpha$ (1).

Dividing Eq. (12) by the square of Eq. (13), we eliminate H and obtain an expression linking only the parameters of the beam and A:

$$F(A) = f_1(A)\, f^2(A) = \frac{2e}{mc^3\pi^3} \frac{(1+q)\, I}{\beta\gamma V_r^2 R^{2q-2}}. \tag{15}$$

Knowing F(A), it is possible to find A as a function of the known parameters of the beam. Then, substituting this quantity in Eq. (13) solved for H, we can obtain the intensity of the focussing field at which the beam will have a stationary distribution function:

$$H = \frac{\pi mc^2 V_r}{2eR^2} f(A). \tag{16}$$

It is of interest to consider two limiting cases which allow the problem to be solved completely in analytic form. Let the coefficient in front of the integral in Eq. (10) satisfy

$$\frac{AR^{2q}}{1+q} \gg 1 \tag{17}$$

("large current" case). Then the function under the integral of Eq. (10) tends to a constant value, $1 - 2\alpha_0$, in the interval $0 \le r \le R$. This takes place because for large A the coefficients C_k with large k in the expansion for α (14) are the largest (it is easy to see that in general each succeeding coefficient is expressed in terms of the product of the preceding coefficients multiplied by A; thus, the higher the number k, the higher the power of A in the numerator of the coefficient C_k. Only after some k does the increase in the denominator, which contains k^2, begin to overcome the growth in the numerator.). As a result, the term x^{2k} has the largest value, corresponding to the largest C_k, and as A increases the quantity $1 - 2\alpha$ (x) approaches a table-shaped (square pulse) form.

Substituting the value of the function $1 - 2\alpha_0$ under the integral into Eq. (10), integrating with x = 1 and approximately solving the resulting equation, we have

$$1 - 2\alpha_0 \approx \left(\frac{1+q^2}{2AR^{2q}}\right)^{1/(1+q)}, \tag{18}$$

Declassified and Approved For Release 2013/09/24 : CIA-RDP10-02196R000400060004-1

Declassified and Approved For Release 2013/09/24 : CIA-RDP10-02196R000400060004-1

from which, taking Eqs. (9) and (11) into account, we find an expression for the constant (across the beam area) charge density:

$$\rho = \frac{e\gamma H^2}{2mc^2}. \tag{19}$$

The dependence of the strength of the focussing field on the beam parameters is obtained from Eq. (12) and is

$$H = \frac{1}{R}\sqrt{\frac{2mc}{\pi e}\frac{I}{\beta\gamma}}. \tag{20}$$

Equation (13) and (11) make it possible to find the relation between the two-dimensional phase volume V_r and A, and to rewrite condition (17) for the applicability of Eqs. (18)-(20) in terms of the beam parameters:

$$\frac{1}{2}\left[\frac{8eIR^2}{\pi^3 mc^3\beta\gamma V_r^2}\right]^{1+q} \gg 1. \tag{21}$$

For small densities ("small current" case)

$$\frac{AR^{2q}}{1+q} \ll 1. \tag{22}$$

We shall neglect α and α_0 in the part of Eq. (10) under the integral. Then

$$\rho = \frac{e\gamma H^2 R^{2q} A}{(1+q)\,mc^2}\left[(1-x^2)^{1+q} - \frac{2AR^{2q}}{2+q}\sum_{p=0}^{1+q}\frac{(1-x^2)^{2+q-p}}{2+q-p}\right]. \tag{23}$$

Integrating Eqs. (12) and (13), including the function α (x) and eliminating A from the result, we find H as a function of the beam parameters,

$$H = \frac{mc^2 V_r}{eR^2}\left[1+\sqrt{1+\frac{eIR^2}{\pi mc^3\beta\gamma V_r^2}\sum_{p=0}^{1+q}\frac{(3+2q-2p)!!}{(2+q-p)!!\,(2+q-p)}}\right], \tag{24}$$

and rewrite Eq. (21) in the form

$$\frac{eIR^2}{4\pi mc^3\beta\gamma V_r^2} \ll 1. \tag{25}$$

Interpretation of Results. In the three-dimensional phase space r, $\dot{r}$, $r\dot{\varphi}$ the trajectories of particles having the same integral i lie on the surface described by Eq. (4). For $i = i_0$ this surface is the boundary of the matched phase volume of the beam. The surface i = const is symmetric with respect to the plane $\dot{r} = 0$. In the case of a small current the surface is an ellipsoid, the projection of which on the plane $r\dot{\varphi} = 0$ is a canonical ellipse, and on the plane $\dot{r} = 0$ is an ellipse with axes rotated relative to the coordinate axes by an angle Ψ (see Fig. 1).

A family of trajectories with the same integral M forms a cylindrical surface parallel to the r axis. It is clear from Eq. (2) that the equation of this surface is independent of the phase density of the current. Evidently, the phase trajectories of the particles are the lines of intersection of the surfaces M = const and i = const. For M = 0 the azimuthal velocity $r\dot{\varphi}$ is also zero. Thus, the projections of the phase trajectory of a particle with M = 0 and $i = i_0$ on the planes r = 0 and $r\dot{\varphi} = 0$ coincide with the boundary of the projection of the phase volume on these planes for arbitrary current, but the amplitude of the oscillations of such a particle is maximal.

Depending on the increase in the phase density, the phase volume begins to transform from an ellipse into a figure whose projection on the plane $r\dot{\varphi} = 0$ approaches a rectangle, and on the plane $\dot{r} = 0$, a parallelogram (The dashed line in the figure denotes the cross section of the phase volumes of the corresponding planes.).

It is easy to see that for any value of the density, n_0, the cross section of the phase volume in the planes r = const has different maximal dimensions in the directions $\dot{r}$ and $r\dot{\varphi}$. For small currents the ratio of the greatest dimension in the $\dot{r}$ direction to the beam radius R (ratio of the semiaxes of the matched volume) is

Declassified and Approved For Release 2013/09/24 : CIA-RDP10-02196R000400060004-1

Declassified and Approved For Release 2013/09/24 : CIA-RDP10-02196R000400060004-1

$$\frac{\dot{r}_{max}}{R} = \frac{eH}{2mc\gamma}. \tag{26}$$

Knowing r_{max}, it is easy to obtain an expression for the values of the phase volume in the $r, \dot{r}$ and $r, r\dot{\varphi}$ planes (We denote the volume in the second case by V_{φ}.). Substitution of the aperture radius a into these formulas transforms them into formulas for the throughputs V_{kr} and $V_{k\varphi}$:

$$V_{kr} = V_{k\varphi} = \frac{eHa^2}{2mc^2}. \tag{27}$$

In the case of large currents the main defocussing factor is Coulomb repulsion of the particles and not the initial scatter of the particles in transverse velocities. Thus, for large currents the choice of the magnetic field strength and the aperture determines the limiting current,

$$I_{lim} = \frac{\pi e\beta\gamma H^2 a^2}{2mc}, \tag{28}$$

and the phase volume of the beam may be arbitrary, subject to Eq. (21). The ratio of the semiaxes of the matched volume is given by

$$\frac{\dot{r}_{max}}{R} = \frac{\pi c V_r}{4\gamma R^2}. \tag{29}$$

All this leads to a need to include a new element in a linear inductive accelerator, a matching channel located between the electron gun and the focussing channel of the accelerator itself. Along the length of the matching channel the phase volume of the beam must be transformed from its initial form (determined by the gun design) to a matched form without destruction of the axial symmetry of the beam. Since both projections (V_r and V_{φ}) of the phase volume must be transformed at the same time and to the same degree, the elements of the matching channel must evidently be lenses with a longitudinal magnetic field. At the moment the beam particles leave the cathode they have equal probability of moving in any transverse direction, i.e., the projections of the phase volume of the beam on the $r, \dot{r}$ and $r, r\dot{\varphi}$ planes are equal. If there is no magnetic field on the cathode, the moment, M, for particles with $\dot{r} = r\dot{\varphi} = 0$ is zero. The quantity M for each particle is kept constant not only in a longitudinally uniform field, but also for H varying along the z axis (law of conservation of the generalized azimuthal momentum [4]). Thus, if the field at the cathode is zero, the phase volume is automatically matched with respect to the angle of inclination to the axis in the $\dot{r} = 0$ plane.

Therefore, a stationary distribution of the particles in phase space may be obtained for any value of the phase density and for various radial drops in the beam density space. For very high values of the phase density, the matched particle density distributions in real and phase space are uniform. Obtaining a stationary distribution function assumes the presence of a definite form for the phase volume of the beam at the inlet of the focussing channel. This leads to a requirement for a new element in the linear inductive accelerator, a matching channel. Matching of the phase volume with respect to the angle of inclination of the axes in the plane of the azimuthal motion takes place automatically if there is no magnetic field at the electron beam cathode of the accelerator.

The author is deeply grateful to V. S. Kuznetsov, R. P. Fidel'skaya, G. I. Trubnikov, I. M. Kapchinskii, and A. A. Drozdovskii for constant interest in this work.

LITERATURE CITED

1. V. S. Kuznetsov and R. P. Fidel'skaya, Zh. Tekh. Fiz., 40, No. 10, 2099 (1970).
2. I. M. Kapchinskii, Particle Dynamics in Linear Resonant Accelerators [in Russian], Atomizdat, Moscow (1966).
3. N. F. Ivanov, Yu. P. Sivkov, and A. I. Solnyshkov, Pribory i Tekh. Éksperim., No. 5, 30 (1965).
4. B. Lepert, The Dynamics of Charged Particles [in Russian] Atomizdat, Moscow (1967).

Declassified and Approved For Release 2013/09/24 : CIA-RDP10-02196R000400060004-1

Declassified and Approved For Release 2013/09/24 : CIA-RDP10-02196R000400060004-1

DEPOSITED PAPERS

A LIQUID-METAL REACTOR CONTROL SYSTEM

É. Ya. Platatsis, É. Ya. Tomsons,
V. V. Gavars, A. É. Mikel'sons,
Yu. A. Roshcheev, N. N. Petrov, and
and Yu. A. Sobolev

UDC 621.039.515:621.039.59

Recently, systematic studies have been made of control and protection systems for nuclear reactors employing various liquids [1, 2]. A liquid-metal control system is considered whose essence is that a molten alloy is supplied to a cavity within the core. Two alloys have been tested: InGaSn which has a high neutron cross section, and GaSn which is an inert alloy.

The control principle is based on replacing one alloy by the other in the controller (Fig. 1). The liquids are separated by elastic membranes and do not mix, and they circulate along pipelines to a balancing tank and controller. The alloys are circulated and kept at the necessary volume relationship in the control unit by electromagnetic pumps.

This system has been used on a critical assembly at the Institute of Physics, Academy of Sciences of the Latvian SSR. The control unit was placed in the graphite reflector at a distance of 70 mm from the edge of the core. The system has been used as a power compensator or manual control for more than two years. The overall change in reactivity on removing the neutron absorber from the controller is 0.375%, and occurs in 7-8 sec.

The system provides stable maintenance of a given power level in the assembly. The performance is dependent on the amount of alloy of each type in the controller, and it varies nearly linearly. Also, such a controller has higher thermal stability than many liquid controllers of other types, while it has a high neutron absorption cross-section and is free from radiolysis products in the absorber. The working materials

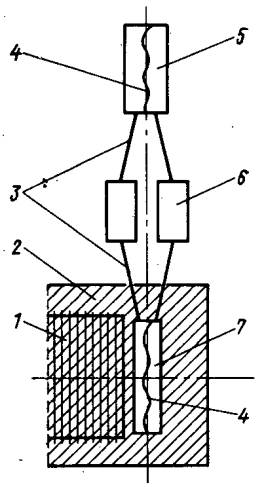

Fig. 1. Structural diagram of the liquid-metal control system: 1) core; 2) reflector; 3) pipework; 4) membranes; 5) compensator; 6) electromagnetic pumps; 7) controller.

Translated from Atomnaya Énergiya, Vol. 39, No. 5, pp. 358-361, November, 1975.

©1976 Plenum Publishing Corporation, 227 West 17th Street, New York, N.Y. 10011. No part of this publication may be reproduced, stored in a retrieval system, or transmitted, in any form or by any means, electronic, mechanical, photocopying, microfilming, recording or otherwise, without written permission of the publisher. A copy of this article is available from the publisher for $15.00.

Declassified and Approved For Release 2013/09/24 : CIA-RDP10-02196R000400060004-1

Declassified and Approved For Release 2013/09/24 : CIA-RDP10-02196R000400060004-1

are liquid metals, so there may be some corrosion of the constructional materials above 600°K, which hinders material choice.

The results indicate that after final development of the individual units, the system can be recommended for use in reactors with small geometrical dimensions.

LITERATURE CITED

1. R. R. Ionaitis, Atomnaya Tekhnika za Rubezhom, No. 5, 15 (1973).
2. R. R. Ionaitis and B. N. Tyunin, Atomnaya Tekhnika za Rubezhom, No. 7, 17 (1974).

Original article submitted December 13, 1974.

THE METHOD OF SUCCESSIVE LINEARIZATION IN PROBLEMS OF OPTIMIZING NUCLEAR REACTOR OPERATING CONDITIONS

V. V. Khromov and A. A. Kashutin

UDC 621.039.516:621.039.526

This paper is devoted to the development of the method of successive linearization [1, 2] for optimizing nuclear reactor operating conditions by computer calculations.

A method is formulated for optimizing refueling for a given reactor power distribution during the operating period. Criteria for optimum conditions are formulated in terms of linear-fractional functionals of the neutron distribution and various characteristics of the isotopic composition of the fuel. The controlling parameters of the problem which are varied to achieve optimum reactor operation are the volume fractions of the fuel with a different power production in each reactor region, the useful life of the reactor between refuelings, the sizes of the regions, the enrichment of the initial fuel loading, the placement of the controls for reactivity compensation and energy release rate, and their volume fractions during the operating period. A broad class of refueling conditions is considered which satisfy the following criteria: from each reactor zone the fuel may not only be discharged into storage but also reloaded into other zones; fuel which has achieved the allowed burnup is discharged only into storage; fuel in storage which has not reached the allowed burnup can be recharged into the reactor in the latter stages of operation; in refueling fresh fuel can be loaded into each reactor zone.

The apparatus of linear perturbation theory has been developed to calculate burnup and refueling [3, 4], and efficient methods are proposed for calculating the spatial and temporal neutron distributions and the isotopic composition of the reactor [3, 5] permitting an appreciable shortening of the calculations involved in solving the optimization problem with an admissible loss in calculational accuracy.

The proposed method serves as a basis for a complex of programs for calculational and optimization studies of fast reactor operating conditions within the limits of an effective four-group diffusion approximation for a one-dimensional space model during six operating intervals between refuelings. The programs of the complex are written in FORTRAN for a BÉSM-6 computer. Test problems run with these programs gave reliable results.

The complex of programs developed can be used to optimize reactor operating conditions in a certain limited interval of time and to optimize transient and steady-state reactor operating conditions.

LITERATURE CITED

1. R. P. Fedorenko, Zh. Vychisl. Matem. i Matem. Fiz., 4, No. 6, 1045 (1964).
2. A. M. Kuz'min et al., in: Physics of Nuclear Reactors [in Russian], No. 1, Atomizdat, Moscow (1968), p. 92.
3. V. V. Khromov, A. A. Kashutin, and V. V. Glebov, At. Énerg., 37, No. 1, 59 (1974).
4. V. V. Khromov, A. A. Kashutin, and L. V. Tochenyi, in: Programs and Methods of Physical Calculation of Fast Reactors [in Russian], Dimitrovgrad, (1975), p. 434.

Declassified and Approved For Release 2013/09/24 : CIA-RDP10-02196R000400060004-1

Declassified and Approved For Release 2013/09/24 : CIA-RDP10-02196R000400060004-1

5. V. V. Khromov, A. A. Kashutin, and V. V. Glebov, At. Énerg., 36, No. 5, 385 (1974).

Original article submitted January 3, 1975

CHARACTERISTICS OF THE γ ACTIVATION OF LIGHT ELEMENTS

M. G. Davydov, A. P. Naumov, and V. A. Shcherbachenko

UDC 543.53

The contemporary level of development of γ-activation analysis, the broadening of its range of application, and the use of calculational methods in the development of specific procedures necessitates a systematization of the material. At the present time there is no handbook on γ-activation analysis. The published tables enable one only to estimate the possibilities in principle of the γ-activation method but do not give a complete collection of nuclear physical constants, particularly the photonuclear cross sections necessary for the development of specific analytical procedures.

We present material on the photoactivation of light elements (up to and including potassium) taking account of the following limitations: the abundance of the irradiated element $\geq 1\%$; the reactions are of the type (γ, n), (γ, p), (γ, pn), $(\gamma, 2n)$, $(\gamma, 2p)$, and (γ, α); the half-lives of the γ-activation products are 10^{-6} sec $\leq T_{1/2} \leq 10^{7}$ sec; the intensity of the β and γ radiation $\geq 1\%$.

The experimental data on photonuclear cross sections were approximated by a sum of Lorentz curves.

The collected material is presented in a table which shows that nearly all the necessary nuclear physical constants, including the characteristics of photonuclear reactions which are of interest for practical γ-activation analysis, are known at the present time. This permits the use of calculational methods for the development of specific analytical procedures of γ-activation determination of light elements.

Original article submitted January 3, 1975.

TISSUE DOSES FROM NEUTRON RADIATION

V. N. Ivanov, L. F. Ivanova, E. N. Parfenov, and Yu. S. Ryabukhin

UDC 577.3:539.12.04+539.125.52

The spatial distribution of tissue dose from neutron beams with radii of 0.5, 1.5, 2.5, 4.5, and 6.5 cm has been calculated by the Monte Carlo method for primary neutron energies of 0.1, 5, 20, 100, 500, and 1000 keV incident normally on the surface of tissue 30 cm thick. Doses from recoil protons, heavier recoil nuclei, protons from the (n, p) reaction in nitrogen, and γ rays from the (n, γ) reaction in hydrogen were computed. In the calculations the chemical composition of tissue in mass % was taken as: H, 10.1; C, 12.1; O, 73.6; and N, 3.1.

Starting from the condition of normal incidence of the beams we have determined the variation of the tissue dose with depth and with the distance from the axis of the beams. The absorbed energy was averaged over hollow cylinders with radii of 0.5, 1.5, 2.5, 3.5, 4.5, 6.5, 8.5, 10.5, 15, 20, 25, and 40 cm. The cylinders were 1 cm high at depths from 0 to 6 cm, 2 cm high at depths from 6 to 20 cm, 4 cm high at depths from 20 to 24 cm, and 6 cm high at depths from 24 to 30 cm.

The results are presented in the form of an atlas of components of tissue doses in rads normalized to a neutron fluence of 1 neutron /cm^2. The dose distributions shown in Fig. 1 are for a beam of 1-MeV neutrons 2.5 cm in radius. The curve for $r = 0$ describes the depth variation of dose in the cross section of the beam. The average radii of the hollow cylinders are shown on the remaining curves. The total energy absorbed in the cylindrical volumes at a given depth corresponds to irradiation by a broad beam of neutrons. These results are shown by dashed curves.

Declassified and Approved For Release 2013/09/24 : CIA-RDP10-02196R000400060004-1

Declassified and Approved For Release 2013/09/24 : CIA-RDP10-02196R000400060004-1

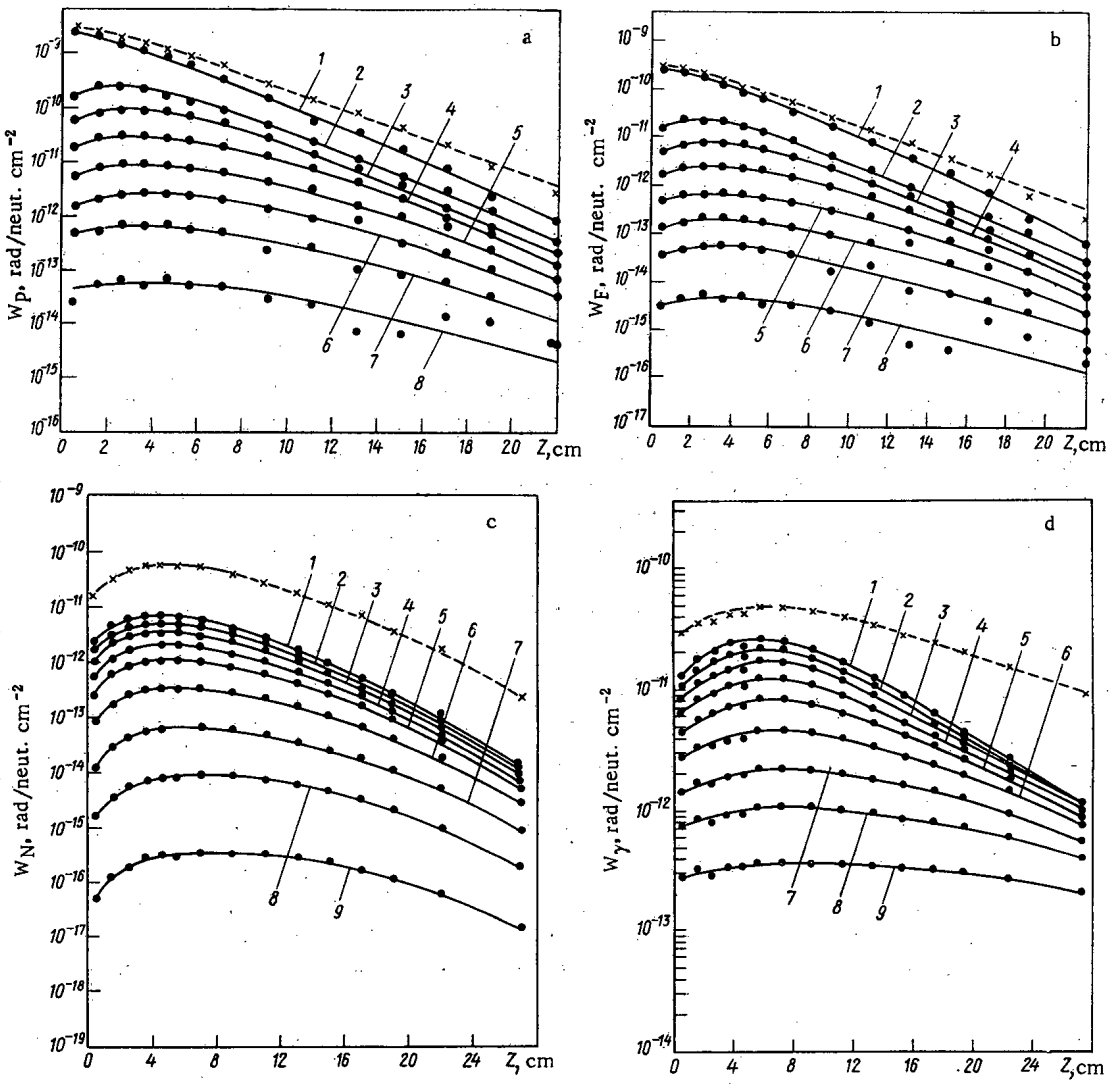

Fig. 1. Components of tissue dose for irradiation by a beam of 1-MeV neutrons 2.5 cm in diameter; a, b) doses from recoil protons and heavier recoil nuclei for various radii in cm: 1) 0; 2) 3; 3) 4; 4) 5.5; 5) 7.5; 6) 9.5; 7) 12.7; 8) 17.5; c, d) doses from protons from the $^{14}N(n,p)$ ^{14}C reaction and γ rays from the $^{1}H(n,\gamma)^{2}H$ reaction for various radii in cm: 1) 0; 2) 4; 3) 5.5; 4) 7.5; 5) 9.5; 6) 12.7; 7) 17.5; 8) 22.5; 9) 32.5; ×) broad beam.

The atlas of dose distributions can be used in clinical dosimetry for planning neutron therapy, in diagnostics by activation analysis, and in emergency dosimetry.

Original article submitted March 3, 1975.

Declassified and Approved For Release 2013/09/24 : CIA-RDP10-02196R000400060004-1

Declassified and Approved For Release 2013/09/24 : CIA-RDP10-02196R000400060004-1

USE OF VARIOUS METHODS OF DETERMINING THE OVERALL ERROR OF ABSORBED-DOSE MEASUREMENT WITH CALORIMETERS AND CHEMICAL DOSIMETERS

V. A. Berlyand, Yu. S. Gerasimov,
V. V. Generalova, M. N. Gurskii,
and A. V. Tultaev

UDC 539.12.08

The paper deals with two methods of determining the overall error in indirectly measured quantities. Detailed derivations are given for the formulas that define the random, systematic, and overall errors, as corresponding to a given confidence level. The derivation is based on the dispersion of a combination of distributions as a sum of the dispersions of the components.

The formulas correspond to independent measured quantities and two types of distribution for the residual systematic errors: normal (Gaussian) and uniform (within a certain range).

Recommendations are made on writing programs for computer calculation of the random, systematic, and overall errors. Results are presented from a Mir-1 computer for the errors of measurement for absorbed dose using calorimeters of two different types and also chemical dosimeters (ferrous sulfate and glucose).

In particular cases, recommendations may be made on the choice of the optimal range for measuring a characteristic in which the error of measurement becomes minimal, and ranges are indicated where the overall error increases rapidly on account of the increase in the influence function.

Then the overall error is less than the sum of the systematic and random errors for a given confidence level, while the overall error is less than the square root of the sum of the squares of the systematic and random errors when there is a uniform distribution for the residual systematic errors. The overall and systematic errors calculated for uniform distributions in the latter are 20-40% higher than the errors for a normal distribution.

A method is given for determining the overall and systematic error for uniform distributions in the latter.

Original article submitted February 20, 1975.

Declassified and Approved For Release 2013/09/24 : CIA-RDP10-02196R000400060004-1

Declassified and Approved For Release 2013/09/24 : CIA-RDP10-02196R000400060004-1

LETTERS TO THE EDITOR

DOSE DEPENDENCE OF POROSITY IN NICKEL ON IRRADIATION WITH NICKEL IONS

S. Ya. Lebedev, S. D. Panin, and S. I. Rudnev

UDC 621.039.51

The development of porosity in nickel samples irradiated with nickel ions in an ILU-100 accelerator [4] as a result of the merging of vacancies was discussed earlier [1-3], and the influence of earlier implanted helium on pore development in nickel was considered. In the present investigation we determined the manner in which the porosity varied with irradiation dose. Samples of commercially pure nickel 0.15 mm thick (previously annealed and thinned for examination in the electron microscope) were irradiated with 46-keV nickel ions at 550°C (dose $2 \cdot 10^{16}$–$3.2 \cdot 10^{17}$ ions/cm^2, current density 3 μA/cm^2).

Electron-microscope examination showed a considerable number of pores, statistically and uniformly distributed over the area under consideration, in all the irradiated samples. Starting from a dose of $8 \cdot 10^{16}$ ions/cm^2 the pores have the shape of cubes with truncated vertices. For doses of $2 \cdot 10^{16}$ and $4 \cdot 10^{16}$ ions/cm^2 (Table 1) the shape of the pores cannot be readily determined because of their small size.

Figure 1 shows the concentration and mean size of the pores as well as the degree of swelling in relation to integrated radiation dose.

In calculating the pore concentration and the degree of swelling, the layer in which the porosity developed was taken as being 400 Å thick [6]. We see from the curves that with increasing dose of irradiation the mean pore size gradually increased, and for a dose of $3.2 \cdot 10^{17}$ ions/cm^2 equalled ~250 Å (the size of individual pores reached ~500 Å). For a dose of $2 \cdot 10^{16}$ ions/cm^2 the minimum pore size was ~20 Å.

It should be noted that with increasing dose of irradiation (up to $8 \cdot 10^{16}$ ions/cm^2) the pore size increased in accordance with the law $\langle d_v \rangle \sim (\Phi t)^{0.74}$, where Φt is the irradiation dose. On further increasing the dose, the increment in mean pore size decelerated. Together with pores, many of the micrographs revealed dislocations and other defects in the form of dark spots. With increasing dose of irradiation there was a reduction in pore concentration. This relationship may be expressed in the form $N_V \sim (\Phi t)^{-0.23}$. The reduction in pore concentrations is evidently associated with the fact that, for sufficiently high doses of irradiation, only the earlier-formed pores continue growing, while no new ones are generated. Since the irradiation temperature is quite high (~0.45 T_m in deg K) it is reasonable to assume that the formation of new pores ceases for irradiation doses of $2 \cdot 10^{16}$–$4 \cdot 10^{16}$ ions/cm^2, and subsequently only the growth of earlier-formed pores is continued. With increasing dose of irradiation the growth of an earlier-generated pore ceases, on account of the reduction in the supersaturation of the material with point defects (vacancies and interstitial atoms). The growth of the pores and dislocation loops evidently causes the dissolution of the finer pores. The swelling $\Delta V/V$ varies in accordance with an $(\Phi t)^2$ law as the dose increases to $8 \cdot 10^{16}$ ions/cm^2, then rises more slowly and for a dose of $3.2 \cdot 10^{17}$ ions/cm^2 reaches 12.3%.

TABLE 1. Results of an Analysis of the Irradiated Samples

Irradiation dose, 10^{16} ions/cm^2	No. of displacements per atom*	N_v, 10^{15} cm^{-3}	$\langle d_v \rangle$, Å	$\Delta V/V$, %
2	5	8,5	55	0,23
4	10	7,5	85	0,7
8	20	6,5	160	4,0
1	40	5	230	9,3
32	80	4,6	250	12,3

*The data for each irradiation dose are taken in accordance with [5].

Translated from Atomnaya Énergiya, Vol. 39, No. 5, pp. 362-363, November, 1975. Original article submitted January 28, 1975.

©1976 Plenum Publishing Corporation, 227 West 17th Street, New York, N.Y. 10011. No part of this publication may be reproduced, stored in a retrieval system, or transmitted, in any form or by any means, electronic, mechanical, photocopying, microfilming, recording or otherwise, without written permission of the publisher. A copy of this article is available from the publisher for $15.00.

Declassified and Approved For Release 2013/09/24 : CIA-RDP10-02196R000400060004-1

Declassified and Approved For Release 2013/09/24 : CIA-RDP10-02196R000400060004-1

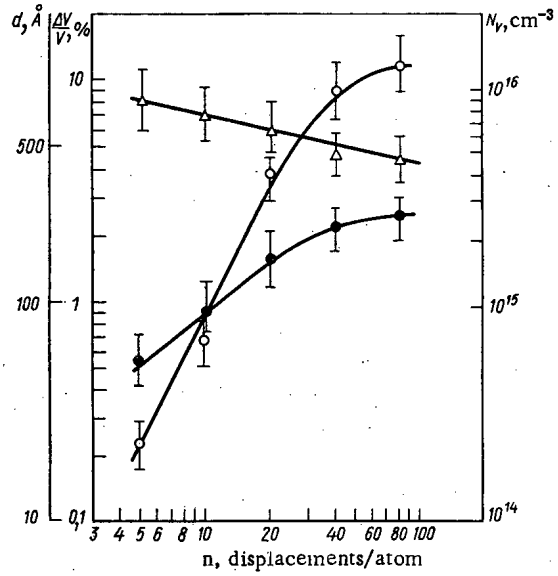

Fig. 1

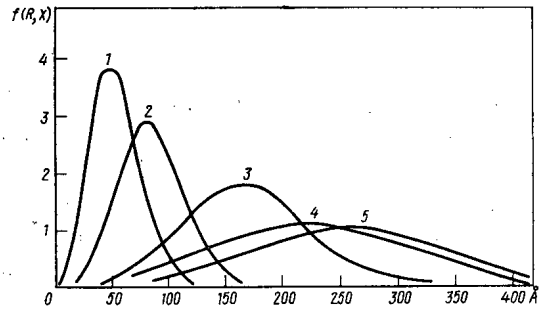

Fig. 2

Fig. 1. Dependence of $\langle d_V \rangle$ (●), N_V (Δ) and $\Delta V/V$ (○) on the irradiation dose of nickel at 550°C.

Fig. 2. Size distribution of pores in nickel for various irradiation doses at 550°C: 1) $2 \cdot 10^{16}$; 2) $4 \cdot 10^{16}$; 3) $8 \cdot 10^{16}$; 4) $1.6 \cdot 10^{17}$; 5) $3.2 \cdot 10^{17}$ ions/cm^2.

The resultant dose dependence of the swelling factor agrees closely with published data [5, 7-9]. For a dose of 25 displacements/atom in [5] the swelling amounted to 6.0%, and for 30-50 displacements/atom [7-9] the swelling reached saturation at a level of 7-10%. According to our present data the swelling amounts to 6% for 25 displacements/atom, while for doses of over 40 displacements/atom there is a tendency toward saturation.

Figure 2 shows the pore size distribution function for various irradiation doses. We see that as the irradiation dose increases both the minimum and the maximum pore sizes do likewise, while the concentration becomes smaller. This confirms the assumption to the effect that no new pore generation occurs; the growth of the earlier-formed pores simply continues.

LITERATURE CITED

1. V. N. Bykov et al., Fiz. Tverd. Tela, 15, No. 3, 910 (1973).
2. S. Ya. Lebedev, S. D. Panin, and S. I. Rudnev, At. Énerg., 38, No. 6, 426 (1975).
3. V. M. Krotov, S. Ya. Lebedev, and V. N. Bykov, At. Énerg., 37, No. 4, 343 (1974).
4. S. Ya. Lebedev and S. D. Panin, Pribory i Tekh. Éksperim., 3, 179 (1973).
5. J. Delaplace, N. Azam, and L. Le Naour, J. Nucl. Mater., 47, No. 3, 278 (1973).
6. C. Chen, A. Mastenbroek, and J. Elen, Radiation Effects, 16, 127 (1972).
7. R. Nelson, D. Mazey, and J. Hudson, J. Nucl. Mater., 41, 241 (1971).
8. D. Norris, J. Nucl. Mater., 40, 66 (1971).
9. G. Kulcinsky et al., ibid., p. 166.

Declassified and Approved For Release 2013/09/24 : CIA-RDP10-02196R000400060004-1

Declassified and Approved For Release 2013/09/24 : CIA-RDP10-02196R000400060004-1

ASSAY OF Zr, Nb, Tc, AND Te IN THE WATER IN NUCLEAR POWER PLANTS

L. N. Moskvin, G. G. Leont'ev,
V. A. Mel'nikov, V. S. Miroshnikov,
I. S. Orlenkov, and E. V. Sosnovskaya

UDC 621.039.534:543.343

If nonvolatile fission products (Zr, Nb, Tc, and Te) appear in the coolant of a reactor, there must be flaws in the fuel-rod sheathes. It is difficult to determine the concentrations of these elements on account of uncertainty as to the form they take in aqueous solutions, and also because of the small contribution from them to the overall activity of the carrier [1]. New studies were made on this topic, after methods had been devised for radiochemical analysis of I, Cs, Ba, and Sr [2] to provide for isolation of these elements from a single sample on a series of selective absorbants of a specified geometrical form and size, which serve simultaneously as sources for γ spectrometry.

Here we consider the scope for using rapid chromatographic radiochemical analysis to determine other fission products. It is necessary to stabilize the process by converting Zr, Nb, Tc, and Te to a single dominant ionic form, for which purpose we used hydrochloric acid. The extraction agents were di-2-ethylhexylorthophosphoric acid D2EHPA to extract Zr [3] and tributyl phosphate TBP for Nb, Te, and Tc [4, 5].

As a rule, iodine isotopes account for most of the fission-activity in a water coolant. As iodine can take a variety of forms, it is necessary to remove it before analysis without losing appreciable amounts of the other elements. It is possible to remove iodine selectively onto sulfonated cation-exchange resins from concentrated hydrochloric acid solutions saturated with chlorine [6]. This method was used to produce radioactive iodine of high purity and highly free from associated elements. A test as a means of removing iodine showed that one did not obtain reasonably high and guaranteed removal factors for solutions of HCl or LiCl saturated with chlorine. We selected two types of extraction agents to remove iodine from concentrated hydrochloric acid solutions: salts of quaternary ammonium basis, such as tetradeclyammonium chloride TDA and aliphatic alcohols, such as n-heptyl alcohol. The latter are effective only for chloride complexes of iodine, which are formed in concentrated hydrochloric acid solutions in the presence of dissolved chlorine (Table 1).

The chromatographic column for isolating the components was similar to that previously described [2] and was intended for three layers of sorbent. The sorbents were of fixed geometrical shape and were cylindrical tablets made of porous PTFE carrying a film of the appropriate extraction agent. These tablets were made as follows. The granulated porous PTFE [7] of grain size 0.1-0.25 mm was poured into a cylindrical metal mound and annealed at 375 ± 5°C. The immobile phase was deposited by soaking the tablet with a 20-30% solution of the extraction agent in ether, with subsequent complete removal of the ether under vacuum. Each disk was pressed into a PTFE holder of internal diameter 0.3-0.6 mm less than the diameter

TABLE 1. Isotope Partition Coefficients

Extraction agent	Aqueous phase	^{131}I	^{95}Zr	^{95}Nb	^{99m}Tc	^{125m}Te
TDA in CCl_4	6 *M* HCl	10^3	1	1	1	0,1
n-Heptanol	6 *M* HCl, sat. with Cl_2	10^2	0,1	5	5	0,1

Translated from Atomnaya Énergiya, Vol. 39, No. 5, pp. 363-365, November, 1975. Original article submitted February 3, 1975.

©1976 Plenum Publishing Corporation, 227 West 17th Street, New York, N.Y. 10011. No part of this publication may be reproduced, stored in a retrieval system, or transmitted, in any form or by any means, electronic, mechanical, photocopying, microfilming, recording or otherwise, without written permission of the publisher. A copy of this article is available from the publisher for $15.00.

Declassified and Approved For Release 2013/09/24 : CIA-RDP10-02196R000400060004-1

Declassified and Approved For Release 2013/09/24 : CIA-RDP10-02196R000400060004-1

TABLE 2. Uptake (%) of Isotopes by Tablets in Relation to Previous Treatment

Conditions	TDA			TBP		D2EHPA	
	ΣJ	^{95}Zr	^{95}Nb	^{95}Zr	^{95}Nb	^{95}Zr	^{95}Nb
Sample made 6 M in HCl and left for 15 min	100	60	70	10	25	30	5
Sample made 6 M in HCl and brought to boiling point	100	15	25	10	75	75	1
Sample made 6 M in HCl, saturated with chlorine, and brought to boiling point	100	5	17	9	82	85	1

TABLE 3. Distributions of ^{99m}Tc, ^{95}Zr, and ^{95}Nb in TDA–TBP–D2EHPA and n-heptanol–TBP–D2EHPA Tablet Systems

Absorber	Isotope	Peak area, counts/sec						% in tablets
		S_1	S_2	S_3	S_4	S_5	S_{cp}	
TDA	^{99m}Tc	15,4	24,3	20,8	16,4	22,5	19,8	12,2
	^{95}Zr	4,0	4,3	3,2	2,8	3,1	3,5	11,0
	^{95}Nb	15,8	13,8	14,2	15,4	13,9	14,5	15,1
TBP	^{99m}Tc	143,5	145,9	144,9	142,5	131,5	142,1	86,5
	^{95}Zr	1,3	1,2	1,4	1,4	1,2	1,3	4,2
	^{95}Nb	74,5	92,1	86,4	76,2	76,6	81,2	84,9
D2EHPA	^{99m}Tc	2,0	3,0	2,4	2,6	2,5	2,5	1,3
	^{95}Zr	25,5	22,8	27,9	27,7	27,2	26,2	84,8
n-Heptanol	^{99m}Tc	15,5	18,4	17,8	16,1	17,7	17,1	10,6
	^{95}Zr	6,2	8,4	5,8	7,6	8,0	7,2	21,4
	^{95}Nb	18,0	15,9	16,4	17,3	16,4	16,8	17,9
TBP	^{99m}Tc	152,5	127,8	131,0	144,3	150,6	141,4	87,7
	^{95}Zr	2,6	1,7	1,8	1,3	1,3	1,7	5,0
	^{95}Nb	84,8	74,8	81,4	71,4	72,8	77,1	82,1
D2EHPA	^{99m}Tc	2,5	3,6	1,9	3,0	2,8	2,7	1,7
	^{95}Zr	24,5	25,1	24,4	24,5	25,6	24,8	73,6

of the disk and height 1 mm greater than the height of the disk. The holder prevented contact between the inner wall of the column and the radioactive solution, and also mutual diffusion of the extraction agents, which could occur if the discs were in direct contact.

Tests on model solutions showed that it was possible to remove virtually all the elements from the solutions onto disks treated with appropriate reagents. On examining real solutions, we checked out various modes of sample preparation. Table 2 gives data for the coolant from the primary loop in the MR reactor at the Kurchatov Institute of Atomic Energy, which indicate that satisfactory results are obtained on chlorinating the sample followed by boiling. However, even in this case there is some partial retention of the Zr and Nb on the first absorber.

The tablets bearing the radioactive isotopes were used in sealed cells with a Ge(Li) detector of volume 25 cm^3, which worked into a multichannel analyzer. The energy resolution was 14.5 keV for the 1332-keV line of ^{60}Co. The instability in the energy calibration over the range 0-1600 keV did not exceed 2 keV over 8 h of continuous operation. The γ spectra was processed with a BÉSM-6 computer using the SIMP3 program [8] written in FORTRAN at Dubna and intended for analysis of complex parts of spectra; the processing time for 10 spectral lines did not exceed 1 min.

Table 3 gives results for five independent analyses. The program provides for reliable determination of the areas of unresolved photoelectric peaks at energies of 756 and 766 keV for ^{95}Zr and ^{95}Nb, respectively. The maximum error of a single measurement was 15% at the 95% confidence level. The tablet treated with TBP showed traces of ^{103}Ru. Tellurium isotopes were not observed in the specimens.

The results indicate that this method can be used in the analysis of nonvolatile fission products in water coolants.

LITERATURE CITED

1. Radiochemical Analysis of Fission Products [in Russian], Akad. Nauk SSSR, Moscow–Leningrad (1960).
2. L. N. Moskvin et al., At. Énerg., 35, No. 2, 83 (1973).
3. K. Samsahl, Analyt. Chem., 40, No. 1, 181 (1968).
4. I. Mikulski, Nucleonika, 6, 775 (1961).

Declassified and Approved For Release 2013/09/24 : CIA-RDP10-02196R000400060004-1

Declassified and Approved For Release 2013/09/24 : CIA-RDP10-02196R000400060004-1

5. L. N. Moskvin et al., Radiokhimiya, 9, 377 (1967).
6. N. G. Zaitsev, Radiokhimiya, 8, 576 (1966).
7. B. K. Preobrazhenskii et al., Radiokhimiya, 10, 375 (1968).
8. S. G. Avramov, Preprint JINR D6-7094, Dubna (1973).

Declassified and Approved For Release 2013/09/24 : CIA-RDP10-02196R000400060004-1

Declassified and Approved For Release 2013/09/24 : CIA-RDP10-02196R000400060004-1

CALCULATION OF PROBE PARAMETERS FOR GAMMA – GAMMA LOGGING

B. E. Lukhminskii and D. K. Galimbekov

UDC 550.835:539.125.52

In the development of new apparatus for the investigation of rock by means of scattered γ radiation, considerable attention has been given in recent times to instrumental methods for the reduction of disturbing influences. In the detection of the soft component of scattered γ radiation in boreholes (selective gamma–gamma logging – GGL-S), the parameter studied is the effective atomic number Z_{eff} of the medium and one of the chief disturbing factors is the uncontrolled variation in rock density. Double-probe instruments with two source collimators are used to eliminate the effect of the variable rock density ρ [1].

Slit collimators for the source and wide collimators for the detector [2] also provide readings independent of rock density in the region of practical interest, 3-4.5 g/cm^3, and furthermore possess a number of advantages over double-probe instruments such as higher sensitivity and greater radiation safety, etc.

Methods for the calculation of the effective probe diameter R_{eff} and of the effective atomic number of the rock determined by this instrument are presented in this report. The calculations were made by the Monte Carlo method using the MOK-20 program developed for optimization calculations of a GGL-S instrument with a slit collimator. The geometry of the instrument is shown in Fig. 1. The calculation was made by simultaneous correlated selection for 12 types of rock composition differing in density and atomic number. One of the calculated functionals was the γ-ray flux through the detector surface $I(\rho, Z, \theta, l_z)$, where θ is the polar angle of γ-ray emission from the source and l_z is the distance from the ^{75}Se source to the detector. The energy threshold was 30 keV.

It is well known that R_{eff} does not coincide with l_z when there is collimation of source and detector (R_{eff} is the distance between the centers of the collimation windows) [1]. For wide collimators, of special shape, this definition is inaccurate. In the calculations, R_{eff} was defined as the average distance (with respect to the number of γ rays detected) between the points of the intersection of γ-ray trajectories with the surface of the collimator windows. In the range of Z (14-23) and density (3-4.5 g/cm^3) considered, the effective length depended rather weakly on density and actual rock composition. For a variation in l_z from 2-9 cm, R_{eff} is approximated by the following simple relation,

$$R_{eff} = l_z - 4.7\cos^2\theta, \quad (1)$$

with the maximum relative error δR_{eff} being no more than 4%. For the optimal configuration of the slit collimator (see Fig. 1) which ensures readings independent of ρ, we find $R_{eff} = 5.6$ cm when $l_z = 6.5$ cm and not 6.8 cm as given by the definition in [1]. The difference between these two values is significant.

It is well known that the atomic number of a multicomponent medium measured by GGL-S depends on the source spectrum and the recorded spectrum of scattered γ rays in addition to the elemental composition of the medium [1]. It is advisable to determine the effective atomic number as applied to a specific instrument and measurement geometry so that this quantity is a parameter not only of the test medium but also of the GGL-S equipment. In this case, the effective atomic number of a test multicomponent medium is equal to the atomic number of a standard medium if the readings of the GGL-S instrument agree for both media. A series of calculations using the MOK-20 program was made for standard media with atomic numbers from 12 to 23 in order to determine Z_{eff}. A standard nomogram of the relation $I(\rho, Z, \theta, l_z)$ was constructed on the basis of these calculations. In the second step, a calculation was made for a model of iron ore in the form $g \cdot Fe + (1-g) \cdot SiO_2$, where g is the mass fraction of iron.

Translated from Atomnaya Énergiya, Vol. 39, No. 5, pp. 365-366, November, 1975. Original article submitted March 10, 1975.

©1976 Plenum Publishing Corporation, 227 West 17th Street, New York, N.Y. 10011. No part of this publication may be reproduced, stored in a retrieval system, or transmitted, in any form or by any means, electronic, mechanical, photocopying, microfilming, recording or otherwise, without written permission of the publisher. A copy of this article is available from the publisher for $15.00.

Declassified and Approved For Release 2013/09/24 : CIA-RDP10-02196R000400060004-1

Declassified and Approved For Release 2013/09/24 : CIA-RDP10-02196R000400060004-1

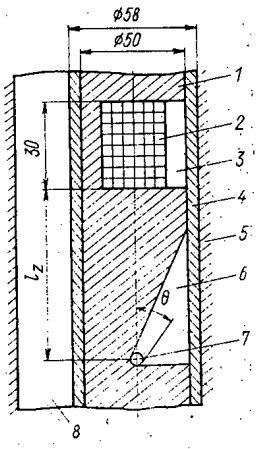

Fig. 1

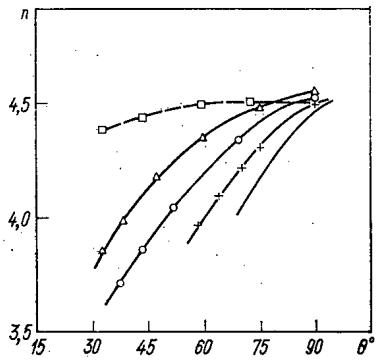

Fig. 2

Fig. 1. Probe geometry: 1) lean shield; 2) detector crystal; 3) pickup collimation channel; 4) aluminum housing; 5) rock; 6) exit collimator for primary γ rays; 7) ^{75}Se point source; 8) borehole.

Fig. 2. Dependence of exponent n on collimation angle for various values of l_z, cm: —) 5; ×) 6; ○) 7; △) 8; □) 9.

To determine Z_{eff} we used a relationship of the general form [1]

$$Z_{eff}=\sqrt[n-1]{\frac{\sum_i q_i \frac{Z_i^n}{A_i}}{\sum_i q_i \frac{Z_i}{A_i}}}. \qquad (2)$$

In accordance with the definition assumed for Z_{eff}, there follows from the equality of the readings of a GGL-S instrument (see Fig. 1) in standard and simulated media a dependence of the exponent n in Eq. (2) on the collimation angle θ and the distance l_z (Fig. 2) from which it is clear that the dependence of the exponent n on polar angle decreases as l_z increases when $\theta > 30°$. After averaging over the polar angles θ in the slit collimator, we obtain for the test instrument (with $l_z = 6.5$ cm) a value of 4.2. For dry ore, the well-known expression

$$Z_{eff}=\sqrt[3]{\sum_i q_i Z_i^3}. \qquad (3)$$

gives acceptable accuracy in the determination of Z_{eff}. Differences between values of Z_{eff} calculated from Eqs. (2) and (3) do not exceed 5%.

Thus, we have demonstrated the possibility of refinement of the parameters of a GGL-S borehole instrument calculated by the Monte Carlo method with the definition introduced for the effective dimension of the probe being markedly different from previously defined values and the value for the effective atomic number of rock practically agreeing with the well-known definitions (2) and (3).

LITERATURE CITED

1. V. A. Artsybashev, Nuclear-Geophysical Exploration [in Russian], Atomizdat, Moscow (1972).
2. I. I. Fel'dman, A. M. Blyumentsev, and V. F. Karanikolo, in: E. V. Karus (editor), Trudy VNIIYaGG, Yadernaya Geofizika [in Russian], No. 9, Nedra, Moscow (1971), p. 141.

Declassified and Approved For Release 2013/09/24 : CIA-RDP10-02196R000400060004-1

Declassified and Approved For Release 2013/09/24 : CIA-RDP10-02196R000400060004-1

SIMULATION OF PROCESSES IN HEAVY CHARGED PARTICLE TRACKS BY PULSED IRRADIATION OF SOLIDS WITH HIGH-DENSITY ELECTRON BEAMS

D. I. Vaisburd, V. P. Kuznetsov, V. A. Moskalev, and M. M. Shafir

UDC 537.226.548:539.121.72.75

The excitation-energy density in tracks of protons and α particles in dielectric crystals reaches 10^{20}-10^{21} eV/cm^3 [1]. With the development of sources of pulsed high-power electron beams, it became possible to produce similar densities of short-lived electron excitations in macroscopic dielectric volumes [2, 3]. Irradiation with a single pulse simulates the situation in a particular track, while periodic pulsed irradiation simulates the space–time overlapping of tracks. For comparison, we performed two series of experiments on the accumulation of elementary radiation defects of F nuclei in ionic crystals irradiated with protons and a pulsed electron beam with the following parameters: top energy of particles – 0.3 MeV; pulse duration controlled within the 2-30 nsec range; beam current density – 5-1500 A/cm^2.

The buildup of defects with the dose (see Fig. 1a) and the yield of defects as a function of the proton beam intensity g(I) were investigated in the first series of experiments. The intensity determines the mean frequency of track overlapping. Assuming a Poisson distribution of the time intervals between successive track superpositions at a given point in the crystal, we obtain

$$g(I) = \int_0^\infty f(t)\, I\sigma \exp(-I\sigma t)\, dt,$$

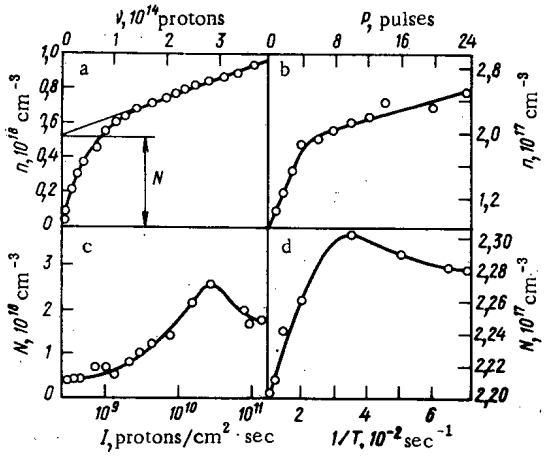

Fig. 1. Irradiation of NaF crystals with 3.5-MeV protons. a and b) Dependences of the density of F nuclei (n) on the density of proton tracks ν and the number of irradiation pulses P; c and d) dependences of the saturation level for the fast stage of accumulation of F nuclei (N) on the proton beam intensity I and the arrival frequency of radiation pulses 1/T.

Translated from Atomnaya Énergiya, Vol. 39, No. 5, pp. 366-367, November, 1975. Original article submitted February 13, 1975.

©1976 Plenum Publishing Corporation, 227 West 17th Street, New York, N.Y. 10011. No part of this publication may be reproduced, stored in a retrieval system, or transmitted, in any form or by any means, electronic, mechanical, photocopying, microfilming, recording or otherwise, without written permission of the publisher. A copy of this article is available from the publisher for $15.00.

Declassified and Approved For Release 2013/09/24 : CIA-RDP10-02196R000400060004-1

Declassified and Approved For Release 2013/09/24 : CIA-RDP10-02196R000400060004-1

where $f(t)$ is the time relaxation law for the number of defects in an individual track, and σ is the effective transverse cross section of the track. It is evident from the expression that the experimental dependence of the yield of radiation defects on the beam intensity can be used for determining the time relaxation of the number of defects in individual tracks. However, this problem pertains to the number of incorrect defects and is solved by means of A. N. Tikhonov's regularization method [4]. The mean period of track overlapping is equal to $T = 1/I\sigma$. If we neglect the statistical fluctuations of track overlapping times and assume that overlappings occur with a strict periodicity, we can use a δ distribution, $\delta\ (t - T)\ dt$, instead of a Poisson distribution. In this case, we obtain $g\ (1/I\sigma) = f(T)$ from the equation, i.e., the yield of radiation defects as a function of the mean track overlapping period constitutes the effective time relaxation law for the number of defects in a track (see Fig. 1c).

In the second series of experiments, crystals were irradiated in a nanosecond electron accelerator by pulses which followed at a fixed period. The pulse duration was equal to 5 nsec, while the amplitude of the current density in the electron beam (140 A/cm^2) was below the brittle failure threshold [2]. Figure 1a and b indicate that the dependence of the density of accumulated defects on the proton track density is similar to the dependence of the defect density on the number of electron irradiation pulses. Figure 1c and d provide a comparison between the yield of defects as a function of the proton beam intensity and the yield of defects as a function of the arrival frequency of electron irradiation pulses. They are similar and display the characteristic maximum. Thus, periodic irradiation with short pulses of high-power electron beams simulates the time overlapping of tracks, while the yield of radiation defects as a function of the arrival period of radiation pulses can be used for reproducing the time relaxation of the number of defects in individual tracks.

LITERATURE CITED

1. D. I. Vaisburd, A. A. Vorob'ev, and L. A. Melikyan, At. Énerg., 30, No. 6, 538 (1971).
2. D. I. Vaisburd and I. N. Balychev, Pis'ma v Zh. Éksperim. i Teor. Fiz., 15, No. 9, 537 (1972).
3. D. I. Vaisburd et al., Izv. Akad. Nauk SSSR, Ser. Fiz., 38, No. 6, 1281 (1974).
4. D. I. Vaisburd and V. P. Kuznetsov, Izv. Vuzov SSSR, Fizika, No. 5, 155, 159 (1974).

Declassified and Approved For Release 2013/09/24 : CIA-RDP10-02196R000400060004-1

Declassified and Approved For Release 2013/09/24 : CIA-RDP10-02196R000400060004-1

RESOLUTION OF TOTAL COINCIDENCE SCINTILLATION SPECTROMETERS

S. V. Shevchenko

UDC 621.387.464.004.13

The method of total coincidences, which has been proposed in [1], is widely used for determining nuclear decay schemes and for activation analysis. The proposed [1-3] statistical description of the method of total coincidences consists in the following:

If

$$f_{1,2}=\frac{1}{\sqrt{2\pi}\,\sigma_{1,2}}e^{-\frac{(\Delta E_{1,2})^2}{2\sigma_{1,2}^2}} \tag{1}$$

and

$$f_s=\frac{1}{\sqrt{2\pi}\,\sigma_s}e^{-\frac{(\Delta E_s)^2}{2\sigma_s^2}} \tag{2}$$

are distribution functions of the total absorption peaks of a cascade of two γ quanta and their sum, then

$$f'_{1,2}(\Delta E_{1,2})=\int_{-\infty}^{+\infty} f_1(\Delta E_1)\,f_2(\Delta E_2)\,f_s(\Delta E_s)\,d(\Delta E_{2,1}) \tag{3}$$

and

$$f'_{1,2}(\Delta E_{1,2})=\frac{1}{\sqrt{2\pi}\,\sigma_{1,2}\sqrt{\sigma_{2,1}^2+\sigma_s^2}}e^{-\frac{1}{2}\frac{(\Delta E_{1,2})^2}{\left(\frac{\sigma_{1,2}\sqrt{\sigma_{2,1}^2+\sigma_s^2}}{\sqrt{\sigma_{1,2}^2+\sigma_{2,1}^2+\sigma_s^2}}\right)}}. \tag{4}$$

On this basis the conclusion has been reached that the spectrometric characteristics of the instrument can be improved without loss of coincidence recording efficiency. The integrand in Eq. (3) remains somewhat vague, since f_S is not a function of an independent variable.

The obtained values of $f'_{1,2}$ have not been normalized to unity, and the probability acquires the dimension 1/E. The conclusion concerning the improvement in resolution without loss of efficiency is not obvious either.

We propose here a calculation method free from these ambiguities. If

$$f_{1,2}=\frac{1}{\sqrt{2\pi}\,\sigma_{1,2}}e^{-\frac{(\Delta E_{1,2})^2}{2\sigma_{1,2}^2}}, \tag{5}$$

we obviously have

$$f_s=\frac{1}{2\pi\sigma_1\sigma_2}\int_{-\infty}^{+\infty} e^{-\frac{(\Delta E_1)^2}{2\sigma_1^2}}e^{-\frac{(\Delta E_1-\Delta E_s)^2}{2\sigma_2^2}}d(\Delta E_1), \tag{6}$$

Translated from Atomnaya Énergiya, Vol. 39, No. 5, pp. 367-368, November, 1975. Original article submitted March 24, 1975.

©1976 Plenum Publishing Corporation, 227 West 17th Street, New York, N.Y. 10011. No part of this publication may be reproduced, stored in a retrieval system, or transmitted, in any form or by any means, electronic, mechanical, photocopying, microfilming, recording or otherwise, without written permission of the publisher. A copy of this article is available from the publisher for $15.00.

Declassified and Approved For Release 2013/09/24 : CIA-RDP10-02196R000400060004-1

Declassified and Approved For Release 2013/09/24 : CIA-RDP10-02196R000400060004-1

where $\Delta E_1 = E_1 - E_{01}$; $\Delta E_2 = E_2 - E_{02}$; $\Delta E_s = E_s - E_{0s}$.

After simple transformations, we obtain

$$f_s = \frac{1}{\sqrt{2\pi}\sqrt{\sigma_1^2 - \sigma_2^2}} e^{-\frac{1}{2}\frac{(\Delta E_s)^2}{\sigma_1^2+\sigma_2^2}}. \quad (7)$$

The introduction in the circuit of a differential discriminator with the window width 2ε, tuned to the total cascade energy, is described mathematically as follows:

$$P_\varepsilon(\varepsilon) = \int_{-\varepsilon}^{+\varepsilon} f_s(\Delta E_s)\, d(\Delta E_s) = \int_{-\varepsilon}^{+\varepsilon} d(\Delta E_s) \int_{-\infty}^{+\infty} f_1(\Delta E_1)\, f_2(\Delta E_1 - \Delta E_s)\, d(\Delta E_1) =$$

$$= \int_{-\infty}^{+\infty} d(\Delta E_1)\, f(\Delta E_1) \int_{-\varepsilon}^{+\varepsilon} f_2(\Delta E_1 - \Delta E_s)\, d(\Delta E_s); \quad (8)$$

then, the function

$$f_1' = \frac{1}{P_\varepsilon} f_1(\Delta E_1) \int_{-\varepsilon}^{+\varepsilon} f_2(\Delta E_1 - \Delta E_s)\, d(\Delta E_s) \quad (9)$$

is the sought distribution function of total absorption peaks:

$$f_1' = \frac{f_1'(\Delta E_1) \int_{-\varepsilon}^{+\varepsilon} f_2(\Delta E_1 - \Delta E_s)\, d(\Delta E_s)}{\frac{1}{\sqrt{2\pi}\sqrt{\sigma_1^2+\sigma_2^2}} \int_{-\varepsilon}^{+\varepsilon} e^{-\frac{(\Delta E_s)^2}{2(\sigma_1^2+\sigma_2^2)}} d(\Delta E_s)}. \quad (10)$$

After transformations, we obtain

$$f_{1,2}'(\Delta E_{1,2}) = \frac{e^{-\frac{(\Delta E_{1,2})^2}{2}\frac{\sigma_1^2+\sigma_2^2}{\sigma_1^2\sigma_2^2}}}{\pi\sigma_1\sigma_2 P_\varepsilon} \int_0^\varepsilon e^{-\frac{\varepsilon^2}{2\sigma_{2,1}^2}} \operatorname{ch}\frac{\Delta E_{1,2}\varepsilon}{\sigma_{2,1}^2}\, d\varepsilon \quad (11)$$

for $\frac{\varepsilon}{\sigma_{1,2}} \ll 1$;

$$f_{01;\,02}'(\Delta E_{1,2}) \approx \frac{\sqrt{\sigma_1^2+\sigma_2^2}}{\sqrt{2\pi}\sigma_1^2\sigma_2^2} e^{-\frac{(\Delta E_{1,2})^2(\sigma_1^2+\sigma_2^2)}{2\sigma_1^2\sigma_2^2}}, \quad (12)$$

i.e., $f'_{1,2}$ is described approximately by a Gaussian function, and

$\sigma_1' \approx \sigma_2' = \frac{\sigma_1\sigma_2}{\sqrt{\sigma_1^2+\sigma_2^2}} \leqslant \frac{\sqrt{\sigma_1^2+\sigma_2^2}}{2}$ for $\sigma_1 \approx \sigma_2$: $\sigma_{1,2}' \approx \frac{\sigma_{1,2}}{\sqrt{2}}$ for $\frac{\varepsilon}{\sigma_{1,2}} < 1$;

$$f_{1,2}'(\Delta E_{1,2}) \sim f_{01,\,02}'(\Delta E_{1,2}) \frac{\sigma_{2,1}^2}{\Delta E_{1,2}} \operatorname{sh}\frac{\Delta E_{1,2}\varepsilon}{\sigma_{2,1}^2}. \quad (13)$$

Consequently, for a certain combination of σ_1, σ_2, and ε, the observed spectrum must contain additional peaks which are symmetric with respect to the total absorption peaks. Thus, for any σ_1 and σ_2, with an increase in the width of the discriminator window ε, the distributions for $E_{\gamma 1}$ and $E_{\gamma 2}$ first deviate from a normal distribution and then pass in the limit $\varepsilon \to 0$ into distributions (5) for an individual detector.

LITERATURE CITED

1. A. Hoogenboom, Nucl. Instrum. and Methods, 3, 256 (1958).
2. Alpha, Beta, and Gamma Spectroscopy [in Russian], Vol. 1, Atomizdat, Moscow (1969).
3. N. A. Vartanov and P. S. Samoilov, Applied Scintillation Gamma Spectroscopy [in Russian], Atomizdat, Moscow (1969).

Declassified and Approved For Release 2013/09/24 : CIA-RDP10-02196R000400060004-1

Declassified and Approved For Release 2013/09/24 : CIA-RDP10-02196R000400060004-1

NEUTRON RESONANCES IN ^{244}Cm, ^{245}Cm, ^{246}Cm, AND ^{248}Cm

T. S. Belanova, Yu. S. Zamyatnin, A. G. Kolesov, N. G. Kocherygin S. N. Nikol'skii, V. A. Safonov, S. M. Kalebin, V. S. Artamonov, and R. N. Ivanov

UDC 621.039.556

Neutron choppers with synchronously revolving rotors suspended in a magnetic field installed at the ITÉF and NIIAR reactors permit the measurement of the transmission of samples containing the isotopes ^{244}Cm, ^{245}Cm, ^{246}Cm, and ^{248}Cm. The resolution of the spectrometer at the NIIAR on a 92-m base is 70 nsec/m [1], and that of the ITÉF spectrometer on a 50-m base is 149 nsec/m [2].

The stable oxide of curium with a known oxygen content (Cm_2O_3) was used in the form of an anhydrous powder. Before charging the targets the powder was baked at a temperature of 900-1100°C. Two samples were made with different isotopic contents of curium (Table 1). They were both contaminated with ^{243}Am and ^{240}Pu: 2 and 1.6% for sample 1; 0.13 and 0.8% for sample 2.

The transmissions of the samples were measured in the energy range above 0.5 eV. A statistical accuracy of 1-2% was maintained; the neutron background varied from 0.5 to 2%. A correction was made for the scattering of neutrons from oxygen.

The resonance parameters were computed by the shape and area method using the single-level Breit–Wigner formula. The resolution function was not approximated by an analytic expression but was calculated directly by computer, taking account of factors characterizing the resolving power of the apparatus. The position of the resonances E_0, the neutron width $2g\Gamma_n$, and the total width Γ were determined.

Measurements were made for several thicknesses of the ^{244}Cm samples with the maximum $n_0 = 0.24 \cdot 10^{22}$ atoms/cm^2. In analyzing the resonances (Table 2) by the area method the radiation width Γ_γ was taken equal to 37 MeV. Calculations gave the average level spacing $\overline{D} = 14.6 \pm 2.2$ eV and the strength function $S_0 = 0.68 \pm 0.30 \cdot 10^{-4}$. It was shown that in ^{244}Cm the reduced neutron widths follow the Porter–Thomas distribution for one degree of freedom, and the level spacing agrees with the Wigner distribution.

Table 3 gives preliminary values of the resonance parameters of ^{245}Cm. A sample of thickness $0.26 \cdot 10^{21}$ atoms/cm^2 was used. Up to 50 eV 21 levels were found. All these were computed by the area method assuming $\Gamma = 40$ MeV.

TABLE 1. Characteristics of Samples

Sample No.	Mass, mg	Isotopes, %					
		^{242}Cm	^{244}Cm	^{245}Cm	^{246}Cm	^{247}Cm	^{248}Cm
1	82,8	0,31	88,62	9,57	1,49	—	—
2	116,4	—	39,28	0,47	51,85	1,61	6,79

TABLE 2. Resonance Parameters of ^{244}Cm

E_0, eV	Γ, MeV	Γ_n, MeV	E_0, eV	Γ_n, MeV
7,67	44±3	10,4±0,4	85,6	26,0±4,8
16,77	37±5	1,90±0,30	95,5	7,8±2,2
22,85	36±10	0,84±0,10	132	16±8
35,0	33±5	5,1±0,8	139	2,2±0,9
52,8	—	0,56±0,15	171	3,6±1,8
69,8	—	0,44±0,25	—	—

Translated from Atomnaya Énergiya, Vol. 39, No. 5, p. 369, November, 1975. Original article submitted June 23, 1975.

©1976 Plenum Publishing Corporation, 227 West 17th Street, New York, N.Y. 10011. No part of this publication may be reproduced, stored in a retrieval system, or transmitted, in any form or by any means, electronic, mechanical, photocopying, microfilming, recording or otherwise, without written permission of the publisher. A copy of this article is available from the publisher for $15.00.

Declassified and Approved For Release 2013/09/24 : CIA-RDP10-02196R000400060004-1

Declassified and Approved For Release 2013/09/24 : CIA-RDP10-02196R000400060004-1

TABLE 3. Resonance Parameters of ^{245}Cm

E_0, eV	$2g\Gamma_n$, MeV	E_0, eV	$2g\Gamma_n$, MeV	E_0, eV	$2g\Gamma_n$, MeV
1,93	—	25,0	2,4±0,4	40,9	1,8±0,9
4,69	1,73±0,35	26,9	—	42,9	3,0±1,5
9,25	0,32±0,05	27,1	1,0±0,3	43,5	—
11,4	0,50±0,20	29,6	4,2±0,7	44,9	1,7±0,5
14,0	0,25±0,08	31,4	0,5±0,2	47,8	5,7±1,4
15,9	—	32,4	0,4±0,2	49,2	2,2±1,2
21,6	2,6±0,4	36,3	3,6±1,8	50,5	1,8±0,7

TABLE 4. Resonance Parameters of ^{246}Cm

E_0, eV	Γ, MeV	Γ_n, MeV	E_0, eV	Γ_n, MeV
4,32	27±2	0,34±0,01	84,5	—
15,29	28±3	0,52±0,01	91,5	9,9±2,5
—	—	—	157	34,1±7,6

TABLE 5. Resonance Parameters of ^{248}Cm

E_0, eV	Γ, MeV	Γ_n, MeV	E_0, eV	Γ_n, MeV
7,26	36±3	1,90±0,04	84	—
26,88	37±3	21,7±7	—	—
35,00	38±5	9,5±2,0	—	—
75,6	—	102,5±13,6	98,6	169±18

Five levels (Table 4) were identified in the sample of ^{246}Cm of thickness $0.21 \cdot 10^{22}$ atoms/cm^2 in the energy range up to 157 eV. The resonance parameters were computed by the shape and energy method assuming $\Gamma_\gamma = 37$ MeV.

The resonance parameters of the ^{248}Cm levels are shown in Table 5 for energies up to 100 eV. The sample thickness was $0.27 \cdot 10^{21}$ atoms/cm^2. In the analysis of the resonances by the area method it was assumed that $\Gamma_\gamma = 40$ MeV.

LITERATURE CITED

1. S. M. Kalebin et al., in: Transactions of a Conference on Neutron Physics [in Russian], Pt. II, Naukova Dumka, Kiev (1972), p. 267.
2. S. M. Kalebin et al., Yadernaya Fizika, 14, 22 (1971).

Declassified and Approved For Release 2013/09/24 : CIA-RDP10-02196R000400060004-1

Declassified and Approved For Release 2013/09/24 : CIA-RDP10-02196R000400060004-1

DIARY OF COLLABORATION

A conference of specialists from the member countries of the Council for Mutual Economic Aid (CMEA) on radiopharmaceutical preparations was held on May 13-16, 1975 in Moscow. It discussed proposals on questions of notices of the day, prepared by the Council Secretariat Department on the basis of reports from the country delegations. It was noted, that within the framework of the Permanent Commision of the Council for Mutual Economic Aid (PC CMEA) on the chemical industry, a large experience has been built up on the development of unique systemmatic data, and also of monographs on specific pharmaceutical preparations included in the "Compendium of Medicines" (CM). The conference deemed it advantageous: to extend this experience to radiopharmaceutical preparations (RPP) and to undertake further work in the field of the creation and application of unified requirements to pharmacopia articles on RPP, used in the member countries of the CMEA, in accordance with the CM, for subsequent inclusion in its approved Material Commissions; and to develop both general monitoring methods, specifically for the RPP and also monographs on specific preparations in the form accepted in the CM. It is considered that specialized RPP mainly are subjected to discussion, and also are widely supplied to the member countries of the CMEA. Taking into account that at the present time in the member countries of CMEA and within the framework of the PC CMEA a number of materials have been developed, which may serve as the basis for carrying out this work, the conference prepared: a list of existing articles, or articles being processed, on RPP; a list of general methods for monitoring RPP, proposed for development, taking account of the general methods (issues 1 to 10) prepared within the framework of the Compendium of Medicine (CM); and a list of the sections of pharmacopia papers on RPP, used in the member countries of the CMEA.

A decision was taken to proceed to the preparation of model monographs according to the form accepted in the CM, with a complete text of monitoring methods for the purpose of verifying the validity of the approach to the preparation of general data and monographs. For this, a number of RPP with different controlling parameters has been chosen, for which different experimental methods are specified, and a list of model monographs on RPP subject to development in 1975-1976 has been agreed; country organizers of work on individual preparations have been established and the corresponding work agendas have been defined.

At the same time, a typical list of monographs on RPP liable for development in the first place, has been prepared. It will be advantageous to consider the orders of development of these monographs after accumulating experience on the preparation of model monographs. Moreover, in the opinion of the participants of the conference, it will be advantageous in future to discuss the designation of the RPP (labelled, carrier-free, with carrier, etc.).

The conference prepared a plan for the decision of the Commission on this problem and the corresponding proposals for refining the work plan of the Commission in 1975-1976. The specialists discussed the draft of the work plan for scientific-technical cooperation in 1976-1980, according to a study of the composition and properties of RPP by physicochemical methods and analysis, stated their interest in the participation and development of individual tasks and agreed to the period of their start and completion, and also defined provisionally their forms of accomplishment.

The draft of a work program was considered concerning the unification of investigations and methods of monitoring essential for obtaining authorization in the clinical study of RPP, and a working plan on the subject was accepted. The purpose of these tasks is the preparation of general instructions on the determination of the volume of experiments in order to obtain authorization in the clinical study of RPP.

An exchange of opinions took place on measures concerned with the conversion of the units of the CMEA to the development of standards of the CMEA. The proposals of the Secretarial Branch of CMEA concerning this problem were discussed and the dates for discussion of the recommendations previously ac-

Translated from Atomnaya Énergiya, Vol. 39, No. 5, pp. 370-371, November, 1975.

©1976 Plenum Publishing Corporation, 227 West 17th Street, New York, N.Y. 10011. No part of this publication may be reproduced, stored in a retrieval system, or transmitted, in any form or by any means, electronic, mechanical, photocopying, microfilming, recording or otherwise, without written permission of the publisher. A copy of this article is available from the publisher for $15.00.

Declassified and Approved For Release 2013/09/24 : CIA-RDP10-02196R000400060004-1

Declassified and Approved For Release 2013/09/24 : CIA-RDP10-02196R000400060004-1

cepted by the Commission on standardization in the field of isotopes and radiation sources were defined.

A conference of specialists on problems of the application of the principles and procedures of price building for specialized isotope production plants, operating within the framework of the Council for Mutual Economic Aid (CMEA), was held on May 20-22, 1975 in Potsdam (German Democratic Republic). Specialists from the Covenant Parties participated on the multilateral international specialization and cooperation of the isotope production industries. The conference deemed necessary the establishment of contract prices on specialized isotope production plants in the mutual trade between member countries of CMEA in 1976-1980, to start from the operating principles and procedures of price building, accepted by the 9th Session of the CMEA and the recommendations of the Executive Committee of the Council, accepted at the 70th Conference (January 1975).

The investigations carried out by the Covenant Parties of the level and development of prices on isotope production plants, established by the leading firms in the world market in the period 1970-1975, showed that these prices changed only insignificantly during the stated period. The existing tendency to increase prices on production, of British and American firms, has given rise mainly to devaluation in a number of capitalist countries. With conversion into rubles over the actual exchange, the increase as a rule is eliminated. By taking account of specifics and the wide assortment of isotope production, agreement was reached concerning the establishment of contract prices on isotope production plants in the mutual trade between member countries of CMEA in 1976-1980, calculated on the basis of prices during 1974, which is considered as the most representative basic year. It should be borne in mind that, in the case of a significant change of prices in isotope production on the world market, any of the Covenant Parties according to necessity can introduce for consideration of the next meeting of the authorized Parties, the question concerning the establishment of contract prices in accordance with the recommendations of the Executive Committee of the Council, i.e., based on a five-year sliding base period.

The Conference approved the draft of the document "Application of the Principles and Procedures operating within the framework of the CMEA, of price building for the establishment of contract prices in mutual trade in specialized isotope production plants in 1976-1980." The draft has been presented for consideration at the Meeting of the Authorized Negotiating Covenant Parties (Hungary, September 1975). In this case, it was taken into account that this document comes into force on the day of signing of the minutes of the meeting so that the principles established in it could be used by the Parties for the conclusion of mutual contracts on the supply of isotope production plants in 1976.

The question of establishing unified prices on irradiation in nuclear reactors was discussed. It was accepted as expedient to consider this question further in the course of work on the program of cooperation in the isotope field in 1976-1980. The Parties acknowledged it to be feasible to extend the principles and procedures of price building, agreed at the conference, to currently nonspecialized isotope production units, supplied to member countries of CMEA.

The 5th Meeting of the Committee for Scientific and Technical Cooperation on Radiation Safety took place on May 27-30, 1975 in Kiev. A list of assignments was agreed on the subject of problems of "Ensuring Radiation Safety" entering into the overall comprehensive program of cooperation of the member countries of CMEA and the Socialist Federated Republic of Yugoslavia (SFRYu), developed by the members of CMEA, in the period 1980 in the field of preservation and improvement of the environment and, associated with this, the rational utilization of natural resources. The final editing was discussed and agreed on the classification of emergency situations in nuclear power stations and methods of determining hazard factors, and recommendations for monitoring the state of the outside medium as a result of the release of I-131 into atmospheric air from industrial effluents. The use of these data for carrying out the appropriate work within national bounds was recommended. A program for undertaking an international comparison of γ-radiation spectrometers for man was considered and the decision was taken to carry out in 1976 a comparison of γ-radiation spectrometers for man and the regular comparison of personal dosimeters, used in the member countries of CMEA. The draft of a report was discussed and prepared by the working group on nuclear instrument design on "The state and prospective developments of portable dosimetric instruments for nuclear power stations and nuclear reactors," and it was recommended to introduce the appropriate changes into the report. Preliminary notification was agreed for the 6th meeting of the Committee for Scientific and Technical Cooperation – Radiation Safety – and a resolution was taken on a number of other questions concerning the plan of work.

Declassified and Approved For Release 2013/09/24 : CIA-RDP10-02196R000400060004-1

Declassified and Approved For Release 2013/09/24 : CIA-RDP10-02196R000400060004-1

BOOK REVIEWS

K. N. Mukhin

EXPERIMENTAL NUCLEAR PHYSICS*

Reviewed by É. M. Tsenter

Mukhin's textbook "Introduction to Nuclear Physics" ran through two editions (1963 and 1965), and it attained a well-deserved reputation in technical colleges and nuclear divisions of physics faculties at universities.

The third edition was published in 1974 under the name Experimental Nuclear Physics with extensive revision and supplementation. A difference from previous editions is that the physics of elementary particles has been transferred to a separate volume.

The present first volume "Physics of Atomic Nuclei" consists of two parts. The first part is "Properties of nuclei and radioactive radiations," which consists of four chapters dealing with the properties of stable and radioactive nuclei, various nuclear models, and the interaction of nuclear radiations with matter.

The second part is called "Nuclear interactions," and consists of eight chapters. The general laws of nuclear reactions are considered along with various forms of nuclear reaction: reactions produced by neutral particles and by charge particles, either involving compound nuclei or direct interaction.

Particular attention is given to fission and thermonuclear reactions. The author devotes sufficient attention to the importance of these reactions for practical applications. This part also deals with topics such as neutron migration in matter, which might better have been included in the chapter "Interaction of nuclear radiations with matter."

The first volume in the main retains the structure of the first two parts of the previous editions, but here each chapter ends with a brief summary of the contents, which is very valuable in a textbook.

The undoubted advantages of this textbook do not compensate for certain defects, however, There are repetitions of formulas (pp. 16, 41, 54, and 122 in formulas 3.4), since the author does not number them, although he might thereby have referred back to them. As students in physics faculties and engineering-physics sections have good mathematical training, it is hardly necessary to give the detailed explanation (p. 64) for the determination of r_0 from the slope of a line. The particular example of two particles is used to prove in two forms (equal and unequal masses) that the overall momentum is zero in the system of the center of inertia, although this follows directly from the definition of that system.

There is not any real justification for altering the name of the third edition as regards the number of experiments described or the level at which they are treated. In future editions, which will undoubtedly be required, these changes should be made; Mukhin's very valuable textbook could only gain from this in our opinion.

*Physics of Atomic Nuclei [in Russian], Vol. 1, Atomizdat, Moscow (1974).

Translated from Atomnaya Énergiya, Vol. 39, No. 5 p. 371, November, 1975.

©1976 Plenum Publishing Corporation, 227 West 17th Street, New York, N.Y. 10011. No part of this publication may be reproduced, stored in a retrieval system, or transmitted, in any form or by any means, electronic, mechanical, photocopying, microfilming, recording or otherwise, without written permission of the publisher. A copy of this article is available from the publisher for $15.00.

Declassified and Approved For Release 2013/09/24 : CIA-RDP10-02196R000400060004-1

Declassified and Approved For Release 2013/09/24 : CIA-RDP10-02196R000400060004-1

CONFERENCES AND MEETINGS

INTERNATIONAL CONFERENCE ON HIGH-ENERGY PHYSICS

V. V. Glagolev

The 4th International Conference on High-Energy Physics was held on June 23-28, 1975 in Palermo, Italy. As many as 660 physicists from Europe, America, and Japan took part in the work of the conference. The largest delegations were from the USA, FRG, France, Italy, and England. Twenty-eight review talks were given at 11 plenary sessions. In addition, 30 invited talks were also given.

Much attention was paid to experimental reports on the observation and study of the new particles ψ (3095) and ψ (3684) and to the theoretical interpretation of these effects. Since the discovery in August, 1974 of a particle with mass 3.1 GeV/c^2 in various laboratories throughout the world, a series of experiments with hadronic, photon, and colliding beams have been performed. It has been shown that the ψ particle production cross section in nucleon–nucleon interactions increases by a factor of 100 in the energy range 60-3000 GeV^2. Experiments done with photon beams show that the interaction cross section of the new particles with nucleons is ~ 1 mb which is characteristic of hadrons. Production of nuclei is diffractive. Experiments at SPEAR, ADONE, and DORIS studying production of new particles in colliding electron–positron beams in the mass region 1.1-7.6 GeV/c^2 have not found other new particles. Data collected up to this point indicate that the new particles are hadrons. Much work has been done studying their characteristics (quantum numbers, decays, and widths). Some results are given in Table 1 (taken from V. Luce's report).

Theoretical reports on the new particles developed schemes with four quarks, introducing a "charmed" quark P'. Variations of this scheme with colored and both colored and charmed quarks were considered. Experiments at SLAC searching for charmed particles in the $K^-\pi^+$, $K^0_S\pi^+\pi^-$, $\pi^+\pi^-$, $K^+\pi^-$, K^+K^- combinations and in other states gave an upper limit of ~ 0.5 nb for their production.

In the section on meson spectroscopy, results on new resonances h ($M = 2020 \pm 30$ MeV/c^2, $\Gamma = 180 \pm 60$ MeV/c^2, $J^p = 4^+$); ω^{0*} ($M = 1669 \pm 11$ MeV/c^2, $\Gamma = 173 \pm 19$ MeV/c^2, $J^p = 3^-$); K^{0*} ($M = 1800$ MeV/c^2, $\Gamma = 200$ MeV/c^2, $J^p = 3^-$) were presented. G. Martin's (France) review talk emphasized the experiment observing the h-meson in the reaction $\pi^-p \to \pi^0\pi^0 n$ at 40 GeV/c^2 (Serpukhov–CERN).

Work using the 2-m CERN hydrogen bubble chamber in a K beam at 4.2 GeV/c stood out in discussion of baryon resonances. With high statistics there is a rather clear $K^-p \to \Lambda K^+K^-$ production evident in the reaction Ξ^{-*} (1820).

K. Goulianos reported on the Soviet–American experiment being performed on the Batavia accelerator using a hydrogen jet target constructed by JINR experts. Results comparing pp and pd collisions at high energies and small momentum transfers were discussed.

A large number of papers (about 150) were devoted to the study of inclusive processes and correlations in a multiplicity of processes. Interesting results on $\gamma\gamma$ correlations were presented from the 2-m propane bubble chamber (Dubna). P. V. Shlyapnikov (IFVE) reported on the study of inclusive reactions in $K^\pm p$ interactions using the "Mirabelle" bubble chamber. It has been shown in experiments on nucleon interactions (Frascati, CERN) that a group of processes exist which can be most naturally interpreted by using neutral currents. No data were presented on the existence of strangeness-changing neutral currents. This is supported by the ratio

$$\frac{K_L \to \mu^+\mu^-}{K^+ \to \mu^+\nu_\mu} = 6 \cdot 10^{-9}.$$

Translated from Atomnaya Énergiya, Vol. 39, No. 5, pp. 372-373, November, 1975.

©1976 Plenum Publishing Corporation, 227 West 17th Street, New York, N.Y. 10011. No part of this publication may be reproduced, stored in a retrieval system, or transmitted, in any form or by any means, electronic, mechanical, photocopying, microfilming, recording or otherwise, without written permission of the publisher. A copy of this article is available from the publisher for $15.00.

Declassified and Approved For Release 2013/09/24 : CIA-RDP10-02196R000400060004-1

Declassified and Approved For Release 2013/09/24 : CIA-RDP10-02196R000400060004-1

TABLE 1. Some Characteristics of the New Particles

Characteristics	$\psi(3,1)$	$\psi(3,7)$
M	3,095±0,04 GeV/c^2	3,684±0,005 GeV/c^2
J^{pc}	1^{--}	1^{--}
$\Gamma_{ee} = \Gamma_{\mu\mu}$	4,8± 0,6 KeV/c^2	2,2±0,3 KeV/c^2
Γ_{had}	59±14 KeV/c^2	220±56 KeV/c^2
Γ	69±15 KeV/c^2	225±56 KeV/c^2
Γ_{ee}/Γ	0,069±0,009	0,0097±0,0016
Γ_{had}/Γ	0,86±0,02	0,981±0,003
$\Gamma_{\mu\mu}/\Gamma$	1,00±0,05	0,89±0,16

A special session was devoted to the experimental verification of quantum electrodynamics. Experiments at Frascati showed that the energy dependence and absolute magnitude of the effective cross section for the purely leptonic process $e^+e^- \to \mu^+\mu^-$ is very accurately (5% error) described by the predictions of quantum electrodynamics when radiative corrections are taken into account. New measurements at CERN of the quantity $a = \frac{g-2}{2}$ have shown that $a_{\text{theor}} - a_{\text{expt}} = (-7 \pm 29) \cdot 10^{-9}$.

New accelerator projects were discussed including EPIC (Rutherford Laboratories, England), PETRA (FRG), and LSR (CERN). The first two are similar projects for colliding electron–positron beam accelerators with luminosity of $\sim 10^{31} \text{cm}^{-2} \cdot \text{c}^{-1}$ (14 and 5-18 GeV, respectively). The CERN project concerns the possibility of building a colliding proton–proton beam accelerator with 400-GeV beam energies. Theoretical papers on the Regge approach to high-energy scattering, dual models and strings, quark confinement, and other topics were discussed, as well as experimental results on the study of total and elastic cross sections, quasi two-body processes, and deep inelastic interactions.

On the whole, the Conference was well organized. The proceedings of the conference will be published in a special CERN publication.

Declassified and Approved For Release 2013/09/24 : CIA-RDP10-02196R000400060004-1

Declassified and Approved For Release 2013/09/24 : CIA-RDP10-02196R000400060004-1

6TH INTERNATIONAL CONFERENCE ON MHD GENERATION OF ELECTRICITY

V. A. Gurashvili

The 6th International Conference on MHD generation of Electricity was held in Washington on June 9-13, 1975. At the conference the latest scientific and technical achievements and new trends in research on MHD energy conversion were discussed. The conference was conducted in the traditional rapporteur manner and was divided into 15 sections covering the following basic directions in MHD research.

Open Cycle Generators and MHD Conversion Systems. The energy crisis in a number of industrial nations in the West has forced them to conduct an intensive search for effective means of energy conversion which will lower the relative expenditure for fuel and substantially reduce environmental pollution. At the present time the main energy source for open cycle MHD stations is coal, large reserves of which are held by a number of countries.

American scientists noted that the goal in the US program is to demonstrate a commercial role for coal-fired MHD stations by the beginning of the 1980's.

The role of the High-Temperature Institute of the Academy of Sciences of the USSR in the development of open-cycle MHD systems was emphasized at the conference. The semicommercial U-25 MHD machine built by the Institute is at present the subject of broad Soviet–American collaboration.

From among the papers presented we should note the studies on the experimental machine Mark-VI, which has worked in a power reducing regime for 182 h with a total energy output of $6.4 \cdot 10^5$ kW-h. The greatest resonance at the conference was received by the paper on construction of a pulsed, self-excited MHD generator using combustion products from a powdered fuel and the application of such a device for deep probing of the earth's core in geophysical studies by the I. V. Kurchatov Institute of Atomic Energy.

Closed Cycle Generators and MHD Conversion Systems. In the last four years substantial progress has been achieved in building highly efficient experimental MHD generator with unbalanced conductivity, in which the energy conversion efficiency reaches 20-30%. This makes it possible to believe that such generators with specific electrical powers of about 500 W/cm^3 may be realized.

To a large extent, progress in building closed cycle MHD stations is determined by the prospects for constructing a high temperature gas-cooled reactor, although in a number of papers combination systems were considered involving a nuclear reactor and subsequent heating of the working medium in a special high temperature combustion product-heat exchanger.

Liquid Metal MHD Generators and Closed Cycle Systems. As for possible utilization of liquid metal systems, not much optimism was noted, since even in this area it is necessary to develop high temperature breeder reactors. All the more, a number of schemes assume construction of a "boiler" reactor. The overall efficiency of such systems remains low, on the order of a few percent; however, the possibility of their use in solar devices was suggested if their overall thermodynamic efficiency turns out to be somewhat higher than that of thermoelectric elements.

New Concepts for Various Energy Systems with MHD Generators. We must note the papers on utilization of the energy from reactors with solid gas-cooled blankets surrounding the fusion zone and with

Translated from Atomnaya Énergiya, Vol. 39, No. 5, p. 373, November, 1975.

©1976 Plenum Publishing Corporation, 227 West 17th Street, New York, N.Y. 10011. No part of this publication may be reproduced, stored in a retrieval system, or transmitted, in any form or by any means, electronic, mechanical, photocopying, microfilming, recording or otherwise, without written permission of the publisher. A copy of this article is available from the publisher for $15.00.

Declassified and Approved For Release 2013/09/24 : CIA-RDP10-02196R000400060004-1

Declassified and Approved For Release 2013/09/24 : CIA-RDP10-02196R000400060004-1

lithium blankets surrounding the fusion zone in pulsed thermonuclear reactors. The papers devoted to hydrogen energetics attracted attention.

The papers on construction and operation of large superconducting magnet systems with magnetic field volumes on the order of several cubic meters are of interest.

Several computational and theoretical papers were presented on various problems in magnetohydrodynamics and the plasma physics of MHD generators.

The conference materials are collected in four volumes and supplementary conference materials and "round table" material will be sent to the conference participants toward the end of 1975.

Declassified and Approved For Release 2013/09/24 : CIA-RDP10-02196R000400060004-1

Declassified and Approved For Release 2013/09/24 : CIA-RDP10-02196R000400060004-1

2ND SESSION OF THE SOVIET-AMERICAN COORDINATING COMMITTEE ON THERMONUCLEAR ENERGY

G. A. Eliseev and D. F. Khokhlova

The second session of the Soviet–American Coordinating Committee on Thermonuclear Energy was held in the United States on July 2-4, 1975. Soviet–American collaboration in controlled thermonuclear fusion research (CTR) is a part of the scientific and technical collaboration on the peaceful uses of atomic energy conducted on the basis of the agreement between the USSR and the USA on June 21, 1973. The basic problems for this joint committee, whose cochairmen are Academician E. P. Velikhov (USSR) and the E.R.D.A. Director of Thermonuclear Research, Dr. Robert L. Hirsch, are the development of yearly and long term programs for cooperation, the coordination of their execution, pointing out the most essential directions for joint efforts, etc.

The notice for the 2nd session of the coordinating committee included a discussion of the current programs and research plans in CTR in both countries and an analysis of the prospects and possible ways of solving the problem of producing thermonuclear energy. The results of the first year of cooperation were considered, the program for cooperation in the current year was made more precise, and a preliminary plan for the program of scientific and technical cooperation in 1976 was drawn up.

During the consideration of the national CTR programs, talks were heard describing in detail the results of the principal experimental and engineering projects, approaches to solving specific scientific and technical CTR problems, and proposed plans for building a thermonuclear power reactor. The American side presented comprehensive information on the demonstration tokamak thermonuclear reactor TFTR, which is intended to begin operation in 1980-1981. The TFTR will be built under the scientific direction of the Princeton Plasma Physics Laboratory at a site adjacent to this laboratory. The basic parameters of TFTR are: torus major radius 2.7 m, plasma column radius 0.85 m, toroidal magnetic field 50 kG, plasma current 2.5 MA, combined power of the reactor power supplies 660 MW, and working pulse length 0.6 sec. Supplementary heating in the reactor is by injection of beams of neutral atoms with energy 150 keV. The expected plasma parameters are $n\tau_E \approx 10^{13}$ cm^{-3} and $T \approx 5$ keV. The overall cost of the reactor is estimated to be 215 million dollars. It is proposed that during 1981-82 experiments with hydrogen plasmas will be conducted on TFTR. Once a plasma has been obtained with parameters such as to ensure a sustained controlled thermonuclear reaction, work with a deuterium–tritium mixture will be begun.

The Soviet delegation reported on the design work on the demonstration thermonuclear tokamak reactor T-20 at the I. V. Kurchatov Institute of Atomic Energy and the D. V. Efremov Scientific-Research Institute for Electrophysical Apparatus. The T-20 reactor is planned for extended operation in a deuterium–tritium experiment with plasma parameters $n\tau_E \approx 10^{14}$ cm^{-3} and $T > 7$ keV. The basic parameters of the system components have been chosen so that a powerful thermonuclear reaction will take place in a D–T plasma and release energy through the reaction neutrons close to the energy delivered to the plasma.

This exchange of opinions gives everyone basis to suppose that construction of the T-20 and TFTR machines together with solution of the physical problems will make it possible to carry out simulations and choose the basic engineering solutions which will be required for development of a power reactor based on a tokamak system. The basic results from studies of pulsed thermonuclear systems and open magnetic mirror systems were discussed. Special attention was paid to analysis of the present state of and plans for

Translated from Atomnaya Énergiya, Vol. 39, No. 5, pp. 374-375, November, 1975.

©1976 Plenum Publishing Corporation, 227 West 17th Street, New York, N.Y. 10011. No part of this publication may be reproduced, stored in a retrieval system, or transmitted, in any form or by any means, electronic, mechanical, photocopying, microfilming, recording or otherwise, without written permission of the publisher. A copy of this article is available from the publisher for $15.00.

Declassified and Approved For Release 2013/09/24 : CIA-RDP10-02196R000400060004-1

Declassified and Approved For Release 2013/09/24 : CIA-RDP10-02196R000400060004-1

developments in the area of technology for thermonuclear systems. In particular, the prospects for constructing high-power 14-MeV neutron sources needed to solve the so-called first wall problem for a thermonuclear reactor were considered.

The commission acknowledged the positive and mutually useful results of this collaboration during 1974. The main goal of the collaboration in 1974 was detailed mutual acquaintance with the national CTR programs. In accordance with the cooperation program, several groups of Soviet and American specialists in plasma physics visited the main thermonuclear centers in both countries. Joint projects were begun on tokamak type machines and on open magnetic traps, on the theory of MHD instabilities and turbulent processes in plasmas, and on the development of fast neutral particle injectors. Successful seminars were conducted involving both countries on CTR materials studies, system analysis of thermonuclear electric generating stations, energy storage and switching, etc.

In the cooperation program for 1975 basic attention is given to production of joint papers, working meetings, and experiments aimed at solving specific scientific and technical problems in CTR, in particular, problems associated with development of a demonstration thermonuclear reactor. The program for this year lays the foundation for selecting the key directions for further collaboration and developing long term joint programs. In 1975 joint development is planned for conceptual designs for a divertor and a 160-keV neutral particle injector for demonstration tokamak reactors. In May there was a joint working meeting in Moscow on the problems of impurities, walls, limiters, and divertors in tokamak systems. A group of Soviet physicists will participate in experiments on the American tokamaks ATC (Princeton), ORMAK (Oak Ridge), and Doublet-IIA (San Diego). American scientists are working on the T-4 and T-11 tokamaks at the I. V. Kurchatov Institute of Atomic Energy. There will be joint working meetings on pulsed thermonuclear reactors at the Leningrad Scientific Research Institute for Electrophysical Apparatus, on tokamaks at the Princeton Plasma Physics Laboratory, and on open magnetic mirrors at the Institute of Nuclear Physics of the Siberian Branch of the Academy of Sciences of the USSR. A seminar on dynamic stabilization of high temperature plasmas is to be held at the Sukhumi Physicotechnical Institute. A group of Soviet specialists in the study of materials will visit US scientific centers working on radiation damage of materials in the autumn.

A preliminary program for cooperation in 1976 was discussed in the meetings at this session. It envisages continued expansion in the volume of joint theoretical, experimental, and design efforts. Agreement was attained on joint development and testing of neutral particle injectors superconducting magnet systems for experimental reactors as well as on joint design and testing of neutron blankets for thermonuclear reactors, in particular, a blanket for a hybrid fission–fusion reactor. The final 1976 program will be confirmed at the third session of the joint Soviet–American commission in November, 1975.

The members of the Soviet delegation visited the Livermore Laboratory, the Princeton Plasma Physics Laboratory, the thermonuclear laboratory of the University of California at Berkeley, and the Electric Power Research Institute (EPRI) in Palo Alto. At the Livermore Laboratory our delegation became acquainted with the work on open magnetic mirrors, in particular, with the experiments on the 2XIIB and "Baseball" machines, and with the work on laser fusion (the "Argus," "Janus," and "Shiva" machines, the latter being under construction). At Livermore and Berkeley the program for developing intense neutral particle injectors for tokamak reactors was discussed. At Princeton the Soviet scientists became acquainted with the progress in setting up the largest American tokamak, PLT, which is planned to be turned on in October, 1975, and with the plans to build the large tokamak with a divertor, PDX. At the EPRI an interesting discussion took place on the prospects for hybrid systems (thermonuclear breeder reactor with a blanket containing fissile material).

Declassified and Approved For Release 2013/09/24 : CIA-RDP10-02196R000400060004-1

Declassified and Approved For Release 2013/09/24 : CIA-RDP10-02196R000400060004-1

SEMINARS AND EXHIBITIONS OF THE ALL-UNION ISOTOPE SOCIETY

A Seminar and Exhibition on "The Atom as a Workman" was held at the Leningrad Interrepublic Section of the All-Union Isotope Society for leaders of enterprises and organizations of the Petrograd District of Leningrad in May 1975. Participants included 43 specialists from 26 enterprises of the district.

A Seminar on "Stable Isotopes in Science and the National Economy," organized by the Kiev Interrepublic Section of the All-Union Isotope Society in conjunction with the Scientific-Research Institute of Stable Isotopes (Tbilisi), was held at Kiev in May 1975. Participants in the work of the seminar included 60 representatives of various branches of the country's economy. Sixteen reports and communications were delivered, and recommendations which will be published and distributed to enterprises were adopted.

An Advanced Experience School on "Methods and Means of Industrial Radiography" was held by the All-Union Isotope Society in conjunction with the All-Union Scientific-Research Institute of Radiation Technology in June 1975 in the demonstration hall of the Sverdlovsk Interregional Section of the All-Union Isotope Society. Participants included 74 representatives from six sections of the All-Union Isotope Society (Leningrad, Kiev, Tashkent, Moscow, Khabarovsk, and Sverdlovsk) and 20 Sverdlovsk industrial enterprises.

A Seminar and Exhibition on "Application of Isotopes and Radioisotope Technology in the National Economy" was held at Saratov in June 1975 by the Moscow Interregional Section of the All-Union Isotope Society in conjunction with the Saratov Interbranch Center of Scientific and Technical Information and Propaganda. Participants in the work of the seminar included 53 specialists from 32 organizations established at Saratov and in the region. The exhibition included demonstrations of new specimens of isotope products, radioisotope instruments, and protective techniques.

An Advanced Experience School on the Introduction of Radioisotope Technology into Industry was held at Dimitrovgrad in June 1975 by the Moscow Interregional Section of the All-Union Isotope Society in conjunction with the V. I. Lenin Scientific-Research Institute of Atomic Reactors for leading workers of industrial enterprises and organizations of Dimitrovgrad and the Ul'yanovsk region. Participants included 150 persons from 78 enterprises of the city and the region. Speakers noted the highly promising outlook for the application of isotope methods and instruments in the city's industry.

A Seminar on "Quality Control for Welded Seams" was held by the Sverdlovsk Interregional Section of the All-Union Isotope Society in conjunction with the "Soyuzshakhtospetsmontazh" Welding Laboratory Trust in June 1975 at Berezovskii in the Sverdlovsk region. Gamma defectoscopes and dosimetric instruments were shown to specialists from industrial enterprises. A communication delivered at the seminar was broadcast over Sverdlovsk television.

An Exhibition and Seminar on "Radioisotope Methods of Control and Automation in Industry" was held by the Sverdlovsk Interregional Section of the All-Union Isotope Society in conjunction with the "Soyuztekhuglerod" All-Union Society and the All-Union Scientific-Research Institute of Technical Carbon (VNIITu) in June 1975 at Omsk. Along 200 specialists visited the exhibition. The work of the exhibition was widely publicized over Omsk radio and television; it showed that radioisotope instruments are being widely used in this branch of the economy. It is expected that a total of 3000 radioisotope instruments will be required by this branch in the future.

A Seminar and Exhibition on "Radioisotope Instruments and Their Application in Various Branches of the National Economy" was organized by the Khabarovsk Interregional Section of the All-Union Isotope

Translated from Atomnaya Énergiya, Vol. 39, No. 5, pp. 375-376, November, 1975.

©1976 Plenum Publishing Corporation, 227 West 17th Street, New York, N.Y. 10011. No part of this publication may be reproduced, stored in a retrieval system, or transmitted, in any form or by any means, electronic, mechanical, photocopying, microfilming, recording or otherwise, without written permission of the publisher. A copy of this article is available from the publisher for $15.00.

Declassified and Approved For Release 2013/09/24 : CIA-RDP10-02196R000400060004-1

Declassified and Approved For Release 2013/09/24 : CIA-RDP10-02196R000400060004-1

Society, the Amur Regional Council of the All-Union Inventors and Rationalizers Society, the Khabarovsk Center for Scientific and Technical Research, and the Amur Regional Council of the Scientific and Technical Association, at Blagoveshchensk in June 1975. Representatives of 25 Blagoveshchensk organizations participated in the seminar. Seven reports were delivered. The exhibition was visited by about 200 specialists. Recommendations aimed at bringing radioisotope techniques into wider use were adopted.

A Seminar on "Radioisotope Methods and Instruments in the Coal and Oil Industry" was organized by the Ukhta Municipal Committee of the Communist Party of the Soviet Union, the Komi Regional Directorate of the Scientific and Technical Association of the Oil and Gas Industry, the House of Technology of the Regional Council of the Scientific and Technical Association, and the Leningrad Interrepublic Section of the All-Union Isotope Society in June 1975 at Ukhta, Komi ASSR. Participants included 52 specialists from 39 industrial organizations of the city; 13 reports and communications were delivered. The recommendations of the seminar will be published and distributed to enterprises.

Three Seminars on "Problems of Safety Techniques and Radiation Safety in Work with Radioactive Substances and Sources of Ionizing Radiation," "What is New in the Practice of Industrial Defectoscopy?" and "Experience and Prospects in the Use of Radioisotope Techniques at Construction Industry Enterprises" were held by the Sverdlovsk Interregional Section of the All-Union Isotope Society in conjunction with the Isotope Committee of the Sverdlovsk Regional Council in June 1975. Specialists from Sverdlovsk industrial enterprises participated in the seminars.

Declassified and Approved For Release 2013/09/24 : CIA-RDP10-02196R000400060004-1

Declassified and Approved For Release 2013/09/24 : CIA-RDP10-02196R000400060004-1

BOOK REVIEWS

Yu. I. Likhachev and V. Ya. Pupko

STABILITY OF THE FUEL ELEMENTS OF NUCLEAR REACTORS *

Reviewed by N. S. Khlopkin

The foremost problems of nuclear-power generation is to ensure reliable operation of the nuclear-reactor fuel elements over a long period and at deep fuel burnups, under conditions of high radiation fluxes, high temperatures and the corrosion action of the coolant, at steady and variable power levels. A knowledge of the stresses and deformations in the core and cladding of the fuel elements, during their entire period of operation, occupies an important place in its solution.

The book being reviewed gives the general theory of the calculation of the stressed–strained state of fuel elements and takes into account their special operating features and the effect of irradiation on the fuel-element materials.

The book comprises two sections. In the first section methods are considered for calculating the stability of fuel elements, the complex form of loading of fuel elements, their nonisothermicity, change of mechanical properties of the materials during operation, swelling of the fissile and structural materials under the action of radiation. The difficulties of the problem posed are large as a result of the small amount of detailed experimental data on the properties of materials under actual conditions.

Experimental investigations of fuel elements serving as the basis for the selection of a numerical model to a considerable extent are full-scale tests and are of a total nature. They do not give the possibility of distinguishing one or another process. The authors show successively the inadequate data, and give a list of experiments and instrumentation by means of which the required characteristics can be obtained.

In the second section a calculation is carried out of the working efficiency of fuel elements, determined by stability characteristics. The kinetics of the stressed and strained states of the fuel and cladding during operation are considered, the accumulation of defects in the cladding material and the change of the physicomechanical properties of the fuel and cladding in a radiation field.

The corrosion–erosion stability of materials in the coolant and the compatibility of the fuel and cladding materials are not considered here, although for fuel elements where the cladding thicknesses are reduced to a minimum for the purpose of reducing the harmful absorption of neutrons, these problems are important. However, their inclusion in the book would sharply increase its volume.

Here, the procedure is given for calculating the stability characteristics which affect the operating efficiency of the fuel elements with pliable and nonpliable cores, in the presence of cohesion of the fuel with the cladding and with the introduction of a liquid or gaseous contact sublayer. The special features of operation of fuel elements with an oxide core are analyzed. A procedure is given for calculating the surrounding nonuniformity of the thermal and neutron fields and the nonuniform swelling of the cladding material. A procedure is described for calculating the stability of a freely deformed cladding, resting on the fuel core.

The solutions of many problems are reduced to computer programs and can raise the problem of experimental verification of the results obtained. Unfortunately, the kinetics of deformation of fuel elements

*Atomizdat, Moscow (1975).

Translated from Atomnaya Énergiya, Vol. 39, No. 5, p. 376, November, 1975.

©1976 Plenum Publishing Corporation, 227 West 17th Street, New York, N.Y. 10011. No part of this publication may be reproduced, stored in a retrieval system, or transmitted, in any form or by any means, electronic, mechanical, photocopying, microfilming, recording or otherwise, without written permission of the publisher. A copy of this article is available from the publisher for $15.00.

Declassified and Approved For Release 2013/09/24 : CIA-RDP10-02196R000400060004-1

Declassified and Approved For Release 2013/09/24 : CIA-RDP10-02196R000400060004-1

during operation of the reactor in the overwhelming majority of cases cannot be monitored. It is possible only to compare certain ultimate results and integrated characteristics of fuel elements, withdrawn from the reactor, with the calculated results – change of its dimensions, change of the mechanical properties of the core and cladding, position of the most damaged places of the cladding, the times to the appearance of cracks and the nature of these cracks.

But these comparisons also permit the values of the empirical coefficients to be refined, the introduction of which is inevitable, and the procedure to be improved.

There is an appendix to the book, where the possibilities are discussed for deriving an adjoint function device for investigating the steady deformed state of fuel elements, in particular for a more accurate computation of the effect of indeterminacy of the mechanical constant values or of the load factors and the effects of a different type of tolerances on the magnitude of the deformations or stresses.

On the whole, the book is very useful for reactor developers. It allows the selection of prospective fuel-element alternatives to be carried out more correctly for further investigation, and the time and costs on development of reliable fuel elements, which will satisfy the requirements of nuclear power generation, to be shortened considerably.

Declassified and Approved For Release 2013/09/24 : CIA-RDP10-02196R000400060004-1

Declassified and Approved For Release 2013/09/24 : CIA-RDP10-02196R000400060004-1

breaking the language barrier

WITH COVER-TO-COVER ENGLISH TRANSLATIONS OF SOVIET JOURNALS

The Soviet Journal of Bioorganic Chemistry

Bioorganicheskaya Khimiya

Editor: **Yu. A. Ovchinnikov**
Academy of Sciences of the USSR, Moscow

Devoted to all aspects of this rapidly-developing science, this important new journal includes articles on the isolation and purification of naturally-occurring, biologically-active compounds; the establishment of their structure; the mechanisms of bioorganic reactions; methods of synthesis and biosynthesis; and the determination of the relation between structure and biological function.

Volume 1, 1975 (12 issues) $225.00

The Soviet Journal of Coordination Chemistry

Koordinatsionnaya Khimiya

Editor: **Yu. A. Ovchinnikov**
Academy of Sciences of the USSR, Moscow

The synthesis, structure and properties of new coordination compounds; reactions involving intraspheral substitution and transformation of ligands, homogeneous catalysis; complexes with polyfunctional and macromolecular ligands; complexing in solutions; and the kinetics and mechanisms of reactions involving the participation of coordination compounds are among the topics this monthly examines.

Volume 1, 1975 (12 issues) $235.00

The Soviet Journal of Glass Physics and Chemistry

Fizika i Khimiya Stekla

Editor: **M. M. Shul'ts**
Academy of Sciences of the USSR, Leningrad

This new bimonthly publication presents in-depth articles on the most important trends in glass technology. Both theoretical and applied research are reported.

Volume 1, 1975 (6 issues) $95.00

Soviet Microelectronics

Mikroélektronika

Editor: **A. V. Rzhanov**
Academy of Sciences of the USSR, Moscow

Offering invaluable reports on the latest advances in fundamental problems of microelectronics, this new bimonthly covers • theory and design of integrated circuits • new production and testing methods for microelectronic devices • new terminology • new principles of component and functional integration.

Volume 4, 1975 (6 issues) $135.00

Lithuanian Mathematical Journal

Lietuvos Matematikos Rinkinys

Editor: **P. Katilyus**

A publication of the Academy of Sciences of the Lithuanian SSR, the Mathematical Society of the Lithuanian SSR, and the higher educational institutions of the Lithuanian SSR.

In joining the ranks of other outstanding mathematical journals translated by Plenum, *Lithuanian Mathematical Transactions* brings important original papers and notes in all branches of pure and applied mathematics. Topics covered in recent issues include complex variables, probability theory, functional analysis, geometry and topology, and computer mathematics and programming. Translation began with the 1973 issues.

Volume 16, 1976 (4 issues) $150.00

Programming and Computer Software

Programmirovanie

Editor: **N. P. Buslenko**
Academy of Sciences of the USSR, Moscow

This important new bimonthly is a forum for original research in computer programming theory, programming methods, and computer software and systems programming.

Volume 1, 1975 (6 issues) $95.00

send for your free examination copies!

PLENUM PUBLISHING CORPORATION, 227 West 17th Street, New York, N.Y. 10011

Prices slightly higher outside the US. Prices subject to change without notice.

Declassified and Approved For Release 2013/09/24 : CIA-RDP10-02196R000400060004-1

Declassified and Approved For Release 2013/09/24 : CIA-RDP10-02196R000400060004-1

The Plenum/China Program

Research in the medical, life, environmental, chemical, physical, and geological sciences from the People's Republic of China

The 15 major scientific journals published in China since the Cultural Revolution are being made available by Plenum in authoritative, cover-to-cover English translations under the Plenum/China Program imprint.

These important journals contain papers prepared by China's leading scholars and present original research from prestigious Chinese institutes and universities. Their editorial boards are affiliated with such organizations as the Chinese Chemical Society, the Academia Sinica in Peking and its Institutes, and the Chinese Microbiological Society.

The English editions are prepared by scientists and researchers, and all translations are reviewed by experts in each field.

Journal Title	No. of Issues	Subscription Price
Acta Astronomica Sinica	2	$65
Acta Botanica Sinica	4	$95
Acta Entomologica Sinica	4	$95
Acta Genetica Sinica	2	$65
Acta Geologica Sinica	2	$75
Acta Geophysica Sinica	4	$95
Acta Mathematica Sinica	4	$75
Acta Microbiologica Sinica	2	$55
Acta Phytotaxonomica Sinica	4	$125
Acta Zoologica Sinica	4	$125
Geochimica	4	$110
Huaxue Tongbao — Chemical Bulletin	6	$95
Kexue Tongbao — Science Bulletin	12	$175
Scientia Geologica Sinica	4	$125
Vertebrata PalAsiatica	4	$95

For further information, please contact the Publishers.

SEND FOR YOUR FREE EXAMINATION COPIES

plenum
PLENUM PUBLISHING CORPORATION
227 West 17 Street, New York, N.Y. 10011
In United Kingdom 8 Scrubs Lane, Harlesden, London, NW10 6SE, England

Declassified and Approved For Release 2013/09/24 : CIA-RDP10-02196R000400060004-1